



N OVA
NOVA SCHOOL OF
SCIENCE & TECHNOLOGY

DEPARTMENT
OF PHYSICS

JOÃO LUÍS FIALHO SIMÃO MARQUES RIBEIRO
Bachelor in Biomedical Engineering

DEVELOPMENT OF RESORBABLE METAL-BASED BIOMEDICAL IMPLANTS

MASTER IN BIOMEDICAL ENGINEERING
NOVA University Lisbon
September, 2022



DEVELOPMENT OF RESORBABLE METAL-BASED BIOMEDICAL IMPLANTS

JOÃO LUÍS FIALHO SIMÃO MARQUES RIBEIRO
Bachelor in Biomedical Engineering

Adviser: João Pedro Oliveira
Assistant Professor, NOVA University Lisbon

Co-adviser: Ana Baptista
Researcher, NOVA University Lisbon

Development of resorbable metal-based biomedical implants

Copyright © João Luís Fialho Simão Marques Ribeiro, NOVA School of Science and Technology, NOVA University Lisbon.

The NOVA School of Science and Technology and the NOVA University Lisbon have the right, perpetual and without geographical boundaries, to file and publish this dissertation through printed copies reproduced on paper or on digital form, or by any other means known or that may be invented, and to disseminate through scientific repositories and admit its copying and distribution for non-commercial, educational or research purposes, as long as credit is given to the author and editor.

ACKNOWLEDGEMENTS

Firstly, I would like to thank my two supervisors, Professor João Pedro Oliveira and Professor Ana Baptista for proposing this topic, which will give way to much research and if all goes well, to an improvement in people's lives. I thank them for the trust they have placed in me since the moment they chose me to explore this theme. Also, their support provided, availability and dedication shown during all these months of work, have made my path to this point a lot clearer but also more challenging.

I would also like to thank the caring and attentive coordinator of the Integrated Masters Course in Biomedical Engineering, Professor Carla Quintão, who always gave everything for me and my colleagues, and helped us to achieve everything we wanted. Obviously never forgetting all the remaining teachers who had a huge impact on my academic life, contributing to both intellectual and personal development. To all the teaching and non-teaching staff of the NOVA School of Science and Technology, and to all my colleagues and good friends I made during these 5 years, who helped me whenever I needed it, never turning me down, a huge gratitude.

To all my family and close friends, for all the moments of fun and support, for helping me to unwind and relax, but also for the serious and more serene moments, for all of this I thank you.

A special thank you would never be enough to make up for all the years of unconditional love and support provided by my beloved Rita. For being constantly by my side, always with the perfect words to lift me up, always making me see the positive side of everything, making everyday of my life brighter and more fulfilling.

Finally, to my mother, father and brother, who have accompanied me since my first day in all situations, who have allowed me to have the life I have today filled with good things. It is because of you that I am who I am and have what I have. Everything I have achieved and will achieve, it is all because of you. For all the good and bad times, all the tears and the smiles, all the arguments and the affection, I will be eternally grateful.

To all of you, those present and those who should be, an enormous gratitude.

“You can’t help anybody else until you can help yourself.”
(Logic)

ABSTRACT

The interest in bioresorbable materials has been increasing throughout the years. Various non-resorbable metals like pure titanium and its alloys, are used to correct bone fractures and some to produce stents for cardiovascular purposes. However, these materials show some limitations, namely the necessity of a second surgery for their removal and so, bioresorbable materials have been studied as an alternative. Additive Manufacturing (AM) is one way to produce the implants and has major advantages over traditional methods. Wire and Arc Additive Manufacturing (WAAM) is one type of AM and has a very promising future in the production of bioresorbable implants due to its high energy efficiency, high deposition rate, and lower equipment cost. Furthermore, a Hydroxyapatite (HA) coating on these implants has been shown to improve corrosion resistance and biocompatibility. In this work, samples of bioresorbable Mg alloys were fabricated using WAAM and a coating of HA was made using electrodeposition. Their microstructures were analysed as well as their electrochemical characterization, *in vitro* degradation and corrosion resistance, before and after the coating. The mass variation experiments in PBS under static conditions were inconclusive because sometimes the substrates gain weight, especially in acid environments. However, the alloys seemed more corroded in that condition than in neutral pH. It was concluded that it is possible to cover the substrates with HA, improving their corrosion resistance. Additionally, lower voltages (3V and 3.5V) seemed to present better results than the others (4V, 4.5V, 5V and 6V), with more homogeneous coatings. Regarding deposition times, too low (30-90 min) revealed seemingly weaker depositions, and too exaggerated times (24 hours) revealed the production of corrosion products. The next steps are the study of the toxicity, biocompatibility, and cell adhesion with the HA coating, and to improve the mass variation experiment, it should be under dynamic conditions, preferably with real body fluids.

Keywords: bioresorbable materials, bioresorbable implants, magnesium, additive manufacturing, wire and arc additive manufacturing, hydroxyapatite, electrodeposition

RESUMO

O interesse por materiais bioabsorvíveis tem vindo a aumentar ao longo dos anos. Diversos metais não reabsorvíveis como o titânio puro e as suas ligas são utilizados para corrigir fraturas ósseas e alguns para produzir *stents* para fins cardiovasculares. No entanto, estes materiais apresentam algumas limitações, sendo a necessidade de uma segunda cirurgia para a sua remoção uma delas, e por conseguinte materiais bioabsorvíveis têm sido estudados como alternativa. A produção aditiva é um dos métodos para os produzir, e tem grandes vantagens sobre os processos tradicionais. *Wire and Arc Additive Manufacturing* (WAAM) é um tipo de produção aditiva, tendo um futuro muito promissor no desenvolvimento de implantes reabsorvíveis devido à sua elevada eficiência energética, elevada taxa de deposição, e menor custo de equipamento. Além disso, foi demonstrado que um revestimento de Hidroxiapatite (HA) nestes implantes melhora a sua resistência à corrosão e biocompatibilidade. Neste trabalho, foram fabricadas através da técnica WAAM amostras de Magnésio (AZ61A) e feito um revestimento HA através da técnica de eletrodeposição. As suas microestruturas foram analisadas, bem como a caracterização eletroquímica, a degradação *in vitro* e a resistência à corrosão, antes e depois do revestimento. As experiências de variação de massa em PBS sob condições estáticas foram inconclusivas porque por vezes os substratos ganham peso, especialmente em ambientes ácidos. No entanto, as ligas pareciam mais corroídas nessa condição do que em pH neutro. Concluiu-se que é possível cobrir os substratos com HA, melhorando a sua resistência à corrosão, tensões mais baixas (3V e 3.5V) parecem apresentar melhores resultados do que as restantes (4V, 4.5V, 5V e 6V), com revestimentos mais homogêneos. No que diz respeito aos tempos de deposição, demasiado baixos (30-90 min) revelaram deposições aparentemente mais fracas, e tempos exagerados (24 horas) revelaram a produção de produtos de corrosão. Os passos seguintes são o estudo da toxicidade, biocompatibilidade, e adesão celular com o revestimento HA, e para melhorar a experiência de variação de massa, deve ser feita em condições dinâmicas, de preferência com fluidos corporais reais.

Palavras-chave: materiais bioabsorvíveis, implantes bioabsorvíveis, magnésio, produção aditiva, wire and arc additive manufacturing, hidroxiapatite, eletrodeposição

CONTENTS

List of Figures	x
List of Tables	xiii
Acronyms	xiv
1 Introduction	1
2 Summary of Theoretical Concepts	2
2.1 Wire and Arc Additive Manufacturing	2
2.2 Bioresorbable Materials	3
2.2.1 Magnesium and its Alloys	4
2.2.2 Hydroxyapatite Coating	6
3 State of the Art	10
3.1 A Brief History of Biomaterials and WAAM Technology	10
3.2 Nowadays	11
4 Materials and Methods	13
4.1 Preparation of the Metallic Substrates by WAAM	13
4.2 Preparation of the Buffer Solutions for Simulation of Body Fluids	15
4.2.1 PBS Solution with pH 7.4	15
4.2.2 PBS Solution with pH 5.5	15
4.3 Degradation Tests	15
4.4 Electrochemical Characterization	15
4.4.1 Cyclic Voltammetry	15
4.4.2 Development of the plastic lid	17
4.5 Electrodeposition of Hydroxyapatite	18
4.6 Analysis and Characterization	20
4.6.1 Chemical Characterization with Raman Spectroscopy	20
4.6.2 Morphological and Structural Characterization with SEM and XRD	20

5 Results and Discussion	22
5.1 Electrochemical and Corrosion Experiments	22
5.1.1 CV with Neutral PBS Solution on Commercial AZ61A alloys . .	22
5.1.2 CV with Acid PBS Solution on Commercial AZ61A alloys	25
5.1.3 CV on WAAM printed AZ61A alloys	27
5.1.4 Mass Variation and Corrosion	28
5.2 Degradation Tests	31
5.3 Hydroxyapatite Coating	31
5.3.1 SEM Results	32
5.3.2 Raman Spectroscopy Analysis	38
5.3.3 XRD Analysis	40
5.3.4 Electrochemical and Corrosion Experiments after the HA Coating	47
6 Conclusion and Future Work	57
Bibliography	59
Annexes	
I Annex	68

LIST OF FIGURES

2.1	Illustration of the WAAM process	3
2.2	Crystal structure of HA	7
4.1	Photograph of the GMAW welding machine, model Pro MIG 501 from KEMPPI	14
4.2	Photograph of a printed wall	14
4.3	Photograph of part of a treated printed wall and a sliced piece used for the study	14
4.4	Illustration of the Cyclic Voltammetry process	16
4.5	Photographs of the setup used for the Cyclic Voltammetry experiment . . .	17
4.6	STL project of the plastic lid	18
4.7	Photograph of the plastic lid	18
4.8	Illustration of the Electrochemical Deposition process	19
4.9	Photograph of the setup used for the electrodeposition method	19
5.1	CV of the Mg alloy with 200 consecutive cycles with a pH of 7.4	23
5.2	CV of the Mg alloy with 50x4 cycles, with a pH of 7.4	24
5.3	CV of the Mg alloy with 200 cycles, with a pH of 5.5	25
5.4	Photographs of the setup after a CV with the acid and the neutral pH . . .	26
5.5	CV of the WAAM printed Mg alloy with 200 cycles, with a pH of 7.4	27
5.6	CV of the WAAM printed Mg alloy with 200 cycles, with a pH of 5.5	28
5.7	Photograph and microscopic image of the WAAM printed Mg commercial alloy AZ61A	30
5.8	Photograph and microscopic image of the WAAM printed Mg commercial alloy AZ61A after a CV experiment with neutral PBS solution	30
5.9	Photograph and microscopic image of the WAAM printed Mg commercial alloy AZ61A after a CV experiment with acid PBS solution	30
5.10	SEM of the commercial Mg wire AZ61A	32
5.11	SEM of a deposition of 3V for 30 minutes after the immersion in NaOH . .	33
5.12	SEM of a deposition of 3 V for 60 minutes after the immersion in NaOH . .	33
5.13	SEM of a deposition of 3 V for 90 minutes after the immersion in NaOH . .	33

5.14 SEM of a deposition of 3 V for 2h after the immersion in NaOH	34
5.15 SEM of a deposition of 3 V for 24 hours after the immersion in NaOH	34
5.16 SEM of a deposition of 3.5 V for 2h after the immersion in NaOH	34
5.17 SEM of a deposition of 4 V for 2h after the immersion in NaOH	35
5.18 SEM of a deposition of 4.5 V for 2h after the immersion in NaOH	35
5.19 SEM of a deposition of 5 V for 2h after the immersion in NaOH	35
5.20 SEM of a deposition of 6 V for 2h after the immersion in NaOH	36
5.21 SEM of a deposition of 3 V for 2h before the immersion in NaOH	36
5.22 SEM of a deposition of 6 V for 2h before the immersion in NaOH	36
5.23 SEM of the WAAM printed Mg alloy AZ61A	37
5.24 SEM of a deposition of 3 V for 2h after the immersion in NaOH in a WAAM printed AZ61A alloy	37
5.25 SEM of a deposition of 3.5 V for 2h after the immersion in NaOH in a WAAM printed AZ61A alloy	37
5.26 SEM of a deposition of 4 V for 2h after the immersion in NaOH in a WAAM printed AZ61A alloy	38
5.27 Raman Spectroscopy of a substrate before the immersion in NaOH, with a electrodeposition of 3 V for 2 hours	39
5.28 Raman Spectroscopy of HA commercial powder and another of a substrate after the immersion in NaOH, with a electrodeposition of 3 V for 2 hours	40
5.29 XRD of the as-deposited coating with a deposition of 3 V for 2 hours	41
5.30 XRD of the coating after the immersion in NaOH with a deposition of 3 V for 2 hours	42
5.31 Comparison of the XRD of the HA powder with the coating after the immer- sion in NaOH with a deposition of 6 V for 2 hours	43
5.32 Comparison of the XRD of the corrosion precipitate powder with the coating after the immersion in NaOH with a deposition of 6 V for 2 hours and the substrate used in a CV experiment in a acid environment	45
5.33 Comparison of the XRD of the coating after the immersion in NaOH with a deposition of 3 V for 24 hours with a deposition of 3V for 2 hours	46
5.34 CV of the Mg alloy with 200 consecutive cycles with a pH of 7.4, after an electrodeposition of 3 V for 2 hours	47
5.35 CV of the Mg alloy with 200 consecutive cycles with a pH of 7.4, after an electrodeposition of 3.5 V for 2 hours	48
5.36 CV of the Mg alloy with 200 consecutive cycles with a pH of 7.4, after an electrodeposition of 4 V for 2 hours	48
5.37 CV of the WAAM printed Mg alloy with 200 consecutive cycles with a pH of 5.5, after an electrodeposition of 3 V for 2 hours	49
5.38 CV of the WAAM printed Mg alloy with 200 consecutive cycles with a pH of 5.5, after an electrodeposition of 3.5 V for 2 hours	49

LIST OF FIGURES

5.39 CV of the WAAM printed Mg alloy with 200 consecutive cycles with a pH of 5.5, after an electrodeposition of 3 V for 2 hours	50
5.40 SEM of a WAAM printed Mg commercial alloy AZ61A after a CV experiment in neutral pH, with a deposition of 3 V for 2h	54
5.41 SEM of a WAAM printed Mg commercial alloy AZ61A after a CV experiment in neutral pH, with a deposition of 3.5 V for 2h	54
5.42 SEM of a WAAM printed Mg commercial alloy AZ61A after a CV experiment in neutral pH, with a deposition of 4 V for 2h	55
5.43 SEM of a WAAM printed Mg commercial alloy AZ61A after a CV experiment in acid pH, with a deposition of 3 V for 2h	55
5.44 SEM of a WAAM printed Mg commercial alloy AZ61A after a CV experiment in acid pH, with a deposition of 3.5 V for 2h	56
5.45 SEM of a WAAM printed Mg commercial alloy AZ61A after a CV experiment in acid pH, with a deposition of 4 V for 2h	56
I.1 Photograph of the commercial wire AZ61A, used to print the WAAM substrates	68
I.2 Photograph of the printed WAAM substrate and the commercial wire, side by side	69
I.3 Raman Spectroscopy of the Hydroxyapatite commercial powder	69
I.4 Raman Spectroscopy of a substrate after the immersion in NaOH, with a electrodeposition of 3V for 2 hours	71
I.5 Comparison of the XRD of the as-deposited coating of depositions of 3V and 6V, both for 2 hours	72
I.6 XRD of the commercial Hydroxyapatite powder	73
I.7 Comparison of the XRD of the HA commercial powder and the coating after the immersion in NaOH with a deposition of 3V for 2 hours	74
I.8 Comparison of the XRD of the coating after the alkaline treatment of depositions of 6V and 3V, both for 2 hours and of the HA commercial powder	75
I.9 XRD of the corrosion precipitate formed during the CV experiment with neutral pH	76
I.10 XRD of the substrates after two CV experiments, one in a acid environment and other in a neutral environment	77
I.11 CV of the WAAM printed substrate with 200 consecutive cycles with a pH of 7.4, after an electrodeposition of 3V for 2 hours	78
I.12 CV of the WAAM printed substrate with 200 consecutive cycles with a pH of 7.4, after an electrodeposition of 3.5V for 2 hours	78
I.13 CV of the WAAM printed substrate with 200 consecutive cycles with a pH of 7.4, after an electrodeposition of 4V for 2 hours	79

LIST OF TABLES

4.1	Parameters' values for the welding process	13
5.1	Mass variation of the Mg commercial alloys after a Cyclic Voltammetry experiment in neutral PBS solution, for 200 cycles and 50x4 cycles	29
5.2	Mass variation of the Mg WAAM printed alloys after a Cyclic Voltammetry experiment in neutral and acid PBS solutions, for 200 cycles	29
5.3	Mass variation of the AZ61A Mg alloys after immersion tests in neutral and acid PBS solutions	31
5.4	Mass variation of the WAAM substrates after Cyclic Voltammetry with 200 cycles in PBS solutions, after the HA coating	51
5.5	Photographs and microscopic images of the WAAM printed Mg commercial alloy AZ61A with a deposition of 3 V, 3.5 V and 4 V with 2 hours, after a CV experiment in neutral pH	52
5.6	Photographs and microscopic images of the WAAM printed Mg commercial alloy AZ61A with a deposition of 3 V, 3.5 V and 4 V with 2 hours, after a CV experiment in acid pH	53
I.1	Physical and mechanical properties of natural bone, Mg and Ti	68
I.2	Photographs and microscopic images of the substrates after the electrodepositions at voltages 3V, 3.5V and 4V, with a duration of 2 hours, after the immersion in NaOH	70

ACRONYMS

AM	Additive Manufacturing
CaP	Calcium Phosphate
CV	Cyclic Voltammetry
DCPD	Dicalcium Phosphate Dihydrate/Brushite
DED	Direct Energy Deposition
GMAW	Gas Metal Arc Welding
GTAW	Gas Tungsten Arc Welding
HA	Hydroxyapatite
Mg	Magnesium
MIG	Metal Inert Gas
OCP	Open-Circuit Potential
OCPphosphate	Octacalcium Phosphate
PAW	Plasma Arc Welding
PBS	Phosphate-Buffered Saline
RS	Raman Spectroscopy
SEM	Scanning Electron Microscopy
TCPphosphate	Tricalcium Phosphate
Ti	Titanium

TIG	Tungsten Inert Gas
WAAM	Wire and Arc Additive Manufacture
XRD	X-ray Diffraction

INTRODUCTION

Firstly, the subject of the dissertation is the Development of resorbable metal-based biomedical implants. Given that a second surgery for hardware removal is almost always necessary, interest in bioresorbable implants has grown exponentially in recent years, and there are many studies proving their efficiency. Despite this, there are still few clinical studies and a number of setbacks to work out, so there is still a long way to go.

This study fits perfectly in the reality lived in today, since the interest in bioresorbable materials and in Wire and Arc Additive Manufacture (WAAM) technology, and the necessity of alternatives to current methods have been increasing in time.

The main goal was to develop bioresorbable Magnesium-based alloys through WAAM. In addition, an Hydroxyapatite (HA) coating was made with electrodeposition, for the purpose of improving the substrates corrosion resistance. Many parameters will be tested during the electrodeposition in order to obtain the most homogeneous coating, thus determining the best options for doing so.

Subsequently, their applicability potential in the biomedical field will be evaluated. For that purpose, the printed substrates will be studied in detail concerning corrosion performance and *in vitro* degradation, before and after the coating. In the mean time, some skills were developed: in the production of metal alloys for medical implants; additive manufacturing processes; materials' characteristics; and evaluation of corrosion phenomena under simulated body fluids.

This document is divided in 6 Chapters: Chapter 2 is related to the Theoretical Concepts, where the WAAM method and the bioresorbable materials are discussed, focusing on the Magnesium (Mg) and the Hydroxyapatite; in Chapter 3 a brief history of the bio-materials and the WAAM method, and the State of the Art are discussed; Chapter 4 is dedicated to the Materials and Methods of this project; Chapter 5 is related to the Results and its discussion; and lastly, the Conclusion of this work is on Chapter 6.

SUMMARY OF THEORETICAL CONCEPTS

In this chapter, the basic theoretical concepts will be presented, such as the WAAM method and the characteristics of bioresorbable materials, specifically Mg and HA.

2.1 Wire and Arc Additive Manufacturing

There are a lot of techniques to produce bioresorbable samples. Additive Manufacturing (AM) has gained credibility in this field due to enabling design capabilities that traditional manufacturing cannot achieve [1]. However, it is a considerably expensive investment, when compared to traditional techniques. Besides that, and being better suited for high production volumes, traditional methods lose to AM when it comes to developing high complexity models or when customization is required [2]. With AM, it is possible to manufacture complex 3D objects, layer by layer, individualizing them to align with anatomical geometries. Additionally, it reduces the manufacturing time, the costs of production and has a clear advantage in terms of environmental impact, reducing waste of material and increasing resource efficiency [1, 2].

Within AM, Direct Energy Deposition (DED) is one of many existing techniques, and it functions by melting materials with thermal energy, fusing them throughout the deposition [1]. There are other methods more often used, such as Selective Laser Sintering and Electron Beam Melting, but they present many restraints due to the essence of their processes, which is why interest in DED is growing [3].

WAAM is classified as a type of DED, and includes an electric arc as a thermal source, and a wire, fed at constant rate, utilized as a feedstock material. The process is shown in Figure 2.1. It has a high energy efficiency, high deposition rate, and a lower equipment cost, when compared to other methods. It is subcategorized in three wire-based welding methodologies: Gas Metal Arc Welding (GMAW) or Metal Inert Gas (MIG), Plasma Arc Welding (PAW), and Gas Tungsten Arc Welding (GTAW) or Tungsten Inert Gas (TIG), where MIG is the most used process in WAAM. In MIG, an electric arc is created between the consumable filament and the metal workpiece, with the wire generally perpendicular to the substrate. The component, the weld pool and adjacent material are protected by an

inert or active shielding gas. Both TIG and PAW use a non-consumable tungsten electrode that creates an electric arc with the workpiece, in the presence of an inert shielding gas. In these techniques, the wire feed orientation is variable, affecting the deposit consistency, making the process planning more challenging. [1, 4, 5]

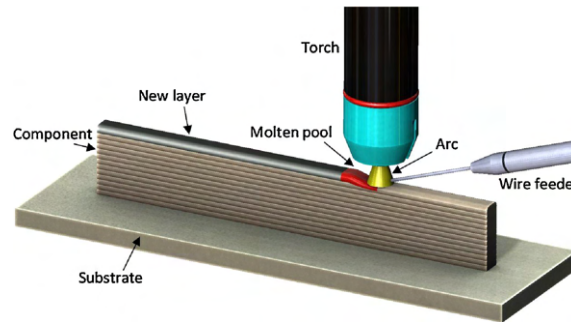


Figure 2.1: Illustration of the WAAM process
(adapted from [6])

2.2 Bioresorbable Materials

Bioresorbable/biodegradable/bioabsorbable materials are materials that corrode gradually *in vivo* with a proper host response, i.e., their derivatives are absorbed completely with no debris and with only slight toxic effects, dissolving entirely while assisting tissue healing [7].

In general, to develop an ideal bioresorbable implant, certain requirements must be fulfilled, such as bioactivity, biocompatibility and be fully degradable. These implants are design to interact with the damaged tissue, liberating products that stimulate tissue healing. Their reaction with the physiological environment should not release toxic products, or even non-toxic products in a high concentration, and the degradation rate needs to be between certain values, in order to give the tissue the support needed, while it is recovering. They can be categorized as polymers, ceramics and metals, and each type has its own advantages and flaws. In this project, a Magnesium alloy - specifically AZ61A - is the substrate that will be studied.

The high incidence of cardiovascular problems and traumatic accidents that results in fractured bone fragments injuries, with the need of surgery, are two of the greatest concerns of public health. Commercially, pure titanium and its alloys, cobalt-chromium-molybdenum alloys, and stainless steel can be found in traditional medical implants often used to stabilize fractured bone fragments. Some metals like steel are also used in coronary stents, to reduce acute and late vessel complications, and avoid vessel recoil [8]. However, these implants require removal operations after a certain time. In addition, besides possessing good mechanical strength, biocompatibility and corrosion resistance, their regular exposure to mechanical, electrochemical, and temperature variations may lead to undesired infections [9, 10]. On the other hand, the degradation products of

the bioresorbable materials are non-toxic, and eventually degrade without affecting surrounding tissues. Yet, these degradation products must not cross the body's tolerance limit. The rate of degradation is not constant, and depends on the contact with body fluid and its flow, temperature, and the material characteristics, such as crystal structure and orientation, and the material's geometry [7].

The metals used to manufacture bioimplants need to have a high purity. Impurities affect the mechanical properties of the material, jeopardizing the efficiency and the validity of the implant.

Regarding orthopaedic implants, their degradation rate should be equal to the rate of bone healing. They should also exhibit mechanical integrity with the bone tissue, that is a Young's Modulus, mechanical strength and fracture toughness, all similar to the bone [11]. For instance, titanium, steel and chromium alloys have elastic modulus very distant to the bone, causing implant failure due to stress shielding of the bone [12].

Stress shielding is the consequence of the change in typical stress/load in the bone, given by the differences between its Young's Modulus and the implant's [13]. If the difference is not substantial, like in the case of Mg, this effect can be reduced. This is coincident with Wolff's Law (1892), that states that mechanics can modify bones' architecture [14]. This leads to bone resorption and loosening of implant which ultimately decreases implant stability [12].

The Table I.1 in I compares the values of some of these properties between natural bone, magnesium and titanium alloys, showing that Mg is much more similar to the bone than titanium is.

In terms of cardiovascular implants, they need to retain their mechanical properties, providing support for approximately six months, after which they fully degrade [15].

In the past years, bioresorbable metals, such as Mg, have been widely studied in the field of bioimplants. This element has several purposes in our body and it is biocompatible and fully degradable. For those reasons, the interest in Mg has been increasing to produce temporary orthopaedic and vascular implants, aiming to avoid a second surgery for hardware removal. However, it has advantages and disadvantages, discussed in 2.2.1.

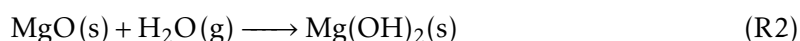
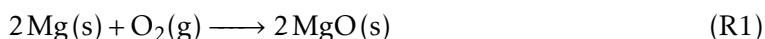
Because there is no perfect element to produce bioresorbable materials, there are many strategies to enhance the properties of each implant such as purification, alloying and coating [16]. In this case, a coating of Hydroxyapatite will be studied in order to increase the biocompatibility and the corrosion resistance of the metallic alloys.

2.2.1 Magnesium and its Alloys

Mg is one of the most studied elements to produce biodegradable materials. It is also an essential micronutrient, and the fourth most abundant cation in the human body. It acts as a cofactor for more than 300 enzymes, plays several roles, including in energy production and bone development, and around 50% to 60% is stored in the bones [17].

As previously mentioned, Mg has a high degradation rate, about 0.62 mm/year in a water solution of pH 7 and 37° C, which can limit its use in some applications, not because of the excessive Mg in the body, but because of the loss of mechanical integrity [7, 9]. The Tolerable Upper Intake Level (maximum daily intake unlikely to cause adverse health effects) for adults is 250-350 mg/day (studied only with supplementation), plus the recommended daily intake that is 310-420 mg/day, depending on the sex. All summed up gives a maximum total of 560-770 mg/day in average. While it is very difficult to cross this limit, which allows the safe use of this element, overtaking it can lead to several complications, including gastrointestinal symptoms [18, 19].

Another disadvantage presented by Mg is the discharge of degradation products, more specifically Hydrogen gas (H₂), as shown in Reaction 7 [20–22]. Mg is very reactive with oxygen (in the air), oxidizing really quickly, forming a thin layer of magnesium oxide (MgO, Reaction 1). When it is in contact with water, this MgO turns into magnesium hydroxide (Mg(OH)₂, Reaction 2). In acidic and neutral environments these two products are soluble, making it non-protective. The dissolution of the hydroxide layer increases the pH value, making it harder to dissolve, as the magnesium hydroxide have lower solubility in alkaline environments. Because of this, the magnesium alloys have less corrosion resistance in acidic environments [21, 23, 24]. In the human body, this undesired pH increase in the surrounding tissues, can adversely affect cell viability [9, 11, 25]. In addition, MgO is more soluble, saturating the surface water layer, leading to the precipitation of Mg(OH)₂ [22].

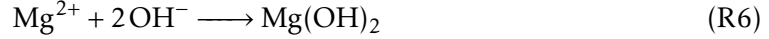


However, besides being soluble, this layer of MgO does not perfectly surrounds the alloy, making it possible for the magnesium to react with water [21]. The formation of H₂ occurs due to the dissociation of magnesium in an aqueous environment (Reaction 3, corresponding to the oxidation/anodic reaction).

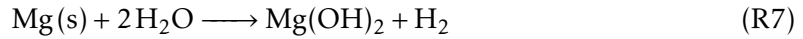


In order to maintain electroneutrality, the electrons formed must be consumed by another species. Next, the release of H₃O⁺ ions by water dissociation (Reaction 4) consume the electrons (Reaction 5), which corresponds to the reduction/cathodic reaction, and the OH⁻ ions consume the Mg²⁺ ions, forming magnesium hydroxide (Reaction 6). According to the Le Chatelier's principle, this affects the balance between water and its ions, giving rise to the water dissociation reaction to return to equilibrium [26].

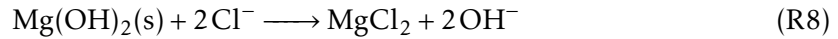




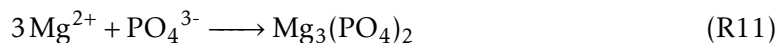
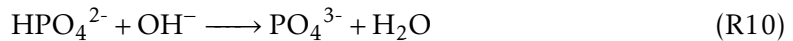
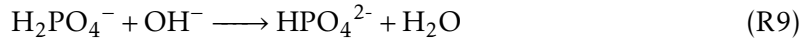
In short, putting all the previous reactions together, the reaction of magnesium with water is given by Reaction 7.



The excessive liberation of H_2 gas can interfere with the bone development process, leading to callus production and cortical flaws [25]. Although acceptable amounts of gas are released, and studies show that exchange through skin can be relatively quick, some strategies are used to overcome the gas formation [15]. The other reaction product, magnesium hydroxide, is only partially soluble. However, since the body fluid is a high chloride environment with a neutral pH, the magnesium hydroxide is converted to magnesium chloride (MgCl_2), which is completely soluble, as shown in Reaction 8. [27, 28]



If the Mg alloy is in an environment where there is phosphate, it can also form magnesium phosphate, following the reactions: [29, 30]



Mg's greatest asset is its mechanical properties alongside with its low density. It is characterized by a hexagonal close-packed structure and has an elastic modulus similar to the cortical bone, which minimizes stress shielding [31]. It is also weldable, it displays high specific strength, and does not cause artifacts in X-ray, computed tomography and magnetic resonance imaging, making it compatible with those exams [11, 32]. All these characteristics make Mg seem the most suitable and studied element to manufacture bioabsorbable implants.

2.2.2 Hydroxyapatite Coating

Hydroxyapatite is a type of Calcium Phosphate (CaP) ceramics which are crystalline materials capable of inducing a direct connection with the bone, given the fact that it has a similar chemical composition to the mineral phase of bone, which represents about 69% of

its composition. Because of its nature, the relevance of HA have been increasing in tissue engineering, as a bone substitute and to improve materials capabilities, specially the bone-bonding. Moreover, issues related to high temperature-sintering can be excluded given the fact that nanostructured ceramics can be sintered at lower temperatures [33, 34].

It has a complex structure (Figure 2.2), with a density of 3.16 g/cm^3 and its formula is $\text{Ca}_5(\text{PO}_4)_3\text{OH}$ [34, 35]. Its mechanical properties vary a lot depending on many factors, such as the porosity, density, crystal size and impurities [34].

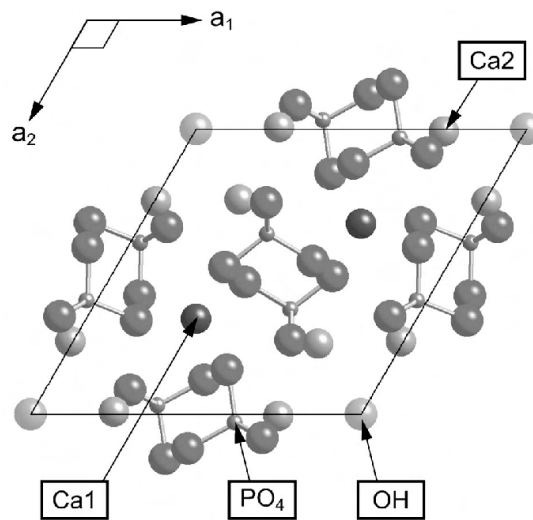


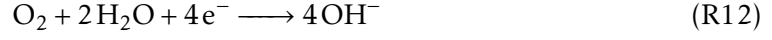
Figure 2.2: Crystal structure of HA
(adapted from [36])

Being one of the most stable and less-soluble Calcium Phosphate ceramics, biocompatible and biodegradable, it is great for orthopedic applications, thanks to its suitable osteointegration, osteoconduction and osteoinduction. In addition, since it is only composed of Ca and phosphate ions, no adverse local or systemic toxicity has been reported. However, given the fact that it has high brittleness and low strength, it is limited to non-load bearing applications. Because of that, HA is usually used only as a coating bioactive material, which is a proven effective method to improve metal's biological properties, allowing a controlled and rapid osseointegration between living bone and the surface of an implant [34, 35, 37, 38].

Furthermore, although the degradation rate of traditional materials do not need to be controlled, when it comes to biodegradable ones like Magnesium, their degradation rate is too high, and so, HA has also the role of reducing that rate [38].

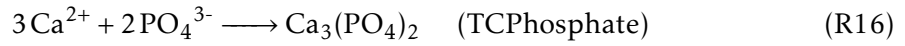
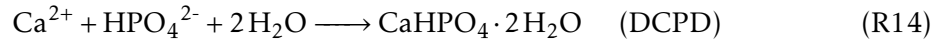
There are various commercial techniques to deposit the HA coating on the metal-based biomaterials, and the chosen for this work was the Electrochemical Deposition or Electrodeposition. In addition, the reagents used were Calcium Nitrate and Ammonium di-Hydrogen Phosphate. In solution, the molecules dissociate resulting in free Ca^{2+} and H_2PO_4^- .

During a electrodeposition using a electrolyte with salts, there are many reactions that may occur at the surface of the cathode (Reactions 5, 9, 10, 12 and 13) [29, 30].



The reduction of water (Reaction 13) leads to the formation of H_2 bubbles near the cathode, along with Reaction 5, prompting an increase of the local pH. By observing Reaction 9 and 10, the increase of OH^- ions can cause the reduction of H_2PO_4^- and HPO_4^{2-} , increasing the concentration of HPO_4^{2-} and PO_4^{3-} , respectfully. [29]

The free Ca^{2+} ions react with the hydrogen phosphate and phosphate ions, forming several CaP phases, such as Dicalcium Phosphate Dihydrate/Brushite (DCPD), Octacalcium Phosphate (OCPhosphate), Tricalcium Phosphate (TCPhosphate) and HA, according to the following Reactions 14, 15, 16 and 17, respectfully: [29]

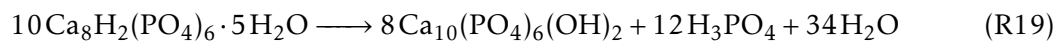
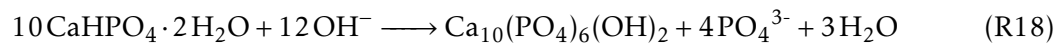


The previous CaPs are precursors of HA. Normally, the as-deposited layers are mainly composed of DCPD, OCPhosphate and HA and during the first moments of the deposition, the formation of DCPD prevails over the HA. There are two reasons that explain this. The first one is related to the absence of OH^- ions in the beginning. As seen in Reactions 9 and 10, there is a necessity of OH^- to form the phosphate ion, needed to the formation of HA. If there is a low concentration of OH^- , the hydrogen phosphate ion will prevail, forming DCPD, according to Reaction 14. Also, there is the direct need of the hydroxyl ion in the Reaction 17 to form HA. The second reason is related to the fact that DCPD is stable at pH lower than 5, condition that exists at the beginning of the process. [29]

According to various work, after an electrodeposition, Brushite is the main constituent of the coating. To transform it into HA, it needs to be immersed in a high pH solution, given that HA is the most stable CaP in alkaline environments. [29, 39–42]

This type of environment provides the sufficient OH^- ions needed for the Reaction 18. What happens is the release of some calcium and phosphate ions from the DCPD coating into the solution, reacting both with the hydroxyl ions, forming HA according to the Reaction 17. Additionally, the post alkaline treatment also meets the thermodynamic

requirements. Likewise, OCPphosphate can also be transformed into HA, according to the Reaction 19. [29]



STATE OF THE ART

This Chapter aims to summarize the history of biomedical implants, their use in orthopaedics and in cardiology, their production, emphasizing WAAM, and the use of Mg and HA. In addition, it provides an overview of the state of the art of WAAM technology and of both biomaterials.

3.1 A Brief History of Biomaterials and WAAM Technology

Biomaterial implants have been around for many years, and have been applied on numerous parts of the body. Throughout the years, three generations of biomaterials have been defined: First Generation, bioinert materials; Second Generation, bioabsorbable or bioactive materials; and Third Generation, involving materials that stimulate specific cellular reactions [43]. These definitions are conceptual, not chronological, because some biomaterials of today can still be categorized as First Generation, for example [44].

In the beginning, the only materials available for implants were the same as for other industrial applications. However, the human body has a very specific environment so not every material sustains there, and some proved to be toxic or pathogenic. This gave way to the First Generation, whose purpose was to have suitable mechanical properties to match the damaged tissue, and to be the least toxic possible [43–45]. With this in mind, stainless steel and cobalt-chrome-based alloys were introduced in orthopaedic applications in the beginning of the 20th century, followed by Titanium (Ti) alloys in 1940, and NiTi alloys in 1960 [44].

By the end of the 20th century, Second Generation biomaterials were introduced, and were characterized as bioactive materials, the ones that strengthen the biological response, and bioresorbable materials, that degrade in the body while the tissue is healing [44]. The application of biomaterials in cardiology happened with the appearance of bare-metal stents in 1987, followed by drug-eluting stents, and later in the 21th century, bioresorbable stents [46–48].

The Third Generation biomaterials are designed to stimulate cell reactions at a molecular level, interacting with cell proliferation, differentiation and organization, and also

to activate genes [44].

First Generation biomaterials were produced by traditional methods, since Additive Manufacturing only started to be studied in the 1960s, and its use with biomaterials only started around 2000 [49].

As mentioned before in Section 2.1, WAAM is a type of Directed Energy Deposition, and DED was patented in 1997 [50]. Apart from that, the WAAM technique, i.e., the process of manufacturing a component from the deposition of weld metal, was first introduced in the 1920s, and is now one of the most significant and promising AM processes [4, 51].

Mg is one of the most used and studied elements to manufacture biomaterials. One of the first clinical reports was in 1878, when Edward C. Huse used Mg wires as bandage for hemorrhagic vessels [52]. However, because of non-absorbable materials like Ti alloys, the interest in these metals eventually declined. With the advancement of technology allowing the production of high purity alloys and bioactive materials, and the necessity of improving bioimplants in the last decades, bioresorbable materials started again to generate a significant interest [9, 16, 52].

Although the era of Hydroxyapatite dates back to the middle of the 20th century, CaPs were used since the end of the 18th. Hydroxyapatite started to be used in regenerative science only as an inert scaffold to correct bone defects, with no interaction with adjacent living tissues. It was only later that HA started to be used as a scaffold that stimulates bone development, being categorized as second generation biomaterial. [34]

3.2 Nowadays

The use of WAAM technology has been increasing, and in the last years some researchers already used it for bioresorbable implants. Still, there are few studies that use WAAM for those purposes, and no *in vivo* studies.

Guo *et al.*, Takagi *et al.*, Holguin *et al.* and Han *et al.* fabricated Mg alloy by means of WAAM. The first three authors investigated the different effects that some parameters have on the mechanical properties and macro and microstructure of the alloy, in a way to improve them. Han *et al.* concluded that a WAAM AZ91D alloy has a higher corrosion resistance than the cast AZ91D because of the $Al_5Mg_{11}Zn_4$ precipitate. All these studies show the versatility of the WAAM technology. Therefore, this method is a potential replacement of traditional manufacture techniques, in some specific cases.

Regarding HA, as it is known to be able to mimic the dimensions of constituents of bone and teeth, there have been some important recent advances. Many studies, including an *in vivo* one, concluded that nanocrystalline HA powder may improve many mechanical properties and fracture toughness because it showed improved densification and sinterability [34]. For the *in vivo* study, Gosain *et al.* used soft tissues sites of adult sheep to investigate the osteoinductive properties of HA biomaterials implanted, and if it is possible to increase it by altering the porosity and the composition. They observed the

occurrence of true osteoinduction within HA-derived biomaterials and concluded that the porosity and bone formation can be enhanced by pairing HA with a fast-resorbing component, as the tricalcium phosphate. [53]

Hing *et al.* studied the influence that microporosity has on early osseointegration and final bone volume on rabbits, within HA bone graft substitutes. They demonstrated that alterations of the microporosity can speed up osseointegration and increase the equilibrium volume of the bone. [54]

Another *in vivo* study by El-Fattah *et al.*, where they made holes in the anteromedial tibial metaphysis of rats, concluded that nano-HA restores materials and enhances the bioactivity of bone implant. They compared three groups of eight rats each: Group 1 with nano-HA, Group 2 with HA and Group 3 with empty bone defects. Group 1 revealed improved biocompatibility and osteointegration of bone graft substitutes, and there was a bigger formation of new reactive bone. Without any application of HA, there was only a partial closure of the hole. [55]

As mentioned earlier, besides increasing the biocompatibility, an HA coating can also improve the corrosion resistance of Magnesium alloys. Song *et al.*, Jamesh *et al.*, Salman *et al.* and Assadian *et al.*, did electrodeposition of HA on Mg alloys in order to enhance its biodegradation performance. The results were consistent among all authors, showing that it is possible to increase the corrosion resistance of the alloys by coating with HA. [39–41, 56]

Regarding only Mg alloys, a small clinical study with bioresorbable materials showed promising results. Herber *et al.* brought together twenty people with the same ankle fractures and treated them with Mg-based ZX00 bioresorbable screws, made only with nutrient elements (0.45 wt% Calcium and 0.45 wt% Zinc). After a year, one person was lost in the follow up, but the other nineteen showed optimal functional outcomes. The screw heads slowly degraded, avoiding complications that usually appear, and no second surgery was necessary. Because this was the first study of this alloying system in human beings, a randomized study was not allowed, and only twenty people participated. However, this study showed very interesting and promising results, showing that bioresorbable materials may be a relevant alternative to use in implants. [31]

MATERIALS AND METHODS

During this work the electrochemical, corrosion and degradation properties of a AZ61A commercial Mg alloy were studied. To do so, a microstructure analysis, *in vitro* degradation evaluation and electrochemical characterization using Cyclic Voltammetry (CV) were made. The samples were also examined by Optical Microscopy, Scanning Electron Microscopy (SEM), X-ray Diffraction (XRD) and Raman Spectroscopy (RS). In addition, an Hydroxyapatite coating was made to cover the alloys using electrochemical deposition, and the same tests were repeated. In the meantime, the alloys were developed with the WAAM technique, proceeding to do the same previous tests.

4.1 Preparation of the Metallic Substrates by WAAM

In this task, WAAM printing of Mg-based alloys was carried out by a colleague in the Mechanic's Department. The goal was to obtain defect-free parts that were subsequently characterized in the next steps. The commercial Mg alloy used for this purpose was AZ61A (92% Magnesium, 5.80%-7.20% Aluminium, 0.40%-1.50% Zinc, 0.15% Manganese, 0.1% Silicon), showed in Figure I.1 in I. To perform the deposition of the layers, a GMAW welding machine, model Pro MIG 501 from KEMPPI (Figure 4.1), and a power source Pro MIG 3200 from same brand were used. The parameter chosen by my colleague are shown in the Table 4.1.

Table 4.1: Parameters' values for the welding process - WFS (Wire Feed Speed, m/min), TS (Travel Speed, mm/min), CTWD (Contact To Work Distance, mm), SGF (Shield Gas Flow/Rate, l/min), ΔV (Voltage Trim)

WFS (m/min)	TS (mm/min)	CTWD (mm)	SGF (l/min)	ΔV
3, 3.5, 4, 5.5	500, 550, 700	12, 14, 17, 19	19	-1, -4, -5

Since the printed substrates were composed of large walls, they needed to be cut, using a precision cutting machine. Also, they were polished with grit paper. The Figure 4.2 shows a finished small wall without any treatment, and the Figure 4.3 shows part of a

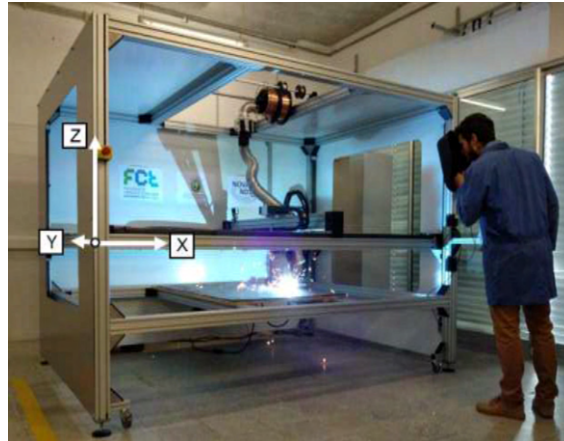


Figure 4.1: Photograph of the GMAW welding machine, model Pro MIG 501 from KEMPPI

(adapted from [4])

treated printed wall and a sliced piece of that wall, used for the study. The Figure I.2 in I shows two examples of the substrates used in this study, the commercial Mg wire and the WAAM printed Mg alloy, side by side.



Figure 4.2: Photograph of a printed wall

(adapted from [4])



Figure 4.3: Photograph of part of a treated printed wall (left) and a sliced piece used for the study (right)

4.2 Preparation of the Buffer Solutions for Simulation of Body Fluids

The first step was to prepare two PBS solutions, to simulate the body fluid, one with a pH around 7.4, and another with 5.5.

4.2.1 PBS Solution with pH 7.4

To prepare this solution, 2 g of NaCl (Sodium Chloride, SIGMA-ALDRICH, $\geq 99.5\%$), 0.05 g of KCl (Potassium Chloride, SIGMA-ALDRICH, 99.5-100.5%), 0.06 g of KH_2PO_4 (Potassium Phosphate Monobasic, SIGMA-ALDRICH, $\geq 99.0\%$) and 0.36 g of Na_2HPO_4 (di-Sodium Hydrogen Phosphate Anhydrous, PanReac AppliChem, $\geq 99.0\%$) were dissolved in water, and then diluted to 500 ml of the same solvent.

4.2.2 PBS Solution with pH 5.5

For this solution two solutions were needed. One with 6.56 g of KH_2PO_4 dissolved in 482 ml of water, and another with 0.64 g of Na_2HPO_4 dissolved in 18 ml of the same solvent. By mixing those solutions, a PBS with a pH 5.5 is formed, with a total volume of 500 ml.

4.3 Degradation Tests

For this phase, an immersion test was made. Its objective was to determine the rate of degradation that the commercial Mg alloy AZ61A has under static simulated body fluids, with a pH of 5.5 and 7.4.

Three Mg wires (approximately 2 cm each) were weighted and added to eight different bottles with 12 ml of PBS solution. Half the bottles had the solution with a pH of 7.4, and the other half had the solution with a pH of 5.5. At the end of 4 months the wires were all weighted again. The first measure was made in 16/05/22, and the last was in 21/09/22.

4.4 Electrochemical Characterization

4.4.1 Cyclic Voltammetry

Used to evaluate the electrochemical behaviour of a electroactive sample immersed in a electrolyte solution, the Cyclic Voltammetry provides information about the redox reactions, electron transfer kinetics and the reaction's reversibility. These information are obtained with the analysis of a cyclic voltammogram. As mentioned before, the solution will be a simulated physiological fluid, a Phosphate-Buffered Saline (PBS) solution.

For this method, usually three electrodes are used: a reference, a working and a counter electrode. The potential of the working electrode is measured in relation to the

reference, and it is scanned back and forth, between two extreme limits, at a constant rate. In the meantime, the current that passes through the working and counter electrodes is recorded, in order to acquire the cyclic voltammogram (current vs. potential). This current is responsible for the oxidation or reduction of the analyte, that are visible in the cyclic voltammogram. The Figure 4.4 represents a schematic of the CV process. [57, 58]

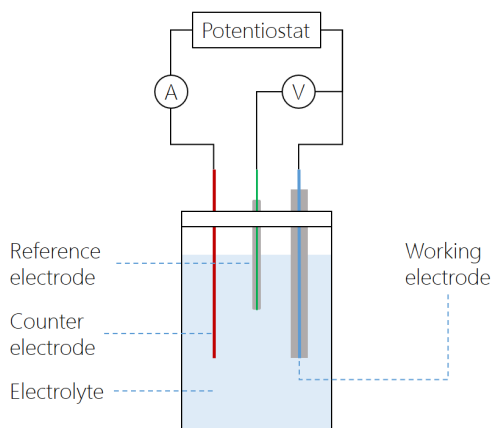


Figure 4.4: Illustration of the Cyclic Voltammetry process
(adapted from [59])

The electrochemical experiments were carried out using a potentiostat *Gamry Instruments - Interface 1010 E*. The metallic structures were immersed in the PBS solutions described in 4.2. A three-electrode configuration was chosen, using the substrates as working electrode (WE), a graphite wire as counter electrode (CE) and Ag/AgCl as reference electrode (RE). To maintain the same distance between electrodes in every characterization, a plastic lid was developed to cover the beaker where the experiment takes place (referred in Section 4.4.2). The Figure 4.5 shows two photographs of the setup used.

The first step was to determine the potential interval where the Magnesium alloy reacts. For that, some experiences were made between -2 V and 2 V, -2 V and 0 V, -3 V and 0 V, for five 5 cycles, with a scan rate of 50 mV/s, with the neutral PBS solution. Since the material behaved like a resistor below -2 V, and above 0 V, and a curve was presented between those intervals, that was the chosen interval. Besides that, at positive potentials a higher formation of precipitate occurred, which may influenced the results. For the acid PBS solution, there was no reaction occurring in that interval, only between -1.5 V and 3 V. The potential was scanned in both directions between -2V and 0 V (pH 7.4) and between -1 V and 3 V (pH 5.5) for 200 cycles with a scan rate of 200 mV/s and 450 mV/s, respectfully, at room temperature. Since the layer formed around the alloy, the increase in pH and the saturation of the solution could influence the results, a different test was made. Every 50 cycles the solution was changed and the alloy rinsed with water,

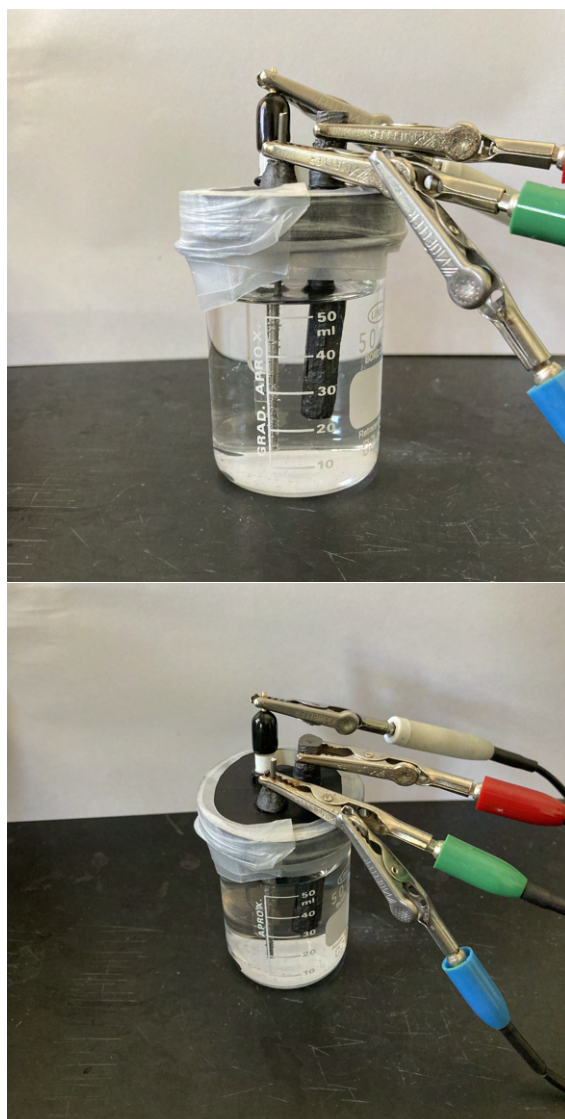


Figure 4.5: Photographs of the setup used for the Cyclic Voltammetry experiment. Red electrode - counter electrode (Graphite); Green and Blue electrode - working electrode (Mg alloy); White electrode - reference electrode (Ag/AgCl)

until cycle 200. It was important to maintain the same length of material immersed in every experiment, as well the same quantity of solution, to be able to compare the results between experiments. For this, it was always used the same beaker filled with 50 ml of PBS solution. The length of the material immersed was around 3 cm.

4.4.2 Development of the plastic lid

Using Autocad, a plastic lid was produced with three holes, separated by 5 mm from each other, and their centers were 1.4 cm apart. The diameter of the lid chosen was 5 cm. The 3D printer used to produce the lid was an Ender-5. This cap aimed to keep the electrodes always at the same distance during all the experiments, so that there could be

a direct comparison between them. Figures 4.6 and 4.7 represent the lid in a STL project and in a photograph, respectfully.

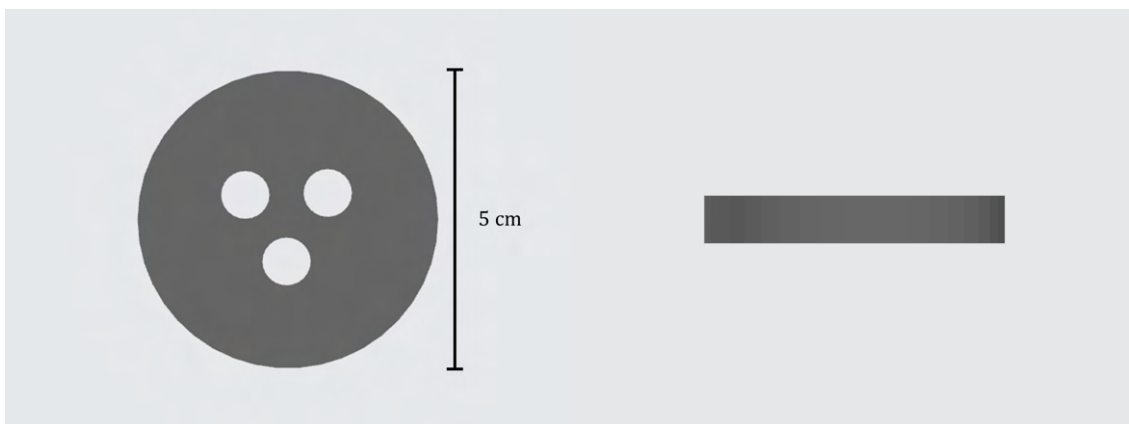


Figure 4.6: STL project of the plastic lid

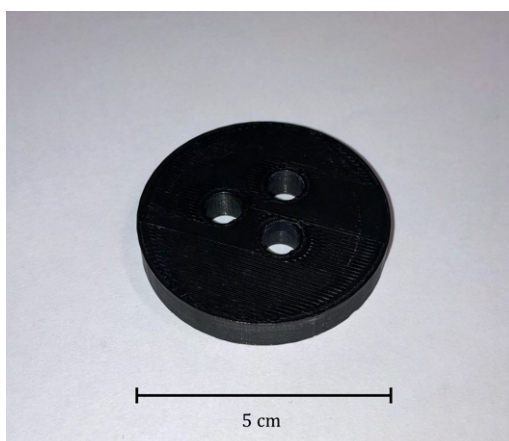


Figure 4.7: Photograph of the plastic lid

4.5 Electrodeposition of Hydroxyapatite

In order to increase the biocompatibility and corrosion resistance of the substrates, a coating of HA was made using the Electrochemical Deposition method. Being very simple and with a low cost associated, this method usually uses two electrode cells, one cathode and one anode. The activation of an electric field charges particles in a stable colloidal suspension, making them move through the electrolyte, lodging in one of the electrodes, creating a homogeneous coating on it. [60, 61]

The protocol followed was based on several articles [39–42]. A voltage source was used, with graphite as the counter electrode (anode) and the Magnesium alloy as the working electrode (cathode). For the positioning of the electrodes it was used the plastic lid mentioned in 4.4.2. The setup is presented in Figure 4.9.

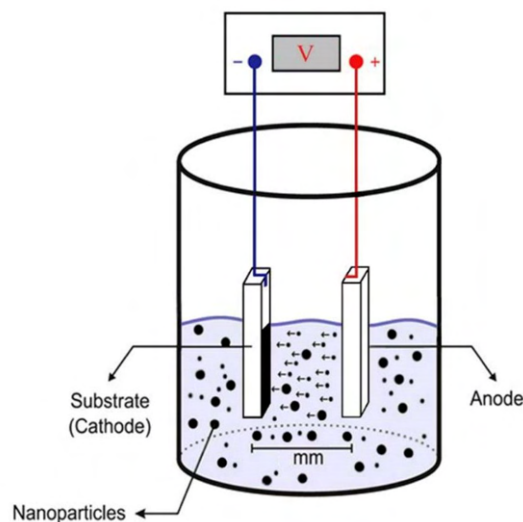


Figure 4.8: Illustration of the Electrochemical Deposition process
(adapted from [62])



Figure 4.9: Photograph of the setup used for the electrodeposition method. Red electrode - anode (Graphite); Black electrode - cathode (Mg alloy)

The first tests were carried out using the commercial Magnesium alloy. The coating solution was 0.1 M $\text{Ca}(\text{NO}_3)_2 \cdot 4\text{H}_2\text{O}$ (Calcium Nitrate 4-hydrate, PanReac AppliChem, 99.0-103.0%), 0.06 M of $\text{NH}_4\text{H}_2\text{PO}_4$ (Ammonium di-Hydrogen Phosphate, PanReac AppliChem, $\geq 99.0\%$) and 30% (v/v) ethanol. The solution was mixed in a stirrer at 500 rpm for 5 minutes, and before the electrodeposition an ultrasound needle was used for 1 minute to fully homogenize it. The electrodeposition was carried out at a stable potential of 3 V, 3.5 V, 4 V, 5 V and 6 V for 30, 60, 90 and 120 minutes, and 24 hours, at room temperature. After the deposition, the substrate was immersed in a solution of 1M NaOH for 2 hours at 80° C.

Cyclic Voltammetry, following the same parameters described in 4.4.1 was used to test the degradation and corrosion of the substrate after the coating.

After all the tests with the commercial alloy, the best parameters for the coating were determined, and tried out on the material printed by WAAM.

4.6 Analysis and Characterization

To analyse the substrates, before and after the corrosion and the coating, and other substances, Optical Microscopy (Leica DMI8), Raman Spectroscopy, SEM and XRD were used.

4.6.1 Chemical Characterization with Raman Spectroscopy

Widely used for tissue characterisation, this optical and vibrational spectroscopic technique is based on the Raman effect, which states that when a light (wavelength 750-850 nm) is incident on a tissue, its molecules will reflect the light with a distinct wavelength. With this new wavelength, characteristic for many chemical components, is it possible to detect the molecular composition and molecular structure of the tissue. [63, 64]

For the chemical characterization of the samples and other substances, a Micro Raman Witec Alpha 300RAS equipped with a 532 nm wavelength laser was used.

4.6.2 Morphological and Structural Characterization with SEM and XRD

4.6.2.1 SEM

SEM is a valuable approach for the analysis of surfaces that are in a vacuum. It is a morphological analysis, providing highly detailed images, and it is widely used for identification of contaminants and for defect characterization. For this technique to work, the surface needs to be conductive, so generally a thin layer of gold is sputtered on the surface. The electron beam scans the surface, interacting with the material, leading to the emission of photons and electrons. These particles are collected by a specialized detector that provides information about the surface. After the beam sweeps all the surface, an image of the sample is produced. [65–67]

The equipment used for the SEM analysis was a Hitachi SU3800.

4.6.2.2 XRD

XRD it's used to describe the crystalline structure of a sample, providing no information about the chemical nature. It is a nondestructive technique and it provides data on structures, crystal orientation and defects, phases, average grain size, for example. It can be conducted at room temperature and pressure.

In this technique, a monochromatic beam of X-rays is scattered in every plane of the substrate at certain angles, producing the XRD peaks. The atomic positions within the

planes determine the peak intensities, and so the XDR pattern is characterized by the periodic atomic arrangements of the material. [67, 68]

The equipment used was the PANalytical's X'Pert PRO MRD X-ray diffractometer, with a monochromatic Cu $K\alpha$ radiation source with wavelength 1.540598 Å. XRD measurements were carried out from 10° to 90° (2θ), with a scanning step size of 0.016°.

RESULTS AND DISCUSSION

This chapter will present the results of this work and their discussion. Its beginning was based on the commercial Mg alloy, first by studying its electrochemical activity and respective corrosion through cyclic voltammetry tests, using acid and neutral PBS solutions, followed by a deposition of HA by electrodeposition. In the meantime, mass variation tests were also carried out to study the degradation of the material *in vitro*, in both environments as well. Only after knowing these characteristics did the study turn to the material printed by WAAM. As already mentioned, the samples were printed by a colleague from Mechanical Engineering using GMAW, and required some treatment in order to be used for the project. The substrates, precipitates and other substances were analysed by Optical Microscope, SEM, XRD and RS in order to draw all possible conclusions.

5.1 Electrochemical and Corrosion Experiments

The electrochemical reactions of the alloy were studied in both environments by using the Cyclic Voltammetry technique. In addition, before and after every experiment the substrates were weighted in order to study the degradation of the material. Both experiences are of great importance since this work is inserted in the subject of biomedical implants. That is, it is always necessary to know which reactions may occur in the material inside the human body, and its degradation rate. Lastly, SEM was used to study the morphology and corrosion of the material after a CV experiment.

5.1.1 CV with Neutral PBS Solution on Commercial AZ61A alloys

The first results to analyse regarding the Cyclic Voltammetry are the differences between changing the solution and cleaning the alloy, or don't. As mentioned in 4.4.1, in order to verify if the saturation of the solution, the protective layer of the alloy and the increase in pH changed the results, two experiments were compared: one where the solution was changed every 50 cycles until the cycle 200 and the substrate was rinsed

(referred as 50x4) , and another where the experiment was left to run until 200 cycles, without changing anything (referred as 200).

The Figures 5.1 and 5.2 are associated to the 200 consecutive cycles, and to the 50x4 cycles, respectfully. In the latter, at the moment the solution is altered and the alloy rinsed (after Cycle 51), it is possible to notice a broadening of the curve (Cycle 53), indicating a more effective reaction. If left unchanged like in the first graph (Figure 5.1), the curve tends more rapidly towards a line, indicating that the material is behaving as a resistor.

These results may indicate that the corrosion was bigger for the 50x4 experiment. This may have occurred because when the solution was changed and the alloy rinsed, part of the protective layer detached. Also, the formation of the corrosion products may make the solution saturated and with a higher pH, influencing the corrosion of the material, decreasing it, because the protective layer is less soluble in more alkaline environments. To check if there really exists a pH increase after the experiment, it was measured giving a value of 11.5.

However, in order to maintain the same parameters between all the experiments to be able to compare the results, only the method with 200 consecutive cycles was chosen.

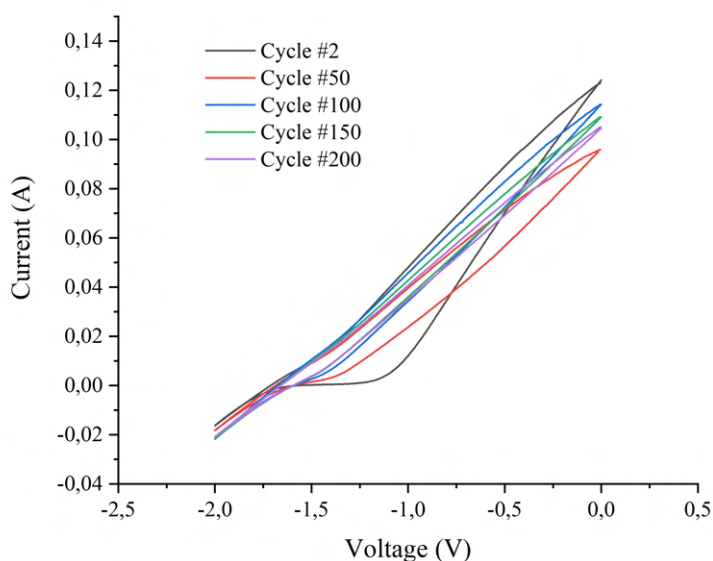


Figure 5.1: CV of the Mg alloy with 200 consecutive cycles (Scan Rate of 200 mV/s) with a pH of 7.4

It was expected that as the experiment progressed, the current would decrease as the alloy corroded, which could be interpreted as a loss of mass. However, this was not always the case. In Figure 5.1 we observe that between the Cycle 50 and 100 there is an increase in current, which would indicate an increase of mass. One justification for this is the detachment of the protective layer of corrosion products. As the layer forms, it protects the alloy, limiting its surface area with the environment, slowing down the reaction and

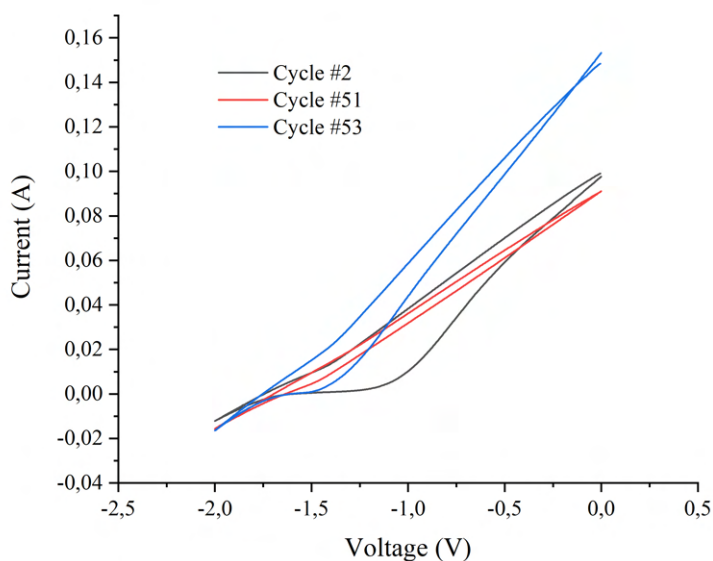


Figure 5.2: CV of the Mg alloy with 50x4 cycles (Scan Rate of 200 mV/s), with a pH of 7.4 (the change of the solution was made at the end of the cycle 51, and cycle 53 is the first stabilised cycle with the new solution)

decreasing the current. When the layer detaches (due to the production of bubbles) or dissolves, the surface area in contact with the PBS solution increases, increasing the current. In the 50x4 experiment, where the solution is changed and the alloy rinsed, this can be verified. By cleaning the corrosion products of the alloy at the end of the Cycle 51, there is an increase of the current at Cycle 53. In this case the new current even goes beyond the first one (Cycle 2). This may be because the alloy is clean and almost free of impurities caused by early air, or because of a slight different setup, mainly in the distance between the electrodes.

Another fact possible to observe is that there is only one reduction peak, which it is possibly related to the cathodic reaction mentioned in 2.2.1 (Reaction 5). This peak starts to open between -1.65V and -1.55V, and below that value, the current changes to negative.

By measuring the potential difference between the reference and working electrode, using a voltmeter, a potential of -1.54V was obtained, which corresponds to the corrosion potential (E_{corr}) or Open-Circuit Potential (OCP). This value is in line with the work of Cain (2014), which mentions that the E_{corr} (vs. Saturated Calomel Reference Electrode, SCE) of the Mg alloy AZ61 measured in quiescent 0.1 M NaCl, is around -1.57 V [69]. This potential is defined as the potential where the anodic (loss of electrons) and cathodic (gain of electrons) reaction rates meet, and so at that point there is no reaction taking place. This was visible during the process because when the current was zero, there were no hydrogen bubbles observed.

5.1.2 CV with Acid PBS Solution on Commercial AZ61A alloys

For the experiment with the acidic environment, the curve is different. The reaction that occurs is in the positive values, and the interval is much larger. Unlike the previous case, in this one the current always decreases throughout the experiment. This may be because, as there is greater dissolution of the reaction products in an acid environment, there is not such a large accumulation, and in turn, the detachment that occurred does not happen, making the decrease in current more linear. This is visible in the graph in Figure 5.3. In this case, the pH of the environment after an experiment was around 6.5, meaning that there is a much bigger increase in neutral pH than in acid. The higher dissolution was also visible during the experiment, because there were almost no precipitate formed, when comparing with the neutral pH (Figure 5.4, the photograph on top corresponds to the acid experiment, and the bottom one to the neutral).

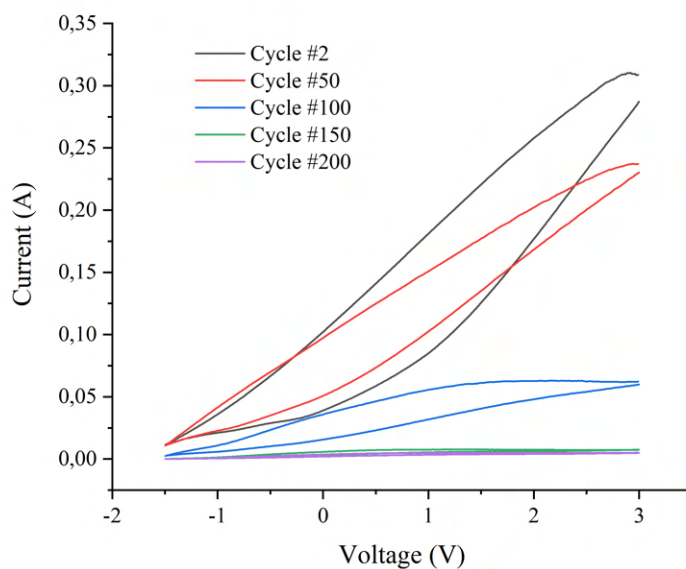


Figure 5.3: CV of the Mg alloy with 200 cycles (Scan Rate of 450 mV/s), with a pH of 5.5

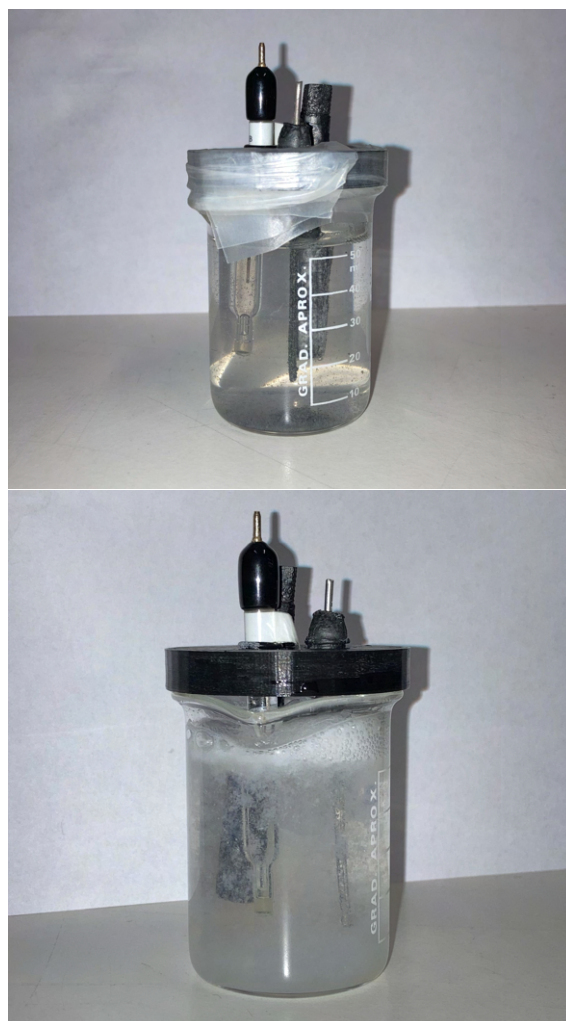


Figure 5.4: Photographs of the setup after a CV with the acid (top) and the neutral pH (bottom)

Again, the saturation of the solution, the increased pH and the formation of the protective layer could influence the results, but there were no experiments made where the solution was changed and the alloy rinsed. Although in the beginning the reaction is more effusive when comparing with the neutral PBS solution, during the last cycles the current is almost zero because the alloy is all covered with the corrosion products that cannot dissolve or detach because of the saturation of the solution, the increased pH and the increased roughness of the material. Furthermore, there can be a difference between the corrosion products from the acid PBS solution and the neutral, which can result in a different adhesion that they have with the material.

There are no explicit reactions in this case. However, these results are not conclusive due to the lack of reproducibility of the electrochemical assays. There may have been a problem with the device as the results varied greatly from experiment to experiment. The data presented here are those which appeared more often in the various trials.

5.1.3 CV on WAAM printed AZ61A alloys

After the tests made with the commercial alloy, the WAAM printed Mg parts were tested. As expected, the reactions were the same yet, since the substrates were much bigger, the current was also bigger. Figure I.2 in I shows a photograph of the printed WAAM substrate and the commercial wire side by side, in order to compare sizes. The CV of the printed substrates in a neutral and acid environment are presented in Figures 5.5 and 5.6, respectfully.

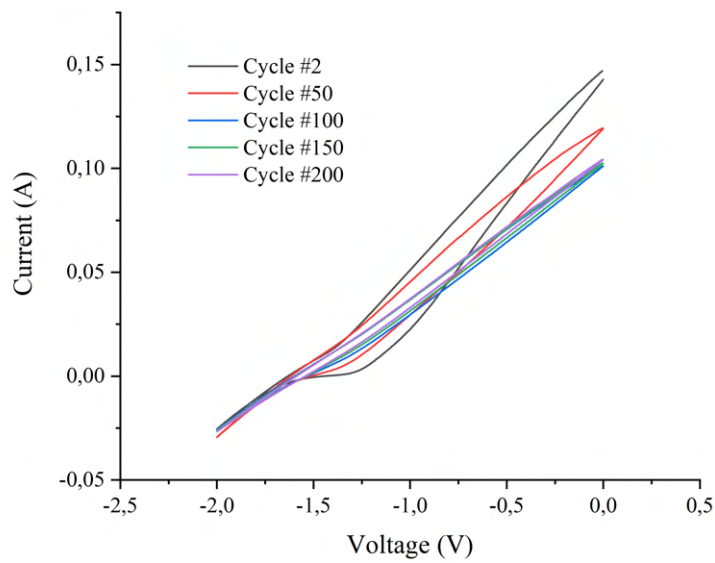


Figure 5.5: CV of the WAAM printed Mg alloy with 200 cycles (Scan Rate of 200 mV/s), with a pH of 7.4

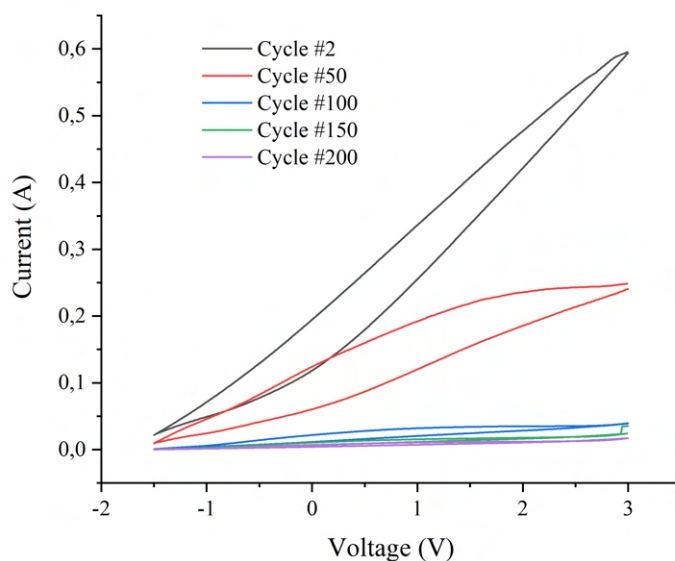


Figure 5.6: CV of the WAAM printed Mg alloy with 200 cycles (Scan Rate of 450 mV/s), with a pH of 5.5

5.1.4 Mass Variation and Corrosion

The first aspect to take into account for a degradation measurement was the loss of mass. Before and after each CV experiment the alloy was weighted, to obtain the percentage of mass that was lost. However, since after every experiment, with acid or neutral pH, the alloy was covered with the corrosion products, the result obtained would never be the real one. The final weight would always be higher than the supposed one. Sometimes the final weight even surpassed the initial. Using ultrasounds and water, a little part of the corrosion layer detached, but the majority was still there. This was also verified by Schille *et al.* They immersed each alloy in a static PBS solution, and measured the weight every hour, and compared it to a situation where blood was used under dynamic conditions. They concluded that under static conditions and with the PBS solution, the Mg alloys revealed weight gain, due to the formation of a corrosion products layer that was insoluble, which could be, magnesium oxide, hydroxide and magnesium phosphate. These corrosion products were also confirmed by Cabeza *et al* [28]. In contrast, in the experiment where blood was used under dynamic conditions, only weight loss was registered, meaning that "it is difficult to evaluate the corrosion behaviour of Magnesium alloys using just standard tests in simply composed simulated body fluids"[70]. Despite this issue, due to lack of time, this work was continued using PBS solution under static conditions.

The Table 5.1 shows the ratio between the final mass and the initial mass of the Mg commercial alloy for the experiment where the solution was changed (50x4) and not

changed (200). From what was mentioned before, it was expected that the mass lost in the CV experiment with 50x4 cycles, would be bigger than for 200 consecutive cycles. Although it is not substantial, there is a difference of 4% which may indicate a bigger degradation for the 50x4 experiment.

Table 5.1: Mass variation (ratio of the final/initial mass) of the Mg commercial alloys after a Cyclic Voltammetry experiment in neutral PBS solution, for 200 cycles and 50x4 cycles

	200	50x4
Ratio	0.92 ± 0.02	0.88 ± 0.02

Theoretically, the mass lost in an acid solution is bigger than in a neutral one. Table 5.2 shows the ratio between the final mass and the initial mass of the Mg WAAM printed alloy, in a neutral and acid solution. Although there is a slight tendency for the substrates tested in acid solution to lose more mass, it is not possible to conclude in which environment the alloy degrades more, because the differences are very small. Again, the ratios calculated for both pHs are not the real ones, because of the layer of corrosion products.

Table 5.2: Mass variation (ratio of the final/initial mass) of the Mg WAAM printed alloys after a Cyclic Voltammetry experiment in neutral and acid PBS solutions, for 200 cycles

pH	Ratio
7.4	0.98 ± 0.01
5.5	0.96 ± 0.01

The Figure 5.7 presents a photograph and a microscopic image of the WAAM commercial alloy before the experiment, the Figure 5.8 shows after the experiment with pH 7.4 and Figure 5.9 with pH 5.5.

Macroscopically, the difference between the three is clear. Logically, after any test the alloy is more corroded and with some corrosion products stuck to it. Between pH 7.4 and 5.5 it is noticeable that in an acid environment the alloy corrodes more, which is borne out by other work. This happens because, like it was mentioned before, part of the protective layer composed with $MgOH_2$ formed during the experiment, is more soluble in acidic environments therefore, it does not protect as much [23, 24]. This indicates that Mg endures less in acidic environments, i.e., in a local where can be an infection.

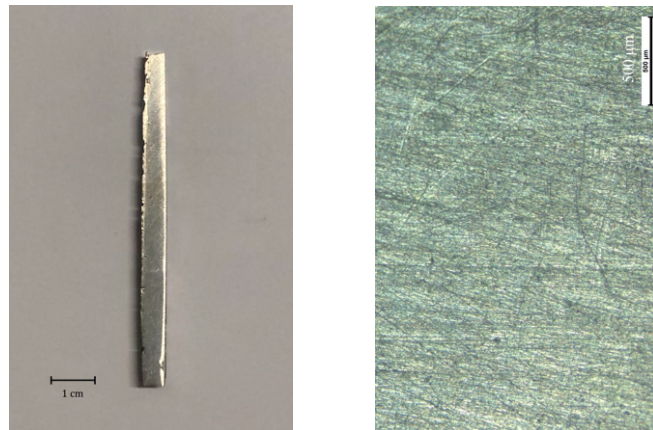


Figure 5.7: Photograph and microscopic image of the WAAM printed Mg commercial alloy AZ61A

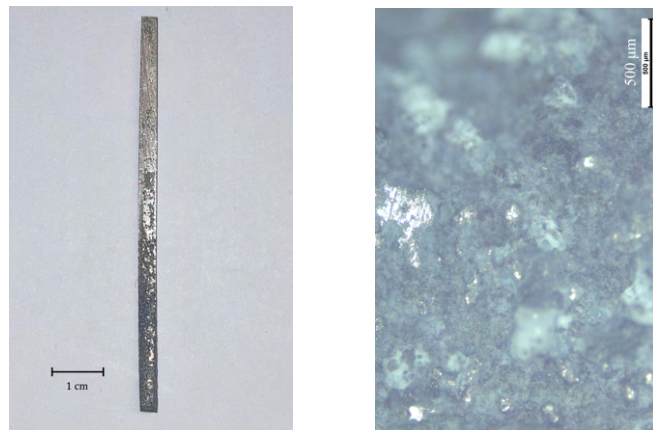


Figure 5.8: Photograph and microscopic image of the WAAM printed Mg commercial alloy AZ61A after a CV experiment with neutral PBS solution

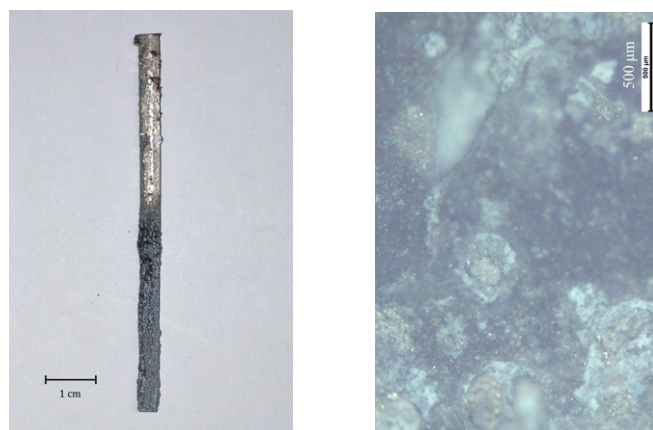


Figure 5.9: Photograph and microscopic image of the WAAM printed Mg commercial alloy AZ61A after a CV experiment with acid PBS solution

5.2 Degradation Tests

In order to determine the degradation rate of the commercial Mg AZ61A alloy a immersion test was made, where 16 samples were immersed in PBS solutions (8 in a neutral solution and 8 a acid solution). The results of the mass variation are exposed in the Table 5.3.

Table 5.3: Mass variation (ratio of the final/initial mass) of the AZ61A Mg alloys after immersion tests in neutral and acid PBS solutions

pH	Ratio
7.4	0.99 ± 0.01
5.5	1.01 ± 0.02

From this experiment it is impossible to conclude anything because of the layer formed by the corrosion products. Just as it happened with the CV experiments in 5.1.4, specially for the experiments in acid environment, the final mass of the alloy does not correspond to the real one. In this case, for the acid PBS solution, the majority of the final mass even surpassed the initial, which is impossible given the fact that the metal is corroding and losing mass. Again, theoretically, the mass loss should be higher in a acid PBS solution, but because of the saturation of the solution, the increase of the pH, and the increase of the roughness can lead to an increase in the adhesion capacity of corrosion products. Also, just as mentioned before, the corrosion products can be different from acid to neutral PBS solution, which can differ in the adhesion that they have with the material. These results corroborate again the work of Schille *et al.*, where in a experiment with blood under dynamic conditions, there was only loss in mass, in contrast with PBS solution under static conditions, that led to a gain of mass.

5.3 Hydroxyapatite Coating

HA is primarily intended to increase biocompatibility and cell adhesion however, when a coating of HA is made on an Mg alloy, it also has the function of increasing its corrosion resistance. This last aspect will be discussed in this work. Initially, the potentials defined were 2 V, 3 V, 3.5 V, 4 V, 4.5 V, 5 V and 6 V. Nevertheless, when a tension of 2 V was tried, the current measured by the voltage source was negative, which resulted in no deposition. As was done with the Cyclic Voltammetry, the OCP was measured, giving a value that varied from 1.85 V to 2.95 V. This value corresponded always to the minimum voltage that results in a positive current measured by the source. With this, the minimum voltage chosen for the electrodepositions was 3 V.

The Table I.2 in I shows the depositions macro and microscopically. Macroscopically is just to have an idea of how does the alloy look after the coating of HA. It is clear

that the bottom half of the three alloys are with a white layer, corresponding to the HA. Microscopically, it is possible to see that there are three homogeneous depositions.

5.3.1 SEM Results

Firstly, Figure 5.10 represents a SEM image of the commercial wire without any deposition, in order to compare with the following depositions.

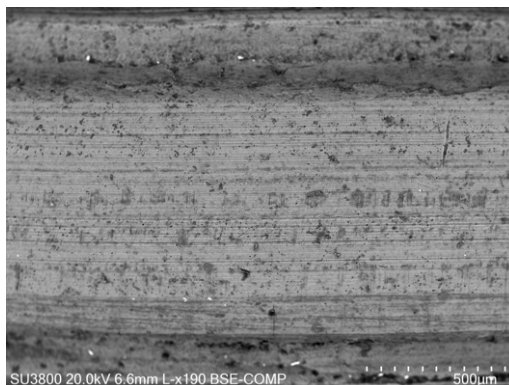


Figure 5.10: SEM of the commercial Mg wire AZ61A

The Figures 5.11, 5.12, 5.13 and 5.14 show the difference between 30, 60, 90, 120 minutes, at 3 V, respectfully. By observing the images, it is noticeable that the higher the deposition time, the thicker the HA layer appears to be. With 30 minutes there was greater deposition in the alloy flaws (red arrow), which was not accompanied in the remaining space. With 60 minutes, the deposition was greater and more homogeneous, however it is only with 90 minutes that a more noticeable layer is deposited. In all of these durations, the flakes vary from plate-shape and needle-shape. With 120 minutes, the layer appears to be even thicker, and the flakes have a different predominant form, which is rod-like. To check if more time is really equivalent to more homogeneous and thicker deposition, an electrodeposition was made with 24 hours. The Figure 5.15 shows what appears to be the thickest and most homogeneous deposition, comparing to the previous ones, with a predominant needle-shaped flakes.

The depositions with less than 90 minutes show less filling and are less homogeneous. With this, a time of 120 minutes was chosen to compare the effect of different voltages.

Figures 5.16, 5.17, 5.18 and 5.19 and 5.20 show the depositions with 3.5 V, 4 V, 4.5 V, 5 V and 6 V, in 120 minutes depositions, respectfully. It is evident that depositions with potentials higher than 4 V show a less homogeneous coating. This can be because of the hydrogen bubbles formation, that is a characteristic feature of Magnesium alloys. The effect of the H_2 bubbles is visible when comparing the depositions with 3 V and 6 V, before the NaOH immersion, in Figure 5.21 and 5.22. It is clear the huge amount of holes (red arrows) in the deposition with 6 V, due to the production of the gas. After immersion, the hydrogen holes are not so noticeable, but they lead to the formation of clusters (red

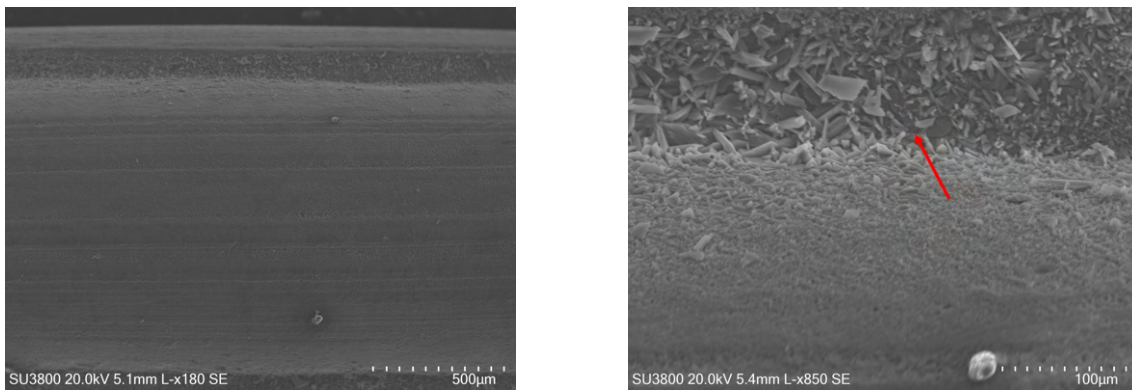


Figure 5.11: SEM of a deposition of 3 V for 30 minutes after the immersion in NaOH. The red arrow points to the flaw of the substrate where the deposition is more noticeable

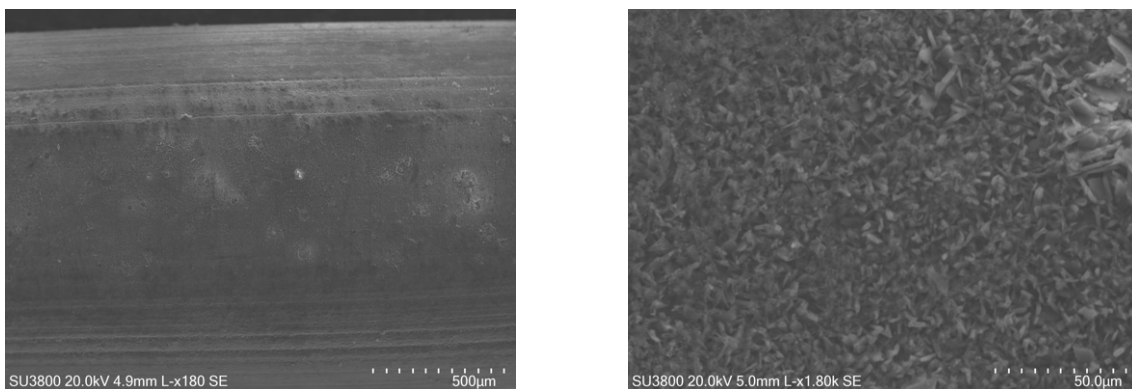


Figure 5.12: SEM of a deposition of 3 V for 60 minutes after the immersion in NaOH

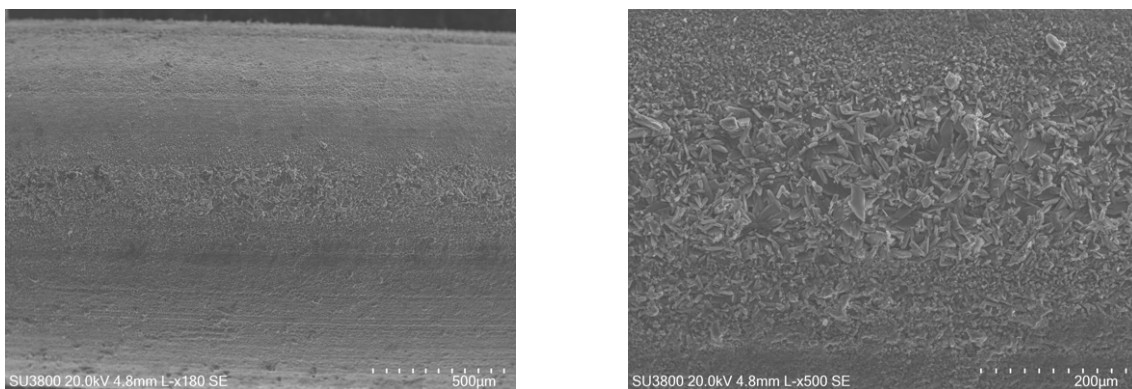


Figure 5.13: SEM of a deposition of 3 V for 90 minutes after the immersion in NaOH

arrows). This is very clear specially with 4.5 V, 5 V and 6 V, where the holes from the H₂ bubbles form clusters, which may be less bound to the alloy, coming out more easily, as it is mentioned in other work [42].

With this, depositions with what seemed the best parameters (3 V, 3.5 V and 4 V, for 2 hours) were made in the WAAM printed Mg alloys. The Figure 5.23 shows the alloy

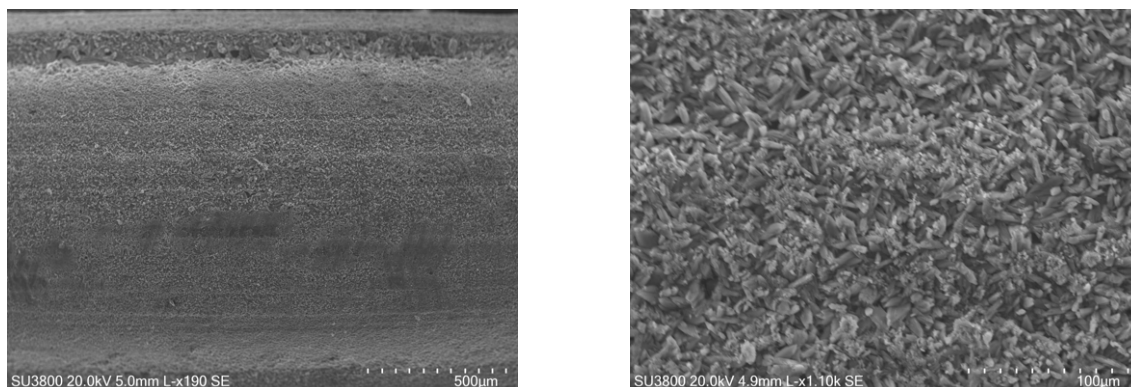


Figure 5.14: SEM of a deposition of 3 V for 2h after the immersion in NaOH

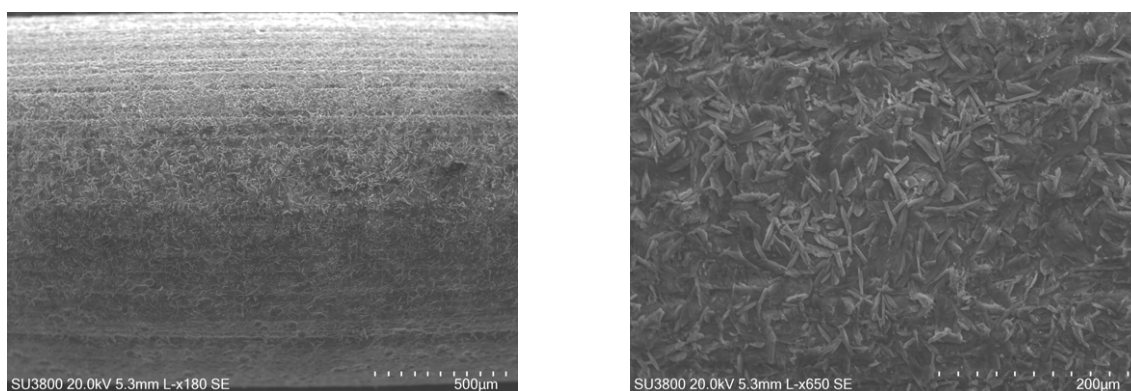


Figure 5.15: SEM of a deposition of 3 V for 24 hours after the immersion in NaOH

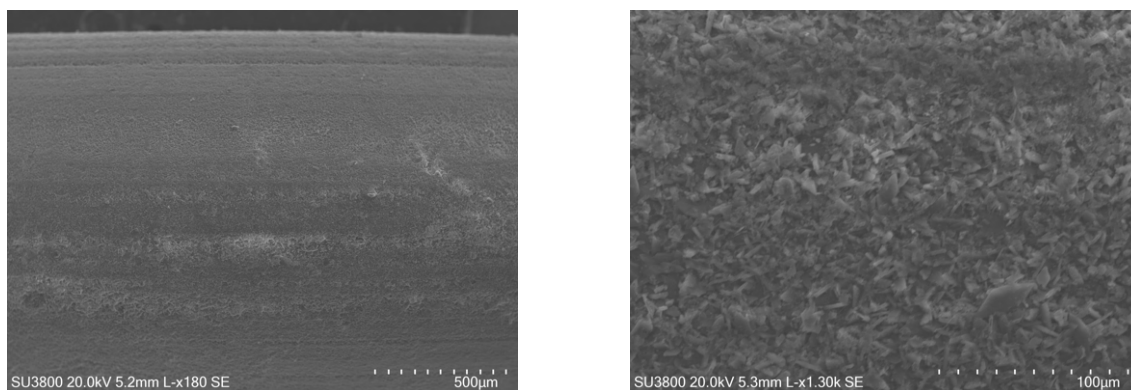


Figure 5.16: SEM of a deposition of 3.5 V for 2h after the immersion in NaOH

without any deposition, and the following show after the deposition with 3 V, 3.5 V and 4 V, with 2 hours (Figure 5.24, 5.25 and 5.26, respectfully). Although they all seem good depositions, it is visible that the 4 V shows shows a slightly less homogeneous coating, with at least a cluster formed by the bubbles (red arrow), indicating that lower voltages may present better results.

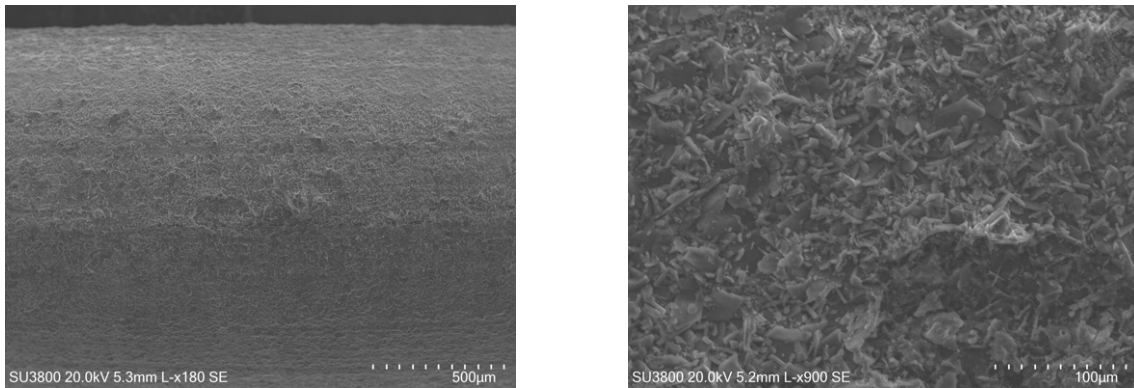


Figure 5.17: SEM of a deposition of 4 V for 2h after the immersion in NaOH

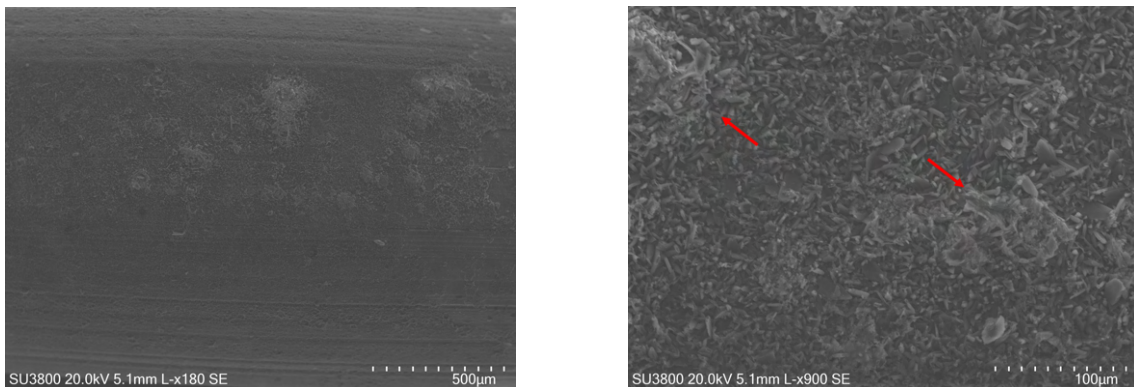


Figure 5.18: SEM of a deposition of 4.5 V for 2h after the immersion in NaOH. The red arrows point to two zones where there are clusters, formed by the Hydrogen bubbles

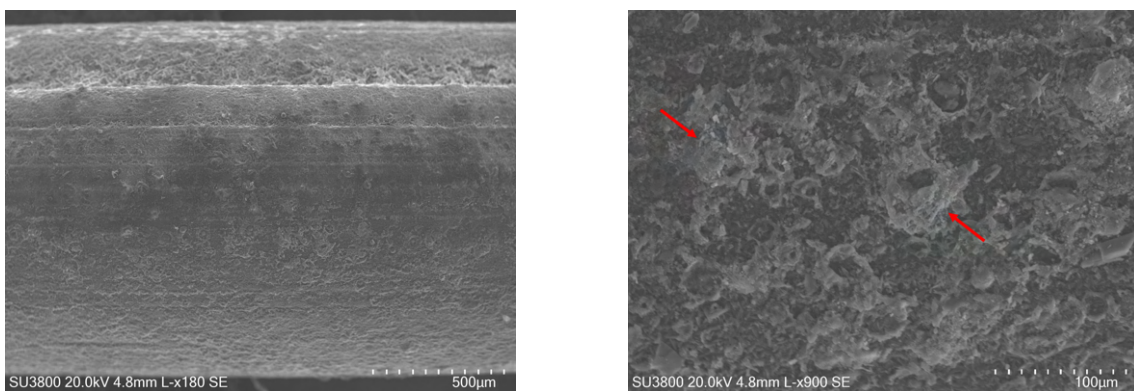


Figure 5.19: SEM of a deposition of 5 V for 2h after the immersion in NaOH. The red arrows point to two zones where there are clusters, formed by the Hydrogen bubbles

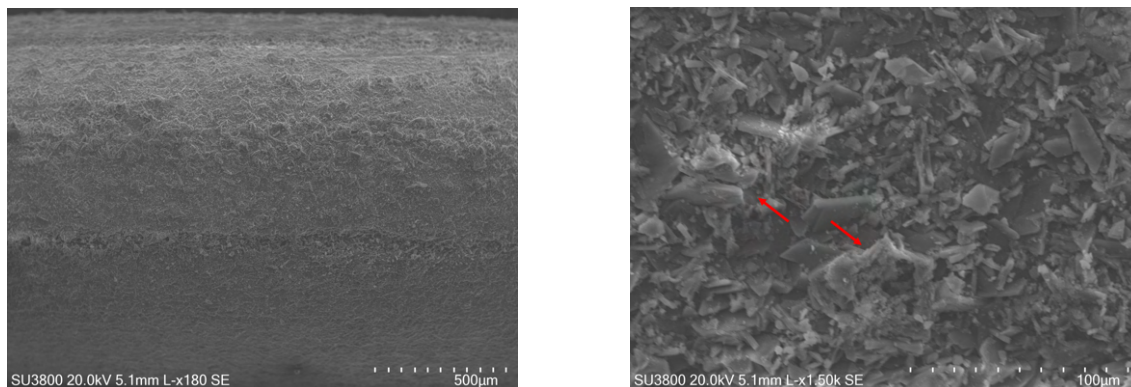


Figure 5.20: SEM of a deposition of 6 V for 2h after the immersion in NaOH. The red arrows point to two zones where there are clusters, formed by the Hydrogen bubbles

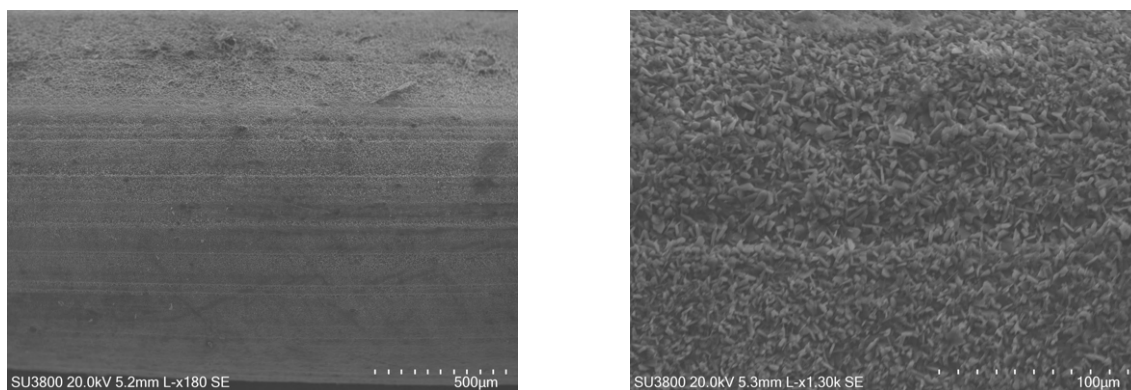


Figure 5.21: SEM of a deposition of 3 V for 2h before the immersion in NaOH

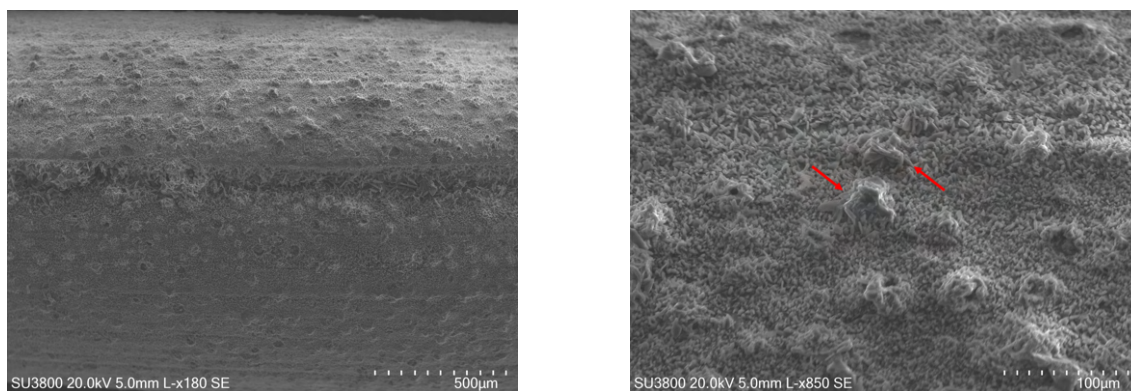


Figure 5.22: SEM of a deposition of 6 V for 2h before the immersion in NaOH. The red arrows point to two zones where there are clusters, formed by the Hydrogen bubbles

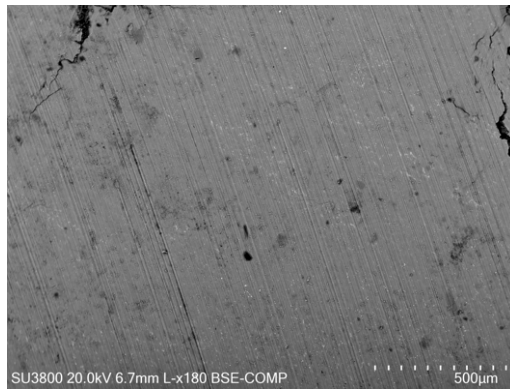


Figure 5.23: SEM of the WAAM printed Mg alloy AZ61A

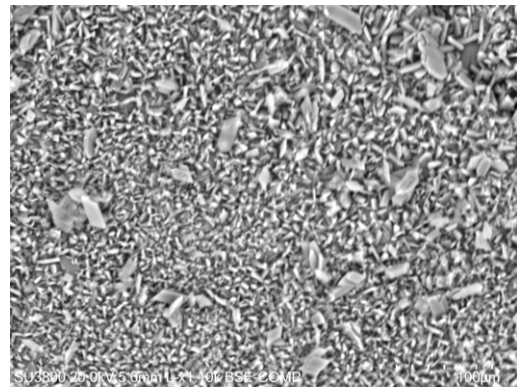
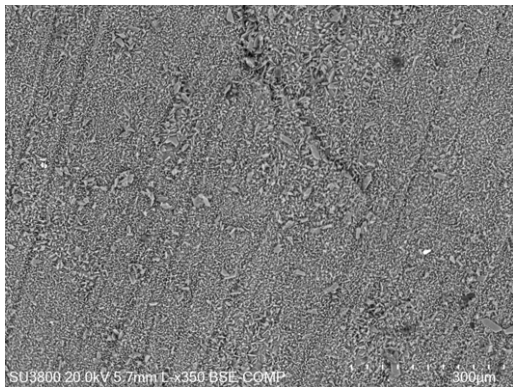


Figure 5.24: SEM of a deposition of 3 V for 2h after the immersion in NaOH in a WAAM printed AZ61A alloy

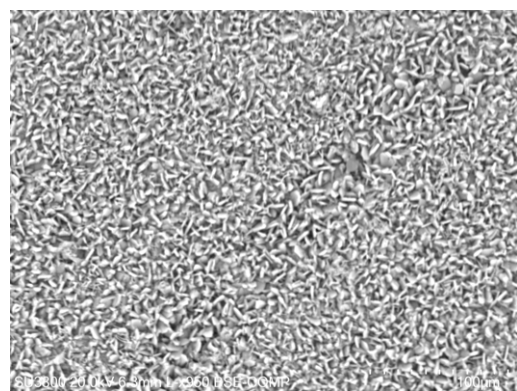
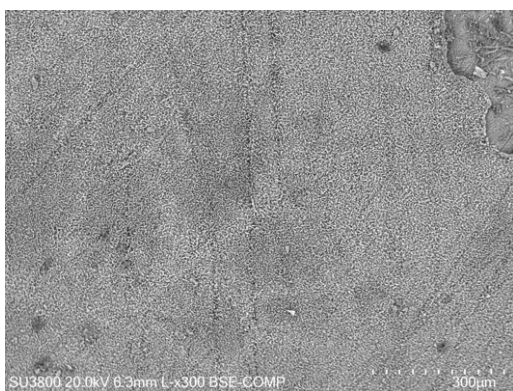


Figure 5.25: SEM of a deposition of 3.5 V for 2h after the immersion in NaOH in a WAAM printed AZ61A alloy

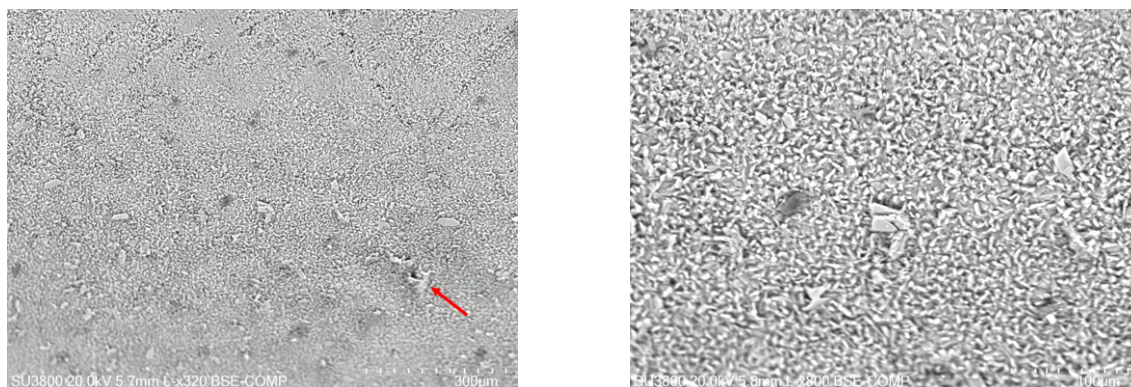


Figure 5.26: SEM of a deposition of 4 V for 2h after the immersion in NaOH in a WAAM printed AZ61A alloy. The red arrow points to one zone where there is a cluster, formed by the Hydrogen bubbles

5.3.2 Raman Spectroscopy Analysis

According to the literature, Brushite is a precedent of Hydroxyapatite, and the main characteristic peaks are: $985\text{-}988\text{ cm}^{-1}$ band due to the PO_4^{3-} ion (ν_1) (P-O symmetrical stretching), and the $872\text{-}879\text{ cm}^{-1}$ due to the HPO_4^{2-} ion (P-OH symmetrical stretching). Other peaks are: $411\text{-}415\text{ cm}^{-1}$ due to the PO_4^{3-} (ν_2) (O-P-O bending), $519\text{-}535\text{ cm}^{-1}$ due to the HPO_4^{2-} (ν_4) (P-OH bending), and a double peak at $1055\text{-}1063\text{ cm}^{-1}$ and $1079\text{-}1086\text{ cm}^{-1}$ due to the PO_4^{3-} (ν_3) (P-O anti-symmetrical stretching). The intervals correspond to the maximum and minimum found in the several articles, depending on the methodologies, like the laser used [71–76].

The Raman Spectroscopy of a deposition with 3 V and a duration of 2 hours before the alkaline treatment (Figure 5.27) indicated that after the electrodeposition the as-deposited coating has as main product DCPD, which is coincident with some articles [39–42].

To convert DCPD to HA, it needs to be immersed in a NaOH solution. HA has many characteristic peaks. The most significant are the ones that correspond to the $(\text{PO}_4)^{3-}$ ion (ν_2) (O-P-O bending) at $423\text{-}447\text{ cm}^{-1}$, $(\text{PO}_4)^{3-}$ ion (ν_4) (O-P-O bending) at $574\text{-}585\text{ cm}^{-1}$, $(\text{PO}_4)^{3-}$ ion (ν_1) (P-O symmetrical stretching) between $950\text{-}965\text{ cm}^{-1}$, $(\text{PO}_4)^{3-}$ ion (ν_3) (P-O anti-symmetrical stretching) between $1030\text{-}1045\text{ cm}^{-1}$. Just like before, the intervals correspond to the maximum and minimum found in the several articles [77–83]. To check these values, an RS of the HA commercial powder (SIGMA-ALDRICH, $\geq 97\%$) was made (Figure I.3 in I). The peaks obtained are coincident with the literature and the existing variations may occur because of different methodologies. With the Raman Spectroscopy of the previous deposition after the immersion in NaOH (Figure I.4 in I), it is possible to see that three of the peaks (442 cm^{-1} , 598 cm^{-1} and 962 cm^{-1}) correspond exactly to commercial HA. The Figure 5.28 shows both RS (of the HA commercial powder and the substrate after an electrodeposition of 3 V and a duration of 2 hours after the alkaline

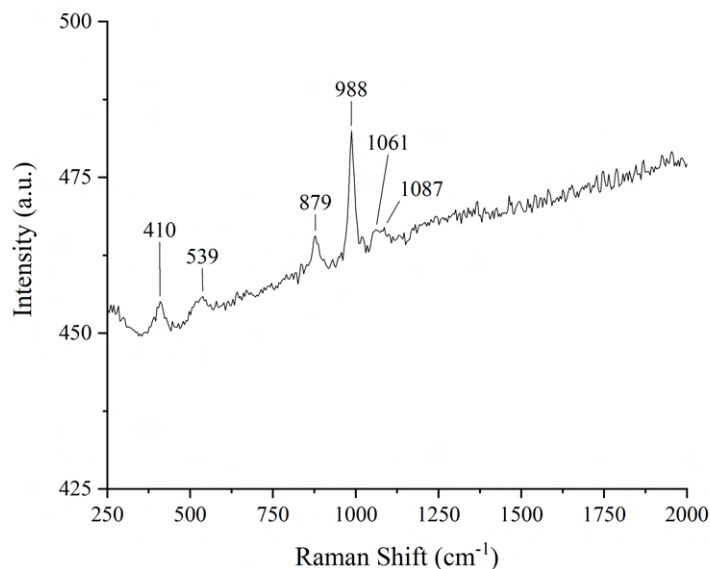


Figure 5.27: Raman Spectroscopy of a substrate before the immersion in NaOH, with a electrodeposition of 3 V for 2 hours

treatment), to facilitate the interpretation. The peak at 1074 cm^{-1} is a bit shifted when compared to the 1052 cm^{-1} of the commercial powder, but according to the literature that peak can also correspond to the $(\text{PO}_4)^{3-}$ ion (ν_3) (P-O anti-symmetrical stretching), assuming that after the alkaline treatment the coating changes to Hydroxyapatite, which is also coincident with the literature [39–41].

There was also an attempt of knowing how was composed the corrosion layer but without success.

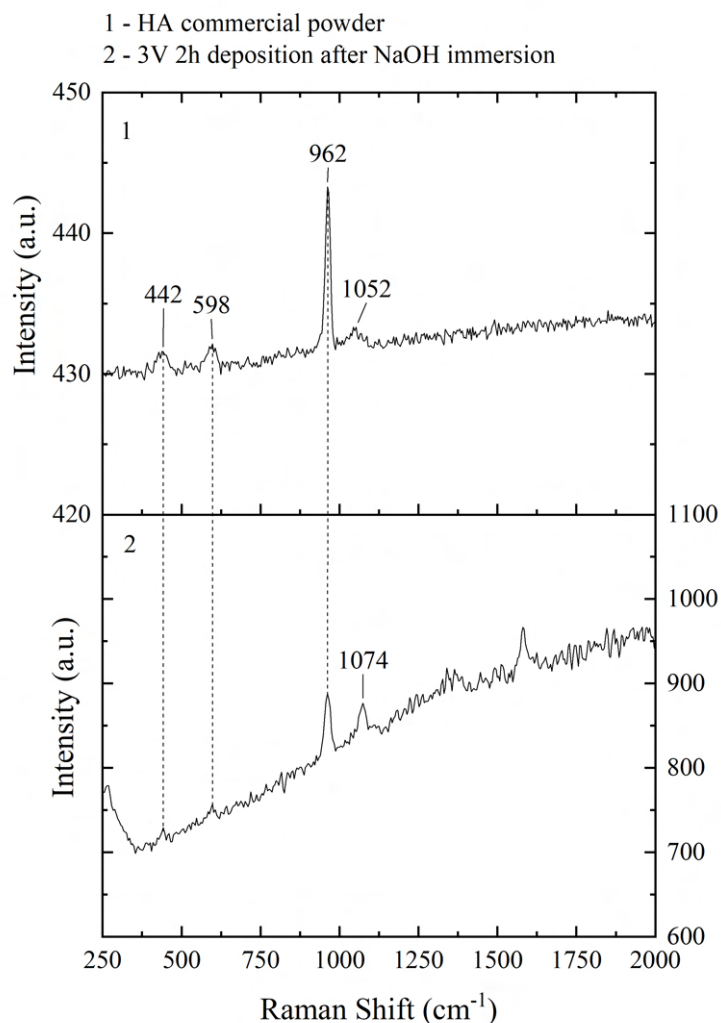


Figure 5.28: Raman Spectroscopy of HA commercial powder (1) and another of a substrate after the immersion in NaOH, with a electrodeposition of 3 V for 2 hours (2)

5.3.3 XRD Analysis

To complement the Raman analysis, XRDs of the substrates, before and after the coating, and of other powders were made. The first two graphs are related to the as-deposited coating (Figure 5.29), and the the following three are related to the coating after the alkaline treatment (Figure 5.30). The largest peaks, present in all graphs with the alloy, correspond to the Magnesium element [84]. The peaks that are going to be analysed are the smaller ones, that may be related to the DCPD, HA or other products related to the corrosion of the substrate.

The many peaks represented by the letter B indicate that the as-deposited coating is Brushite, as it is described in the literature [39–42]. The peaks were also confirmed in other work [85].

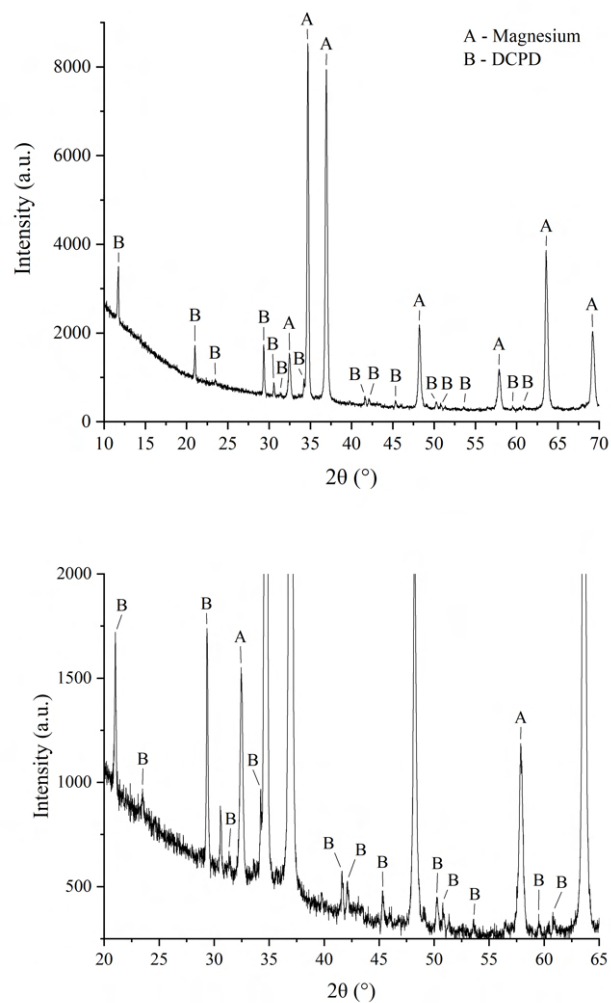


Figure 5.29: XRD of the as-deposited coating with a deposition of 3 V for 2 hours

By comparing the XRD of 3 V and 6 V, both for two hours, before the alkaline treatment, it is clear that both have the same results (Figure I.5 in I).

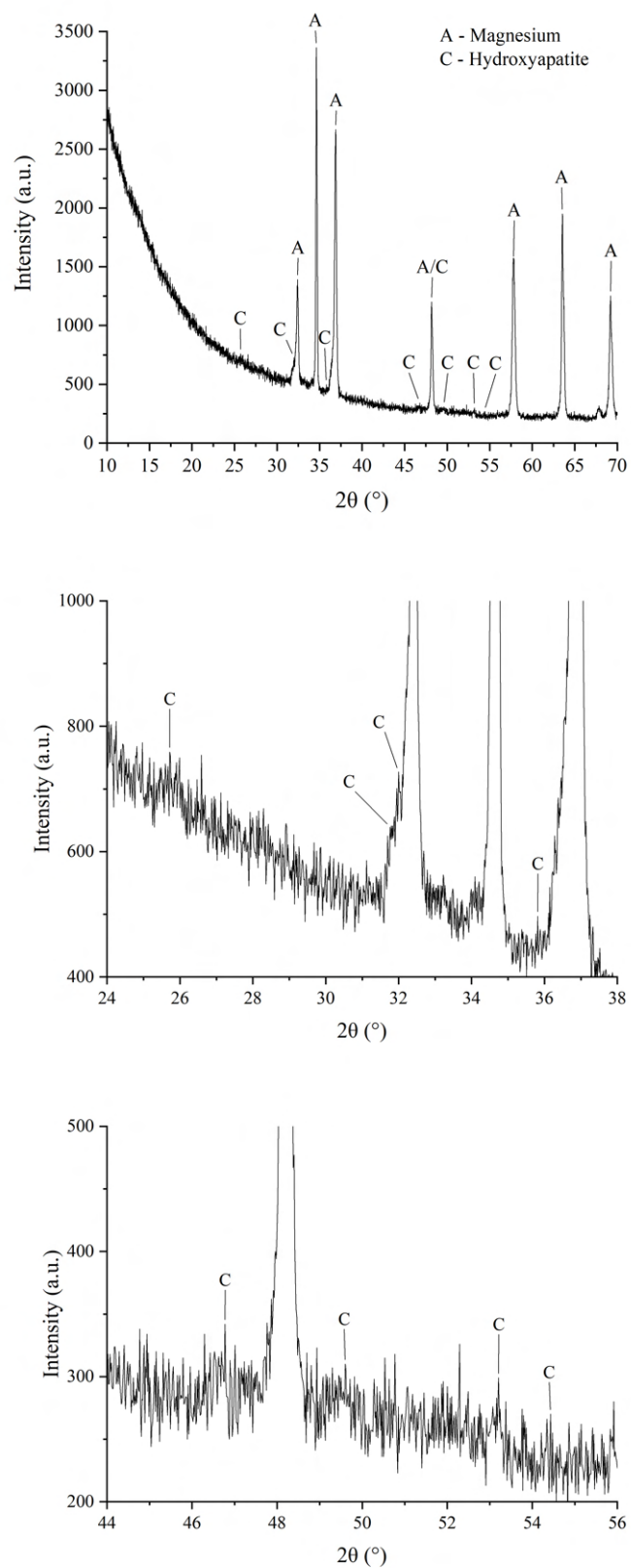


Figure 5.30: XRD of the coating after the immersion in NaOH with a deposition of 3 V for 2 hours

In order to detect the small HA peaks present in the substrate, an XRD of commercial Hydroxyapatite powder was also performed (Figure I.6 in I). Since the powder has a high purity, all peaks that appear are considered to be from HA. Many of these peaks are also coincident with the literature [86]. The Figure I.7 in I shows the overlay of the XRD plot of the HA powder with the 3 V deposition after the alkaline treatment. Thus, it is possible to identify in Figure 5.30 the peaks that may correspond to the deposition of HA on the alloy, indicating that the layer covering the alloy is Hydroxyapatite.

When comparing the 3 V with 6 V after the immersion, the 6 V has more and more intense peaks corresponding to the HA, but it has a few peaks that may correspond to the corrosion products (Figure I.8 in I). By overlaying the graph of the HA powder and the 6 V, it is noticeable that the 6 V has at least three extra peaks besides the ones that correspond to the HA (Figure 5.31).

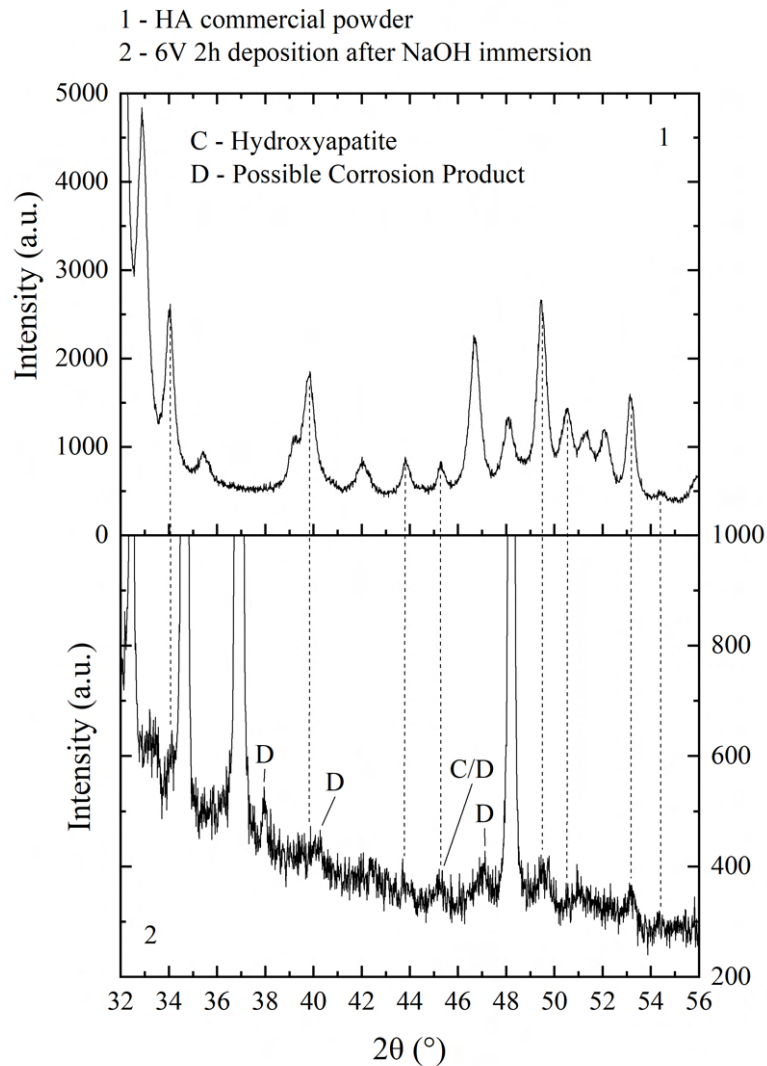


Figure 5.31: Comparison of the XRD of the HA powder (1) with the coating after the immersion in NaOH with a deposition of 6 V for 2 hours (2)

To check this fact, an XRD of the corrosion products powder from the CV experiment (with neutral pH) was made, and of two substrates after a CV with neutral and acid PBS solutions (Figures I.9 and I.10 in I). To analyse how the powder from the tests in neutral pH was composed, the the PBS solution was evaporated, leaving only the powder.

All visible peaks in any of the graphs (except those related to Mg) are considered to be related to corrosion products. Regarding the precipitate, although there are peaks that could not be identified, some of the them could, and matched with the literature, suggesting that the precipitate is composed by magnesium hydroxide, magnesium oxide, magnesium chloride and magnesium phosphate [87–90]. These results are quite consistent with the information discussed earlier in 2.2.1.

The first thing noticed between these three graphs is that there are some different peaks. Between the precipitate and the other two, there is a clear difference in the peaks that can be related to the magnesium chloride. This may be because this substance is more soluble, and therefore does not stick to the substrate, being in suspension in the solution. The opposite also happens for the substrate tested in acid conditions, meaning that there can be different corrosion products between the acid and neutral experiments. Between the substrate tested in a neutral environment and in a acid one, there are more and more intensive peaks in the latter. There can be two justifications for this: the fact that in the acid environment the substrate ends up with a thicker layer of corrosion products; and the possibility of different corrosion products between the two experiments.

With this, the XRD of the 6 V deposition was compared with the XDR of the precipitate and the substrate in a acid environment (Figure 5.32).

By observing the Figure 5.32, it can be seen that there are coincident peaks with the corrosion products powder and the substrate after a CV in an acid environment, which may indicate the presence of unwanted corrosion products.

This may indicate that during the electrodeposition with 6 V, the metal starts to react a bit to much with the solution, leading to corrosion. With this information, it is plausible to assume that every voltage that leads to a big production of hydrogen bubbles, can also lead to the formation of corrosion products.

Lastly, comparing two of the 3 V depositions, one with 2 hours and the other with one day, it is possible to see that with one day of deposition, there are more peaks related to the HA, however, as was also the case with the 6 V, there may be some corrosion related peaks (Figure 5.33). If that is the case, the reason for these peaks could be due to the high immersion time that the alloy was subjected to.

In summary, the XRD analysis corroborates both the RS and SEM analysis, in the sense that it shows that the as-deposited coating after the electrodeposition is DCPD, becoming HA after the alkaline treatment, and that high voltages and deposition times do not produce satisfactory results, leading to the formation of corrosion products.

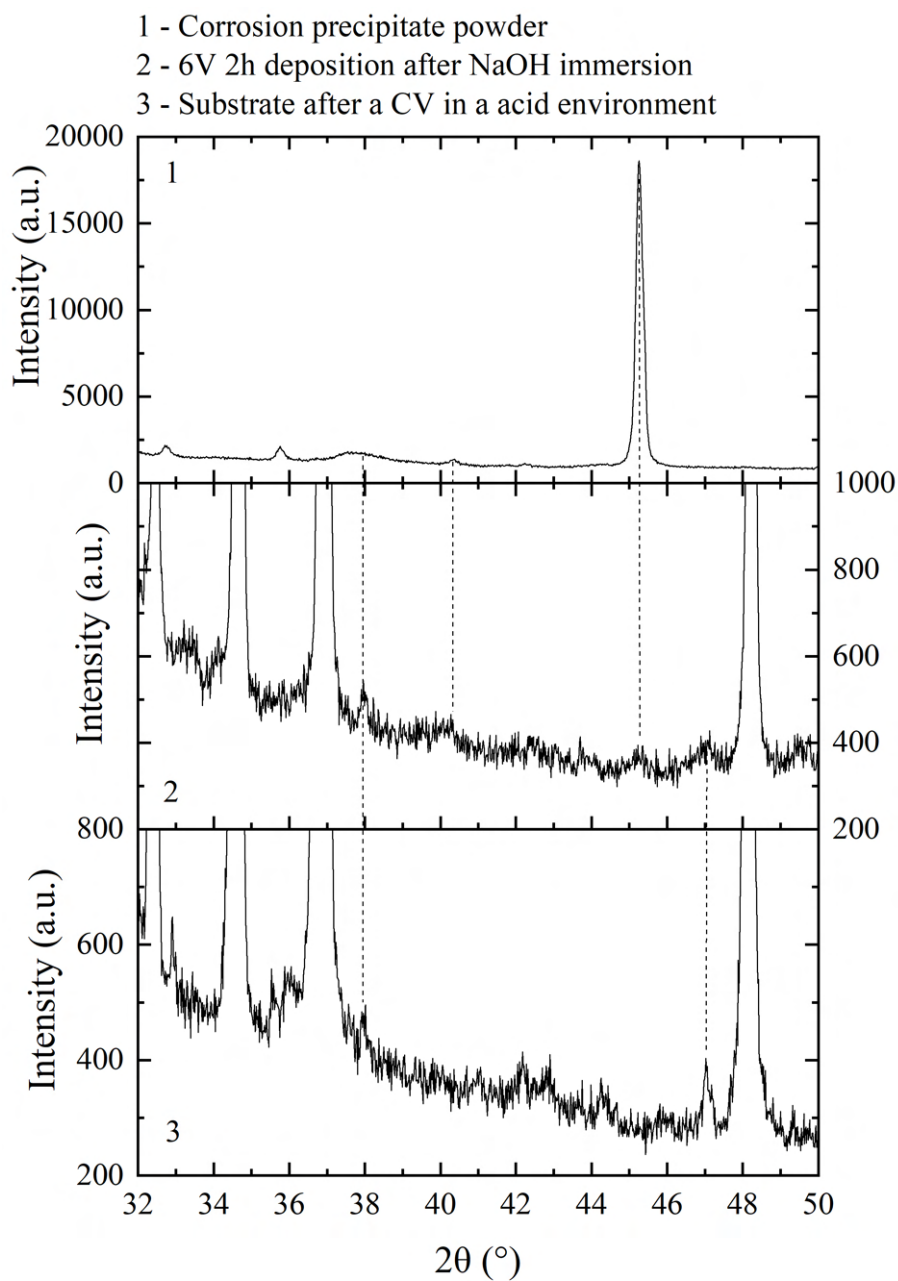


Figure 5.32: Comparison of the XRD of the corrosion precipitate powder (1) with the coating after the immersion in NaOH with a deposition of 6 V for 2 hours (2) and the substrate used in a CV experiment in a acid environment (3)

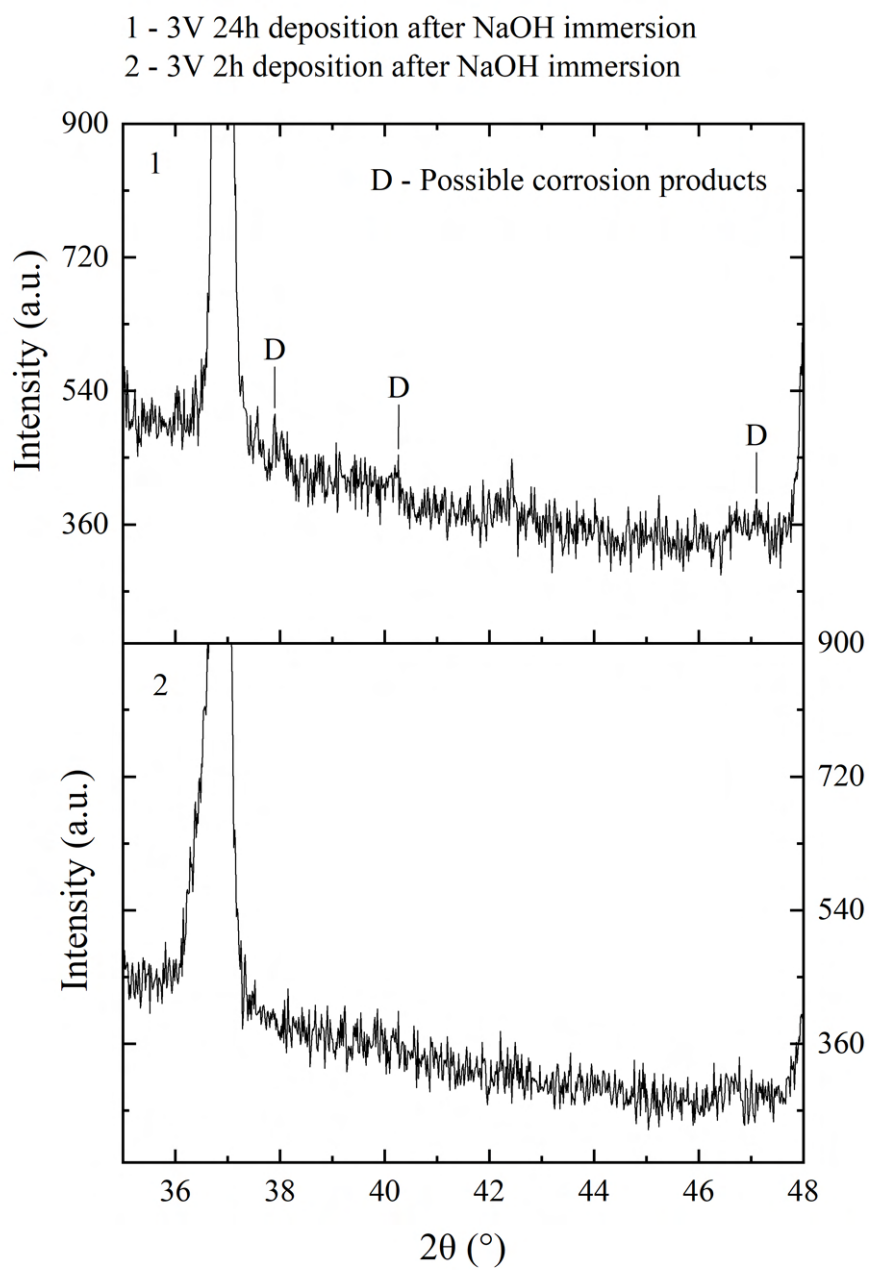


Figure 5.33: Comparison of the XRD of the coating after the immersion in NaOH with a deposition of 3 V for 24 hours (1) with a deposition of 3 V for 2 hours (2)

5.3.4 Electrochemical and Corrosion Experiments after the HA Coating

5.3.4.1 Cyclic Voltammetry

By observing the cyclic voltammograms of the commercial alloys after the depositions (3 V, 3.5 V and 4 V, all with 2 hours), it is noticeable that besides the reduction peak, there is also a clear oxidation reaction with neutral pH, that didn't exist. Figures 5.34, 5.35 and 5.36, refer to the graphs of the commercial alloy after depositions at 3 V, 3.5 V and 4 V.

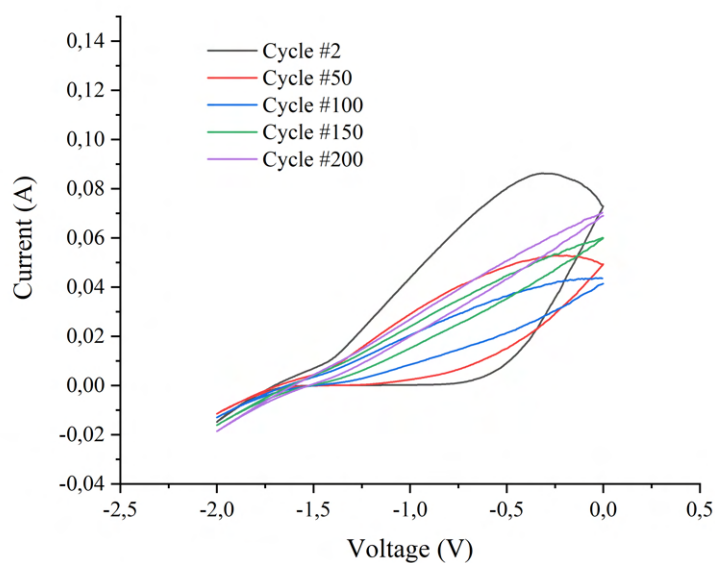


Figure 5.34: CV of the Mg alloy with 200 consecutive cycles with a pH of 7.4 (Scan Rate of 200 mV/s), after an electrodeposition of 3 V for 2 hours

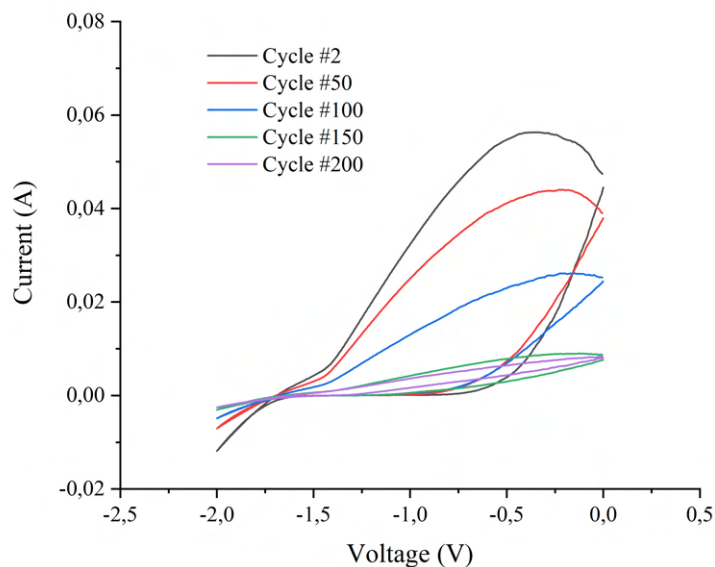


Figure 5.35: CV of the Mg alloy with 200 consecutive cycles with a pH of 7.4 (Scan Rate of 200 mV/s), after an electrodeposition of 3.5 V for 2 hours

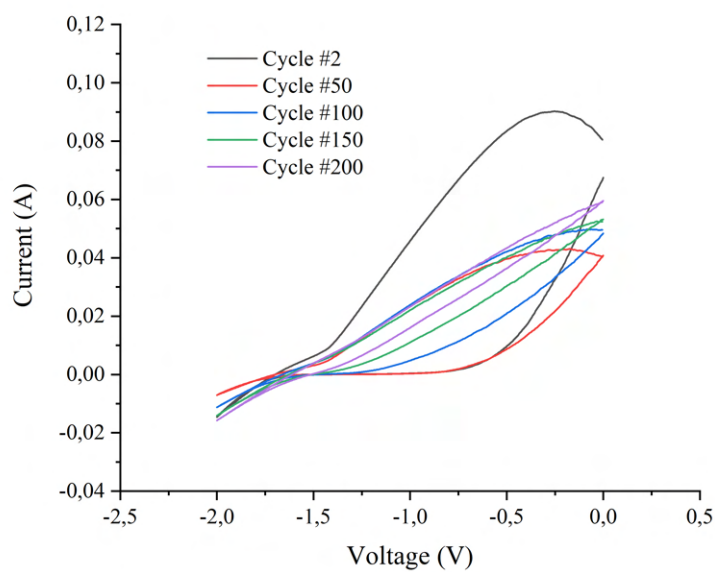


Figure 5.36: CV of the Mg alloy with 200 consecutive cycles with a pH of 7.4 (Scan Rate of 200 mV/s), after an electrodeposition of 4 V for 2 hours

For the WAAM substrates the oxidation peak is not so visible. Figures I.11, I.12 and I.13 in I, refer to the CVs of the these substrates after depositions at 3 V, 3.5 V and 4 V.

For the acid pH, there were only made CVs for the WAAM substrates, shown in Figures 5.37, 5.38 and 5.39, for 3 V, 3.5 V and 4 V, respectfully.

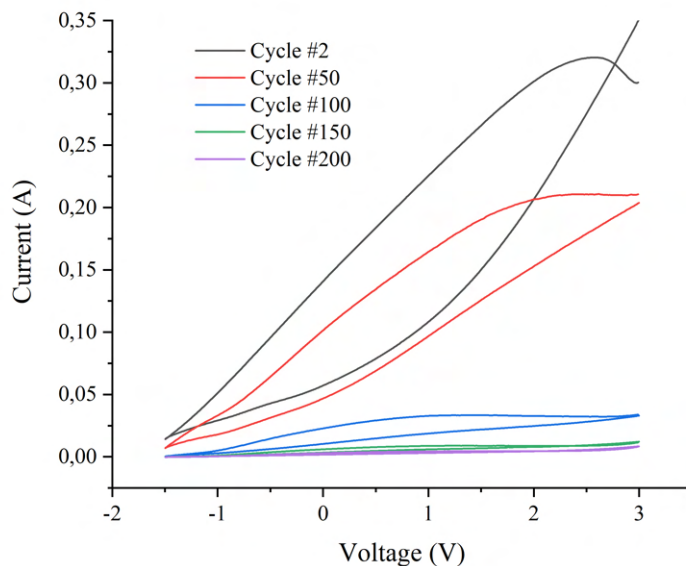


Figure 5.37: CV of the WAAM printed Mg alloy with 200 consecutive cycles with a pH of 5.5 (Scan Rate of 450 mV/s), after an electrodeposition of 3 V for 2 hours

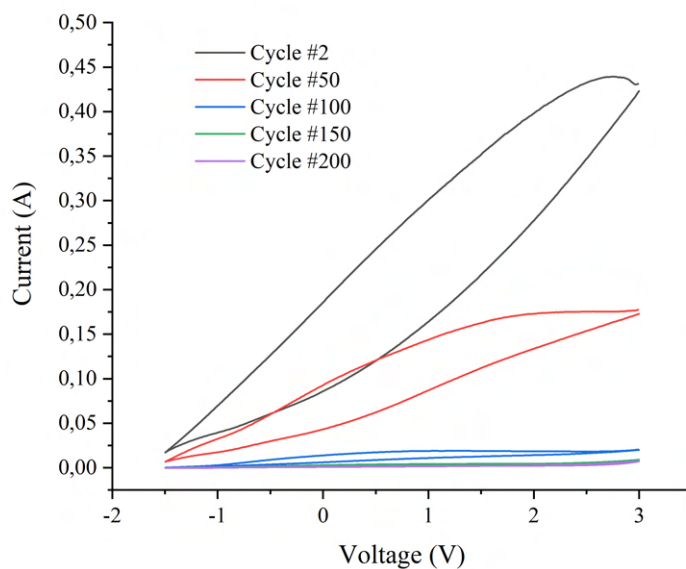


Figure 5.38: CV of the WAAM printed Mg alloy with 200 consecutive cycles with a pH of 5.5 (Scan Rate of 450 mV/s), after an electrodeposition of 3.5 V for 2 hours

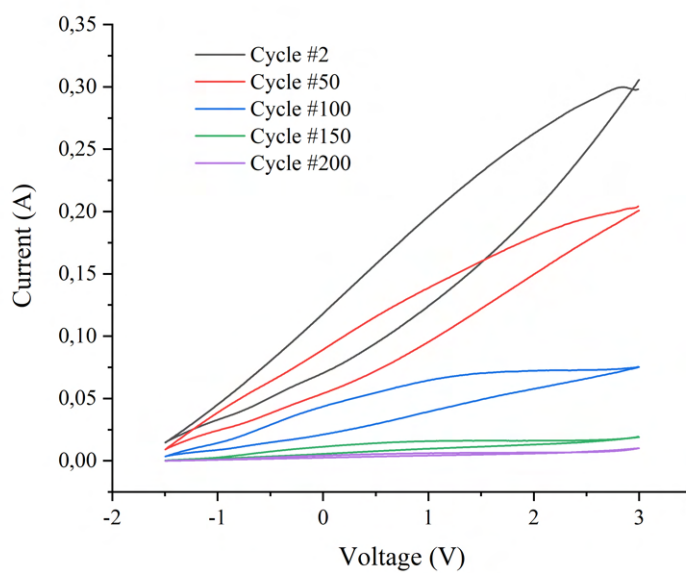


Figure 5.39: CV of the WAAM printed Mg alloy with 200 consecutive cycles with a pH of 5.5 (Scan Rate of 450 mV/s), after an electrodeposition of 3 V for 2 hours

5.3.4.2 Mass Variation and Corrosion

Just like before, the substrates were weighted before and after the CV experiment to check the mass variation. In this case the sample is very short, with only one example for each voltage. The Table 5.4 shows the ratio between the final mass (after the CV) and the initial mass of the WAAM printed alloy, for 200 cycles, at pH 7.4 and 5.5, after the depositions of 3 V, 3.5 V and 4 V.

Table 5.4: Mass variation (ratio of the final/initial mass) of the WAAM substrates after Cyclic Voltammetry with 200 cycles in PBS solutions, after the HA coating, for 3 V, 3.5 V, 4 V

pH	Voltage		
	3 V	3.5 V	4 V
7.4	0.98	0.98	0.97
5.5	0.97	0.97	0.96

Again, the final weights are not the real ones given the corrosion layer formed during the experiment. Although it is rather complicated to conclude anything, there is a slight inclination towards a greater mass loss by the substrates tested in acidic solution, just like the results in the Table 5.2 suggests. Between these results and the results related to the mass variation without the HA coating, there is no significant difference.

According to the literature, the HA coating increases the corrosion resistance of the alloys [39–41, 56]. By comparing the previous photograph and microscopic image of the WAAM alloy after a CV with neutral pH (Figure 5.8) with the same experiment with alloys with depositions of 3 V, 3.5 V and 4 V (Table 5.5), it is possible to assume that there is a slight improvement regarding the corrosion resistance, in the alloys with the HA coating. This improvement exists for all the voltages. Furthermore, there seems to be a better corrosion resistance for lower voltages however only with the help of SEM it was possible to compare the results between the three voltages, in order to determine which voltage leads to the best results.

For the acidic environment, the same results were acquired (comparing with Figure 5.9), as shown in Table 5.6.

Table 5.5: Photographs and microscopic images of the WAAM printed Mg commercial alloy AZ61A with a deposition of 3 V, 3.5 V and 4 V with 2 hours, after a CV experiment in neutral pH


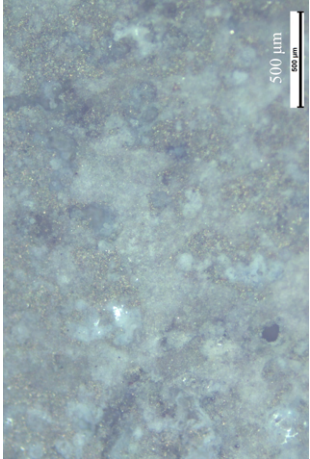

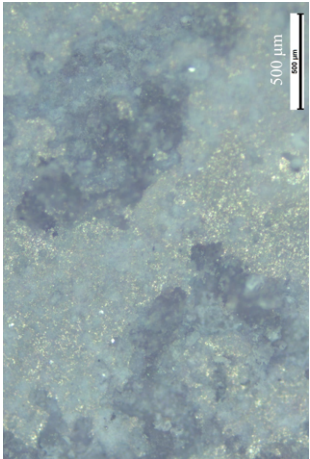

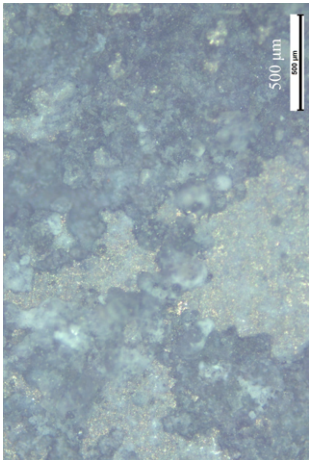

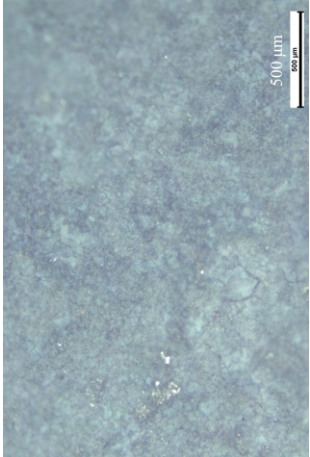

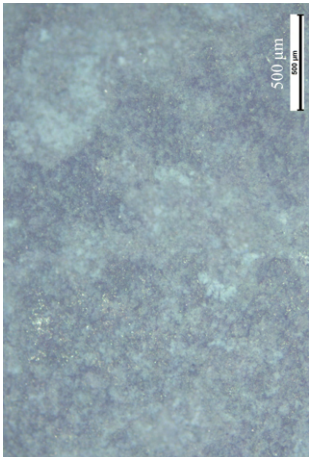

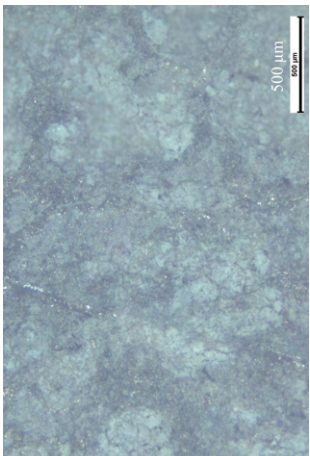
Voltage	Photographs	Microscopic
3 V		
3.5 V		
4 V		

Table 5.6: Photographs and microscopic images of the WAAM printed Mg commercial alloy AZ61A with a deposition of 3 V, 3.5 V and 4 V with 2 hours, after a CV experiment in acid pH

Voltage	Photographs	Microscopic
3 V		
3.5 V		
4 V		

For the CV with neutral pH, there are the SEM Figures 5.40, 5.41 and 5.42, referring to the depositions of 3 V, 3.5 V and 4 V, in that order. These images show that with 3 V there are smaller cracks, with a minor depth, and the substrate surface seems much more intact when comparing with the other two, which may indicate a better corrosion resistance. The differences between the 3.5 V and 4 V depositions are less prominent however the 3.5 V may appear to have cracks with a smaller depth, and a more intact surface. These results are consistent with other work, which claims that an HA coating can improve the corrosion resistance of Mg alloys. In addition, some of these papers concluded that depositions with a lower voltage also appear to have a better corrosion resistance results. [27, 39–42, 56]

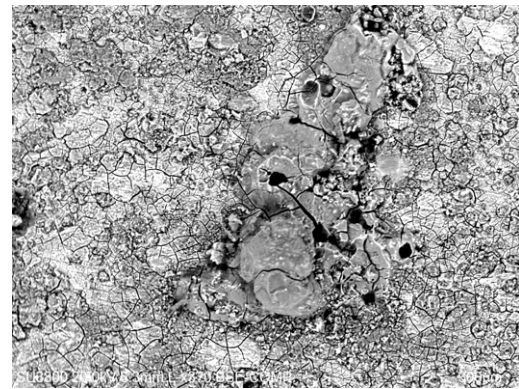
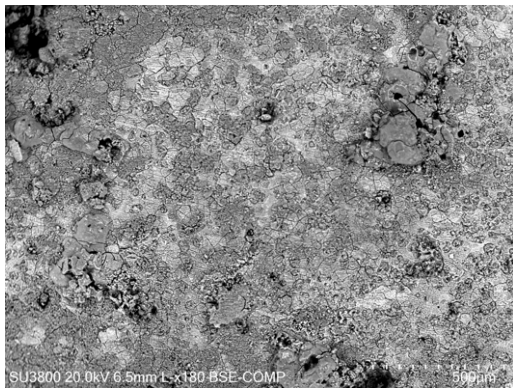


Figure 5.40: SEM of a WAAM printed Mg commercial alloy AZ61A after a CV experiment in neutral pH, with a deposition of 3 V for 2h

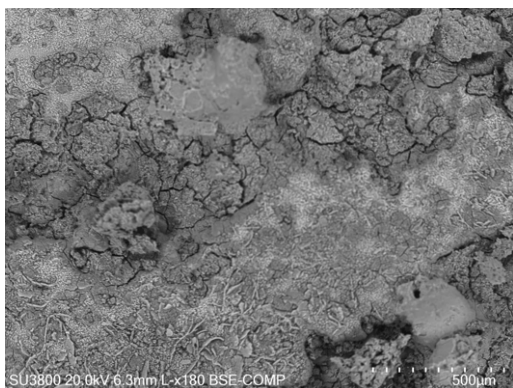


Figure 5.41: SEM of a WAAM printed Mg commercial alloy AZ61A after a CV experiment in neutral pH, with a deposition of 3.5 V for 2h

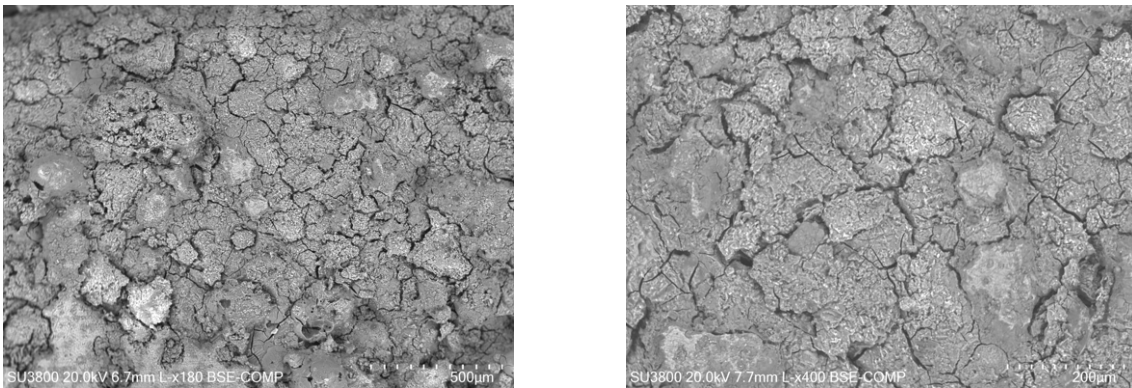


Figure 5.42: SEM of a WAAM printed Mg commercial alloy AZ61A after a CV experiment in neutral pH, with a deposition of 4 V for 2h

Although it is rather more difficult to assume which deposition shows better corrosion results (due to the layer of corrosion products stuck in the substrate), it can be noted that also in acidic environments, lower voltages seem to indicate better results. The following Figures 5.43, 5.44 and 5.45, show these results for 3 V, 3.5 V and 4 V, respectively. The 3 V and 3.5 V show a smoother and less heterogeneous surface, and the 4 V shows a more degraded and damaged substrate.

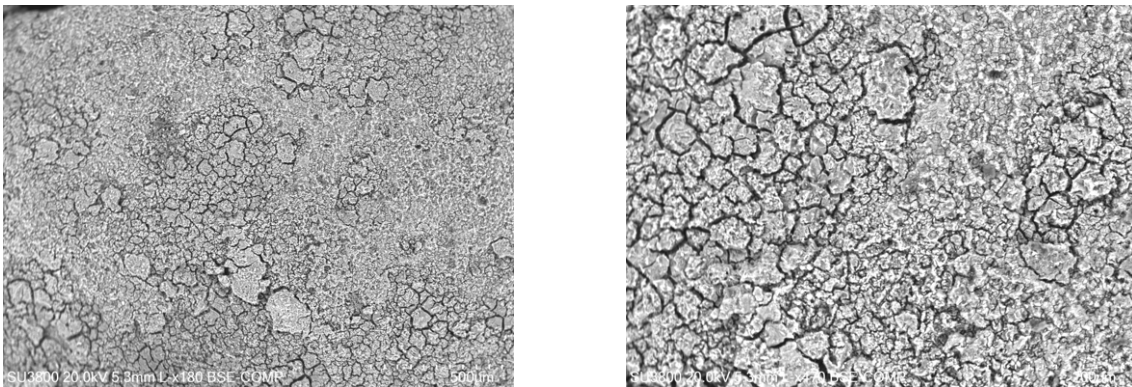


Figure 5.43: SEM of a WAAM printed Mg commercial alloy AZ61A after a CV experiment in acid pH, with a deposition of 3 V for 2h

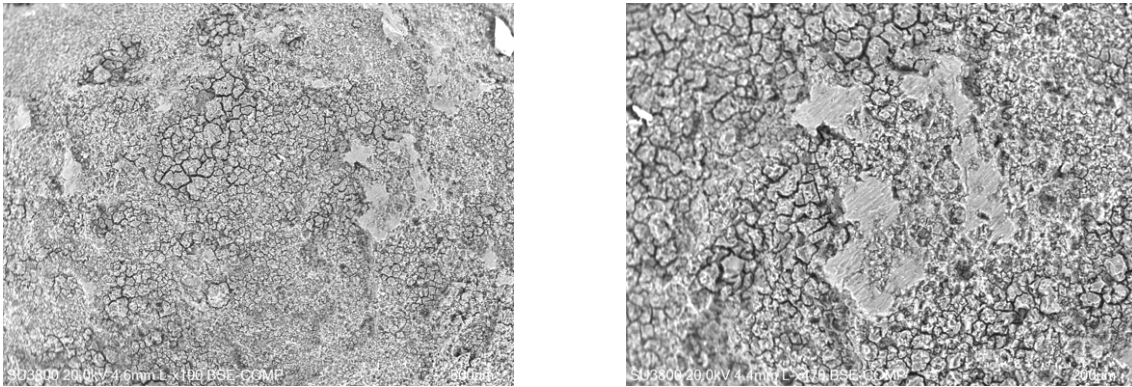


Figure 5.44: SEM of a WAAM printed Mg commercial alloy AZ61A after a CV experiment in acid pH, with a deposition of 3.5 V for 2h

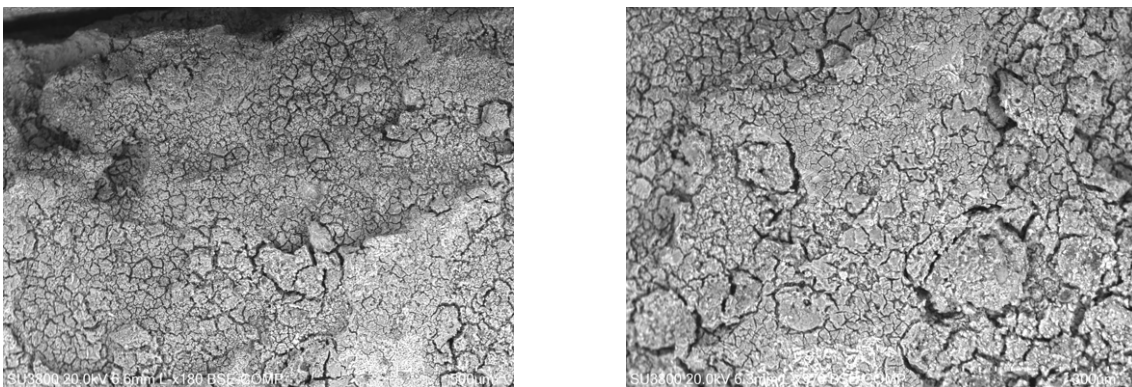


Figure 5.45: SEM of a WAAM printed Mg commercial alloy AZ61A after a CV experiment in acid pH, with a deposition of 4 V for 2h

CONCLUSION AND FUTURE WORK

To verify the possibility of using the WAAM technology to produce of Mg based bioresorbable implants it was first necessary to study the behaviour of the commercial alloy (AZ61A in specific) in two static simulated body fluids environments: one with a pH of 5.5 and another of 7.4, in order to simulate an infection and the normality of the body.

To check the electrochemical characterization, Cyclic Voltammetry was used, and the samples were weighted before and after every experiment to investigate the mass variation.

It was possible to conclude that Mg reacts with the environment releasing bubbles (hydrogen according to the literature), forming different corrosion products, some soluble and others insoluble. It was observed that the dissolution of some of these products increases the pH of the surrounding environment.

In the beginning of an acid CV, the Magnesium alloy seems to be less resistant when comparing with a neutral environment because the corrosion layer is more soluble in a lower pH. However, as the tests proceed, the reactions in acid environment cease to be so effusive, because of the thick layer formed by the corrosion products. In opposition to the experience in a neutral environment, this layer does not detach as much, which ultimately protects the material, which is contradictory to literature. This can be justified by: the saturation of the solution; the increased roughness of the material; the increased pH; and the difference between the corrosion products from the acid PBS solution and the neutral, which can result in a different adhesion that they have with the material. In a dynamic environment, like the human body, this may differ because of the constant solution renovation, and the light cleansing of the alloy.

Regarding the mass variation of the Magnesium alloys, it is difficult to study given the formation of the layer of corrosion products that sticks to the alloy. Some results even appoint to a gain of mass, instead of a loss. Again, in a dynamic environment, this may differ. These results were similar between the commercial alloys and the WAAM printed ones.

To try to improve the corrosion resistance of the substrates, an Hydroxyapatite coating

was made, using Electrodeposition. It is possible to use it to cover both the commercial Mg alloy wire and the printed WAAM Mg alloy, with DCPD, and immerse it in a alkaline solution to transform the layer into HA. The composition of each layer was confirmed with the Raman Spectroscopy and XRD, matching with the literature.

Focusing on the corrosion, both macro and microscopically images show that this protective layer appears to help the alloy with the corrosion rate by slowing it down.

With SEM it was possible to verify that besides appearing to improve corrosion resistance, lower voltages seem to indicate a more homogeneous coating, and therefore more effective protection. This can be related to the higher production of hydrogen bubbles, given by higher voltages. In addition, XRD could indicate that higher voltages also lead to the production of corrosion products, which is not appropriate. With reference to the deposition time, higher times lead to a more homogeneous and apparently thicker deposition, however from a certain point onwards there may start to be a production of corrosion products, as indicated by the XRD. Between the voltages 3 V, 3.5 V, 4 V, 4.5 V, 5 V and 6 V, and times of 30, 60, 90, 120 minutes and 24 hours, the best results seemed to be the 3 V and 3.5 V for depositions of 120 minutes.

This work lays the foundations for future work to be pursue. The next steps will be the toxicity, biocompatibility and cell adhesion tests to study the biological properties that the substrates have with the Hydroxyapatite coating. Some possible amendments that could be made are the the tests under dynamic environments, and the usage of real body fluids. Also, the use of different electrochemical techniques, like the Open Circuit Potential measurements, can be beneficial for a better understanding of the corrosion resistance, with and without the HA coating.

The future use of bioresorbable implants is a tremendous step forward in the evolution of public health. In addition to the project having succeeded in achieving its main objectives, it provides useful contributions for the future use of these methods in medical approaches. This, in turn, can play a part in the improvement of the quality of life of the patients.

BIBLIOGRAPHY

- [1] R. Karunakaran et al. “Additive manufacturing of magnesium alloys”. In: *Bioactive Materials* 5 (1 Mar. 2020), pp. 44–54. ISSN: 2452-199X. DOI: 10.1016/j.bioactmat.2019.12.004 (cit. on pp. 2, 3).
- [2] T. Pereira, J. V. Kennedy, and J. Potgieter. “A comparison of traditional manufacturing vs additive manufacturing, the best method for the job”. In: vol. 30. Elsevier B.V., 2019, pp. 11–18. DOI: 10.1016/j.promfg.2019.02.003 (cit. on p. 2).
- [3] S. Han et al. “Optimization of AZ91D Process and Corrosion Resistance Using Wire Arc Additive Manufacturing”. In: *Appl. Sci.* (Aug. 2018). DOI: 10.3390/app8081306 (cit. on p. 2).
- [4] T. A. Rodrigues et al. “Current status and perspectives on wire and arc additive manufacturing (WAAM)”. In: *Materials* 12 (7 2019). ISSN: 1996-1944. DOI: 10.3390/ma12071121 (cit. on pp. 3, 11, 14).
- [5] D. Jafari, T. H. Vaneker, and I. Gibson. “Wire and arc additive manufacturing: Opportunities and challenges to control the quality and accuracy of manufactured parts”. In: *Materials and Design* 202 (Apr. 2021). ISSN: 1873-4197. DOI: 10.1016/j.matdes.2021.109471 (cit. on p. 3).
- [6] A. R. McAndrew et al. “Interpass rolling of Ti-6Al-4V wire+arc additively manufactured features for microstructural refinement”. In: *Additive Manufacturing* 21 (May 2018), pp. 340–349. ISSN: 2214-8604. DOI: 10.1016/j.addma.2018.03.006 (cit. on p. 3).
- [7] S. Chatterjee et al. “Futuristic medical implants using bioresorbable materials and devices”. In: *Biosensors and Bioelectronics* 142 (Oct. 2019). ISSN: 1873-4235. DOI: 10.1016/j.bios.2019.111489 (cit. on pp. 3–5).
- [8] D. Lindholm and S. James. “Bioresorbable Stents in PCI”. In: *Current Cardiology Reports* 18 (8 Aug. 2016). ISSN: 1534-3170. DOI: 10.1007/s11886-016-0750-9 (cit. on p. 3).

- [9] Y. Chen et al. “Recent advances on the development of magnesium alloys for biodegradable implants”. In: *Acta Biomaterialia* 10 (11 Nov. 2014), pp. 4561–4573. ISSN: 1878-7568. DOI: 10.1016/j.actbio.2014.07.005 (cit. on pp. 3, 5, 11).
- [10] K. F. Farraro et al. “Revolutionizing orthopaedic biomaterials: The potential of biodegradable and bioresorbable magnesium-based materials for functional tissue engineering”. In: *Journal of Biomechanics* 47 (9 June 2014), pp. 1979–1986. ISSN: 1873-2380. DOI: 10.1016/j.jbiomech.2013.12.003 (cit. on p. 3).
- [11] A. C. Bîrcă et al. “Mg-Zn alloys, most suitable for biomedical applications”. In: *Rom J Morphol Embryol* 59 (1 2018), pp. 49–54. ISSN: 2066-8279 (cit. on pp. 4–6).
- [12] R. Parai and S. Bandyopadhyay-Ghosh. “Engineered bio-nanocomposite magnesium scaffold for bone tissue regeneration”. In: *Journal of the Mechanical Behavior of Biomedical Materials* 96 (Aug. 2019), pp. 45–52. ISSN: 1878-0180. DOI: 10.1016/j.jmbbm.2019.04.019 (cit. on p. 4).
- [13] P. J. Denard et al. “Stress shielding of the humerus in press-fit anatomic shoulder arthroplasty: review and recommendations for evaluation”. In: *Journal of Shoulder and Elbow Surgery* 27 (6 June 2018), pp. 1139–1147. ISSN: 1532-6500. DOI: 10.1016/j.jse.2017.12.020 (cit. on p. 4).
- [14] F. H. M. “Wolff’s Law and bone’s structural adaptations to mechanical usage: an overview for clinicians”. In: *The Angle orthodontist* (1994), pp. 175–188. DOI: 10.1043/0003-3219(1994)064<0175:WLABSA>2.0.CO;2 (cit. on p. 4).
- [15] Y. Liu, B. Lu, and Z. Cai. “Recent Progress on Mg- And Zn-Based Alloys for Biodegradable Vascular Stent Applications”. In: *Journal of Nanomaterials* 2019 (2019). ISSN: 1687-4129. DOI: 10.1155/2019/1310792 (cit. on pp. 4, 6).
- [16] V. Herber et al. “Bioresorbable magnesium-based alloys as novel biomaterials in oral bone regeneration: General review and clinical perspectives”. In: *Journal of Clinical Medicine* 10 (9 May 2021). ISSN: 2077-0383. DOI: 10.3390/jcm10091842 (cit. on pp. 4, 11).
- [17] A. M. A. Alawi, S. W. Majoni, and H. Falhammar. *Magnesium and Human Health: Perspectives and Research Directions*. 2018. DOI: 10.1155/2018/9041694 (cit. on p. 4).
- [18] E. C. S. C. on Food., Nutrition, and A. E. F. S. A. S. P. on Dietetic Products. *Tolerable upper intake levels for vitamins and minerals*. European Food Safety Authority, 2006, p. 478. ISBN: 9291990140 (cit. on p. 5).
- [19] I. of Medicine. *Dietary Reference Intakes for Calcium, Phosphorus, Magnesium, Vitamin D, and Fluoride*. National Academies Press, 1997, p. 448. ISBN: 0309063507 (cit. on p. 5).

- [20] M. B. Kannan et al. "Biocompatibility and biodegradation studies of a commercial zinc alloy for temporary mini-implant applications". In: *Scientific Reports* 7 (1 Dec. 2017). ISSN: 2045-2322. DOI: 10.1038/s41598-017-15873-w (cit. on p. 5).
- [21] M. Esmaily et al. "Fundamentals and advances in magnesium alloy corrosion". In: *Progress in Materials Science* 89 (Aug. 2017), pp. 92–193. ISSN: 00796425. DOI: 10.1016/j.pmatsci.2017.04.011 (cit. on p. 5).
- [22] S. V. Prasad, S. Singh, and S. B. Prasad. "A review on the corrosion process in magnesium". In: vol. 2341. American Institute of Physics Inc., May 2021. ISBN: 9780735440951. DOI: 10.1063/5.0050016 (cit. on p. 5).
- [23] S. Johnston, Z. Shi, and A. Atrens. "The influence of pH on the corrosion rate of high-purity Mg, AZ91 and ZE41 in bicarbonate buffered Hanks' solution". In: *Corrosion Science* 101 (Dec. 2015), pp. 182–192. ISSN: 0010938X. DOI: 10.1016/j.corsci.2015.09.018 (cit. on pp. 5, 29).
- [24] K. Sun et al. "Effect of pH on the corrosion and crack growth behavior of the ZK60 magnesium alloy". In: *Corrosion Science* 179 (Feb. 2021). ISSN: 0010938X. DOI: 10.1016/j.corsci.2020.109135 (cit. on pp. 5, 29).
- [25] H. Yang et al. "Alloying design of biodegradable zinc as promising bone implants for load-bearing applications". In: *Nature Communications* 11 (1 Dec. 2020). ISSN: 2041-1723. DOI: 10.1038/s41467-019-14153-7 (cit. on pp. 5, 6).
- [26] S. Bender et al. "Corrosion and corrosion testing of magnesium alloys". In: *Materials and Corrosion* 58 (12 Dec. 2007), pp. 977–982. ISSN: 09475117. DOI: 10.1002/maco.200704091 (cit. on p. 5).
- [27] M. Kannan. "Hydroxyapatite coating on biodegradable magnesium and magnesium-based alloys". In: *Hydroxyapatite (Hap) for Biomedical Applications* (Jan. 2015), pp. 289–306. DOI: 10.1016/B978-1-78242-033-0.00013-4 (cit. on pp. 6, 54, 68).
- [28] S. Cabeza et al. "Corrosion behaviour of mg98.5nd1zn0.5 (at. %) alloy in phosphate buffered saline solution". In: *Metals* 10 (1 Jan. 2020). ISSN: 20754701. DOI: 10.3390/met10010148 (cit. on pp. 6, 28).
- [29] M. S. Safavi et al. "Electrodeposited Hydroxyapatite-Based Biocoatings: Recent Progress and Future Challenges". In: *Coatings 2021, Vol. 11, Page 110* 11 (1 Jan. 2021), p. 110. ISSN: 2079-6412. DOI: 10.3390/COATINGS11010110. URL: <https://www.mdpi.com/2079-6412/11/1/110/htm%20https://www.mdpi.com/2079-6412/11/1/110> (cit. on pp. 6, 8, 9).
- [30] H. Peng et al. "Effect of Galvanic Corrosion on the Degradability of Biomedical Magnesium". In: *Frontiers in Materials* 8 (Dec. 2021). ISSN: 22968016. DOI: 10.3389/FMATS.2021.767179 (cit. on pp. 6, 8).

- [31] V. Herber et al. “Can Hardware Removal be Avoided Using Bioresorbable Mg-Zn-Ca Screws After Medial Malleolar Fracture Fixation? Mid-Term Results of a First-In-Human Study”. In: *Injury* (2021). ISSN: 1879-0267. DOI: 10.1016/j.injury.2021.10.025 (cit. on pp. 6, 12).
- [32] J. Guo et al. “Wire arc additive manufacturing of AZ31 magnesium alloy: Grain refinement by adjusting pulse frequency”. In: *Materials* 9 (10 Oct. 2016). ISSN: 1996-1944. DOI: 10.3390/ma9100823 (cit. on p. 6).
- [33] A. El-Ghannam and P. Ducheyne. *Bioactive ceramics*. Oct. 2011 (cit. on p. 7).
- [34] V. S. Kattimani, S. Kondaka, and K. P. Lingamaneni. “Hydroxyapatite—Past, Present, and Future in Bone Regeneration”. In: *Bone and Tissue Regeneration Insights* 7 (Jan. 2016), BTRI.S36138. ISSN: 1179-061X. DOI: 10.4137/BTRI.S36138 (cit. on pp. 7, 11).
- [35] M. Rahman, Y. Li, and C. Wen. “HA coating on Mg alloys for biomedical applications: A review”. In: *Journal of Magnesium and Alloys* 8 (3 Sept. 2020), pp. 929–943. ISSN: 22139567. DOI: 10.1016/j.jma.2020.05.003 (cit. on p. 7).
- [36] K. Sato. “Mechanism of hydroxyapatite mineralization in biological systems”. In: *Journal of the Ceramic Society of Japan* 115 (1338 2007), pp. 124–130. ISSN: 13486535. DOI: 10.2109/JCERSJ.115.124 (cit. on p. 7).
- [37] W. S. Harun et al. *A review of powder additive manufacturing processes for metallic biomaterials*. Mar. 2018. DOI: 10.1016/j.powtec.2017.12.058 (cit. on p. 7).
- [38] J. Chen et al. “Recent advances on development of hydroxyapatite coating on biodegradable magnesium alloys: A review”. In: *Materials* 14 (19 Oct. 2021). ISSN: 19961944. DOI: 10.3390/ma14195550 (cit. on p. 7).
- [39] M. Assadian et al. “Topography, wetting, and corrosion responses of electrodeposited hydroxyapatite and fluoridated hydroxyapatite on magnesium”. In: *Bio-Medical Materials and Engineering* 27 (2-3 Aug. 2016), pp. 287–303. ISSN: 18783619. DOI: 10.3233/BME-161585 (cit. on pp. 8, 12, 18, 38–40, 51, 54).
- [40] Y. W. Song, D. Y. Shan, and E. H. Han. “Electrodeposition of hydroxyapatite coating on AZ91D magnesium alloy for biomaterial application”. In: *Materials Letters* 62 (17-18 June 2008), pp. 3276–3279. ISSN: 0167577X. DOI: 10.1016/j.matlet.2008.02.048 (cit. on pp. 8, 12, 18, 38–40, 51, 54).
- [41] M. Jamesh, S. Kumar, and T. S. Narayanan. “Electrodeposition of hydroxyapatite coating on magnesium for biomedical applications”. In: *Journal of Coatings Technology and Research* 9 (4 2012), pp. 495–502. ISSN: 15470091. DOI: 10.1007/s11998-011-9382-6 (cit. on pp. 8, 12, 18, 38–40, 51, 54).
- [42] M. B. Kannan and L. Orr. “In vitro mechanical integrity of hydroxyapatite coated magnesium alloy”. In: *Biomedical Materials* 6 (4 2011). ISSN: 1748605X. DOI: 10.1088/1748-6041/6/4/045003 (cit. on pp. 8, 18, 33, 38, 40, 54).

- [43] L. L. Hench and J. M. Polak. "Third-Generation Biomedical Materials". In: *Science* 295 (5557 2002), pp. 1014–1017. DOI: 10.1126/science.1067404 (cit. on p. 10).
- [44] M. Navarro et al. "Biomaterials in orthopaedics". In: *Journal of the Royal Society Interface* 5 (27 Oct. 2008), pp. 1137–1158. ISSN: 1742-5662. DOI: 10.1098/rsif.2008.0151 (cit. on pp. 10, 11).
- [45] L. L. Fiench and J. Wilson. "Surface-Active Biomaterials". In: *Science* 226 (4675 1984), pp. 630–636. DOI: 10.1126/science.6093253 (cit. on p. 10).
- [46] U. Sigwart et al. "Intravascular stents to prevent occlusion and restenosis after transluminal angioplasty". In: *The New England journal of medicine* 316 (10 1987), pp. 701–706. DOI: 10.1056/NEJM198703193161201 (cit. on p. 10).
- [47] M.-C. Morice et al. "A Randomized Comparison of a Sirolimus-Eluting Stent with a Standard Stent for Coronary Revascularization". In: *New England journal of medicine* 346 (23 2002), pp. 1773–1780. DOI: 10.1056/NEJMoa012843 (cit. on p. 10).
- [48] P. W. Serruys, H. M. Garcia-Garcia, and Y. Onuma. "From metallic cages to transient bioresorbable scaffolds: Change in paradigm of coronary revascularization in the upcoming decade?" In: *European Heart Journal* 33 (1 Jan. 2012), pp. 16–25. ISSN: 0195-668X. DOI: 10.1093/eurheartj/ehr384 (cit. on p. 10).
- [49] T. Wohlers and T. Gornet. "History of additive manufacturing". In: *Wohlers report* 24.2014 (2014), p. 118 (cit. on p. 11).
- [50] B. Dutta. "Directed Energy Deposition (DED) Technology". In: *Encyclopedia of Materials: Metals and Alloys*. Ed. by F. G. Caballero. Oxford: Elsevier, 2022, pp. 66–84. ISBN: 978-0-12-819733-2. DOI: <https://doi.org/10.1016/B978-0-12-819726-4.00035-1> (cit. on p. 11).
- [51] K. S. Derekar. "A review of wire arc additive manufacturing and advances in wire arc additive manufacturing of aluminium". In: *Materials Science and Technology (United Kingdom)* 34 (8 May 2018), pp. 895–916. ISSN: 1743-2847. DOI: 10.1080/02670836.2018.1455012 (cit. on p. 11).
- [52] F. Witte. "The history of biodegradable magnesium implants: A review". In: *Acta Biomaterialia* 6 (5 2010), pp. 1680–1692. ISSN: 1742-7061. DOI: 10.1016/j.actbio.2010.02.028 (cit. on p. 11).
- [53] A. K. Gosain et al. "A 1-year study of osteoinduction in hydroxyapatite-derived biomaterials in an adult sheep model: part I". In: *Plastic and reconstructive surgery* 109 (2 2002), pp. 619–630. ISSN: 0032-1052. DOI: 10.1097/00006534-200202000-00032. URL: <https://pubmed.ncbi.nlm.nih.gov/11818845/> (cit. on p. 12).

- [54] K. A. Hing et al. "Microporosity enhances bioactivity of synthetic bone graft substitutes". In: *Journal of materials science. Materials in medicine* 16 (5 May 2005), pp. 467–475. ISSN: 0957-4530. DOI: 10.1007/S10856-005-6988-1. URL: <https://pubmed.ncbi.nlm.nih.gov/15875258/> (cit. on p. 12).
- [55] H. A. El-Fattah et al. "In vivo animal histomorphometric study for evaluating biocompatibility and osteointegration of nano-hydroxyapatite as biomaterials in tissue engineering." In: *Journal of the Egyptian National Cancer Institute* 22 (4 2010), pp. 24–50 (cit. on p. 12).
- [56] S. A. Salman, K. Kuroda, and M. Okido. "Preparation and characterization of hydroxyapatite coating on AZ31 Mg alloy for implant applications". In: *Bioinorganic Chemistry and Applications* 2013 (2013). ISSN: 15653633. DOI: 10.1155/2013/175756 (cit. on pp. 12, 51, 54).
- [57] P. S. Nnamchi and C. S. Obayi. "Chapter 4 - Electrochemical Characterization of Nanomaterials". In: *Characterization of Nanomaterials*. Ed. by S. Mohan Bhagyaraj et al. Micro and Nano Technologies. Woodhead Publishing, 2018, pp. 103–127. ISBN: 978-0-08-101973-3. DOI: <https://doi.org/10.1016/B978-0-08-101973-3.00004-3> (cit. on p. 16).
- [58] Y. S. Choudhary, L. Jothi, and G. Nageswaran. "Chapter 2 - Electrochemical Characterization". In: *Spectroscopic Methods for Nanomaterials Characterization*. Ed. by S. Thomas et al. Micro and Nano Technologies. Elsevier, 2017, pp. 19–54. ISBN: 978-0-323-46140-5. DOI: <https://doi.org/10.1016/B978-0-323-46140-5.00002-9> (cit. on p. 16).
- [59] T. Forrister. *Analyzing Cyclic Voltammetry at a Microdisk Electrode with Simulation | COMSOL Blog*. July 2018. URL: <https://www.comsol.fr/blogs/analyzing-cyclic-voltammetry-at-a-microdisk-electrode-with-simulation/> (cit. on p. 16).
- [60] R. Devasia et al. "Continuous fiber reinforced ceramic matrix composites". In: *Fiber Reinforced Composites: Constituents, Compatibility, Perspectives and Applications* (Jan. 2021), pp. 669–751. DOI: 10.1016/B978-0-12-821090-1.00022-3 (cit. on p. 18).
- [61] J. Chang, Y. L. Zhou, and Y. Zhou. *Surface modification of bioactive glasses*. Jan. 2018. DOI: 10.1016/B978-0-08-100936-9.00008-3 (cit. on p. 18).
- [62] A. Khanaki, H. Abdizadeh, and M. R. Golobostanfard. "Electrophoretic Deposition of CuIn_{1-x}Ga_xSe₂ Thin Films Using Solvothermal Synthesized Nanoparticles for Solar Cell Application". In: *J. Phys. Chem. C* 119 (2015), p. 12. DOI: 10.1021/acs.jpcc.5b07300. URL: <https://pubs.acs.org/sharingguidelines> (cit. on p. 19).
- [63] W. T. Mason. *Fluorescent and luminescent probes for biological activity : a practical guide to technology for quantitative real-time analysis*. Academic Press, 1999, pp. 433–455. ISBN: 0124478360 (cit. on p. 20).

- [64] A. Synetos and D. Tousoulis. *Invasive imaging techniques*. Jan. 2018. DOI: 10.1016/B978-0-12-811908-2.00018-0 (cit. on p. 20).
- [65] M. Henini. "Scanning electron microscopy: an introduction". In: *III-Vs Review* 13 (4 July 2000), pp. 40–44. ISSN: 0961-1290. DOI: 10.1016/S0961-1290(00)80006-X (cit. on p. 20).
- [66] S. Ebnesajjad. "Surface and material characterization techniques". In: *Handbook of Adhesives and Surface Preparation*. Plastics Design Library. Oxford: William Andrew Publishing, 2011, pp. 31–48. ISBN: 9781437744613. DOI: 10.1016/B978-1-4377-4461-3.10004-5 (cit. on p. 20).
- [67] R. Kohli and K. Mittal. "Methods for Assessing Surface Cleanliness". In: *Developments in Surface Contamination and Cleaning, Volume 12*. Elsevier, 2019, pp. 23–105. ISBN: 978-0-12-816081-7. DOI: <https://doi.org/10.1016/B978-0-12-816081-7.00003-0> (cit. on pp. 20, 21).
- [68] N. Fleck et al. "Characterization techniques in energy generation and storage". In: *Emerging Nanotechnologies for Renewable Energy* (Jan. 2021), pp. 259–285. DOI: 10.1016/B978-0-12-821346-9.00003-1 (cit. on p. 21).
- [69] T. Cain et al. "A compilation of corrosion potentials for magnesium alloys". In: *Corrosion* 70 (10 Oct. 2014), pp. 1043–1051. ISSN: 00109312. DOI: 10.5006/1257 (cit. on p. 24).
- [70] C. Schille et al. "Corrosion of experimental magnesium alloys in blood and PBS: A gravimetric and microscopic evaluation". In: *Materials Science and Engineering: B* 176 (20 Dec. 2011), pp. 1797–1801. ISSN: 0921-5107. DOI: 10.1016/J.MSEB.2011.04.007 (cit. on p. 28).
- [71] E. M. Schotsmans et al. "Raman spectroscopy as a non-destructive screening technique for studying white substances from archaeological and forensic burial contexts". In: *Journal of Raman Spectroscopy* 45 (11-12 2014), pp. 1301–1308. ISSN: 10974555. DOI: 10.1002/jrs.4526 (cit. on p. 38).
- [72] G. Penel et al. "Raman Microspectrometry Studies of Brushite Cement: In Vivo Evolution in a Sheep Model". In: *Bone* 25 (2 1999), 81S–84S (cit. on p. 38).
- [73] M. M. Mirković et al. "Adsorption of malathion on mesoporous monetite obtained by mechanochemical treatment of brushite". In: *RSC Advances* 6 (15 2016), pp. 12219–12225. ISSN: 20462069. DOI: 10.1039/c5ra27554g (cit. on p. 38).
- [74] R. L. Frost, S. J. Palmer, and Y. Xi. "A Raman spectroscopic study of the mono-hydrogen phosphate mineral dorfmanite $\text{Na}_2(\text{PO}_3\text{OH})\cdot 2\text{H}_2\text{O}$ and in comparison with brushite". In: *Spectrochimica Acta - Part A: Molecular and Biomolecular Spectroscopy* 82 (1 Nov. 2011), pp. 132–136. ISSN: 13861425. DOI: 10.1016/j.saa.2011.07.015 (cit. on p. 38).

- [75] R. L. Frost et al. "Raman spectroscopy of synthetic $\text{CaHPO}_4 \cdot 2\text{H}_2\text{O}$ - and in comparison with the cave mineral brushite". In: *Journal of Raman Spectroscopy* 43 (4 Apr. 2012), pp. 571–576. ISSN: 03770486. DOI: 10.1002/jrs.3063 (cit. on p. 38).
- [76] M.-N. D. Noirfontaine et al. "Amorphization of a Proposed Sorbent of Strontium, Brushite, $\text{CaHPO}_4 \cdot 2\text{H}_2\text{O}$, Studied by X-1 ray Diffraction and Raman Spectroscopy". In: (2020). URL: <https://www.sciencedirect.com/science/article/pii/S0022311520313593> (cit. on p. 38).
- [77] R. Cuscó et al. "Differentiation between Hydroxyapatite and β -Tricalcium Phosphate by Means of p-Raman Spectroscopy". In: *Journal of the European Ceramic Society* 18 (1998), pp. 1301–1305 (cit. on p. 38).
- [78] L. F. Sukhodub et al. "Collagen-hydroxyapatite-water interactions investigated by XRD, piezogravimetry, infrared and Raman spectroscopy". In: *Journal of Molecular Structure* 704 (1-3 Oct. 2004), pp. 53–58. ISSN: 00222860. DOI: 10.1016/j.molstruc.2003.12.061 (cit. on p. 38).
- [79] P. E. Timchenko et al. "Experimental studies of hydroxyapatite by Raman spectroscopy". In: *Journal of Optical Technology* 85 (3 Mar. 2018), p. 130. ISSN: 1070-9762. DOI: 10.1364/jot.85.000130 (cit. on p. 38).
- [80] J. A. Stammeier et al. "In-situ Raman spectroscopy of amorphous calcium phosphate to crystalline hydroxyapatite transformation". In: *MethodsX* 5 (Jan. 2018), pp. 1241–1250. ISSN: 22150161. DOI: 10.1016/j.mex.2018.09.015 (cit. on p. 38).
- [81] B. Yilmaz and Z. Evis. "Raman spectroscopy investigation of nano hydroxyapatite doped with yttrium and fluoride ions". In: *Spectroscopy Letters* 47 (1 2014), pp. 24–29. ISSN: 00387010. DOI: 10.1080/00387010.2013.778296 (cit. on p. 38).
- [82] L. M. Reis de Vasconcellos et al. "Porous titanium associated with CaP coating: In vivo and in vitro osteogenic performance". In: *Materials Research* 21 (2 2018). ISSN: 15161439. DOI: 10.1590/1980-5373-mr-2017-0557 (cit. on p. 38).
- [83] I. Rehrnan et al. "Structural evaluation of human and sheer, bone and comparison with synthetic hydroxyapatite by FT-Rarnan spectroscopy". In: *Journal of Biomedical Materials Research* 29 (1995), pp. 1287–1294 (cit. on p. 38).
- [84] D. Guzmán et al. "Effect of the milling energy on the production and thermal stability of amorphous $\text{Mg}_{50}\text{Ni}_{50}$ ". In: *Journal of Alloys and Compounds* 471 (1-2 Mar. 2009), pp. 435–441. ISSN: 09258388. DOI: 10.1016/J.JALLCOM.2008.03.130 (cit. on p. 40).
- [85] M. P. Binitha and P. P. Pradyumnan. "Dielectric Property Studies of Biologically Compatible Brushite Single Crystals Used as Bone Graft Substitute". In: *Journal of Biomaterials and Nanobiotechnology* 04 (02 2013), pp. 119–122. ISSN: 2158-7027. DOI: 10.4236/JBNB.2013.42016 (cit. on p. 40).

-
- [86] S. A. Manafi et al. "Synthesis of nano-hydroxyapatite under a sonochemical/hydrothermal condition". In: *Biomedical Materials* 3 (2 June 2008). ISSN: 17486041. DOI: 10.1088/1748-6041/3/2/025002 (cit. on p. 43).
- [87] A. Almontasser, A. Parveen, and A. Azam. "Synthesis, Characterization and antibacterial activity of Magnesium Oxide (MgO) nanoparticles." In: *IOP Conference Series: Materials Science and Engineering* 577 (1 Dec. 2019). ISSN: 1757899X. DOI: 10.1088/1757-899X/577/1/012051 (cit. on p. 44).
- [88] T. D. Munusamy et al. "Catalytic performance and antimicrobial activity of Mg(OH)₂/MgO colloidal nanoparticles in alkyd resin nanocomposite derived from palm oil". In: *Polymer Bulletin* 77 (9 Sept. 2020), pp. 4571–4586. ISSN: 14362449. DOI: 10.1007/S00289-019-02993-8 (cit. on p. 44).
- [89] K. Suvarnna et al. "Corn silk extract-based solid-state biopolymer electrolyte and its application to electrochemical storage devices". In: *Ionics* 28 (4 Apr. 2022), pp. 1767–1782. ISSN: 18620760. DOI: 10.1007/S11581-021-04415-0 (cit. on p. 44).
- [90] C. Berg. "Influence of Magnesium in the Formation of Phosphate Spheres". Uppsala Universitet, July 2017. URL: urn:nbn:se:uu:diva-326255 (cit. on p. 44).



Figure I.1: Photograph of the commercial wire AZ61A, used to print the WAAM substrates

Table I.1: Physical and mechanical properties of natural bone, Mg and Ti; Compressive Yield Strength - CYS (adapted from [27])

Properties	Natural bone	Magnesium	Titanium alloy
Density (g/cm^3)	1.8-2.1	1.74-2.0	4.4-4.5
CYS (MPa)	3-20	41-45	110-117
Elastic Modulus (GPa)	130-180	65-100	758-1117

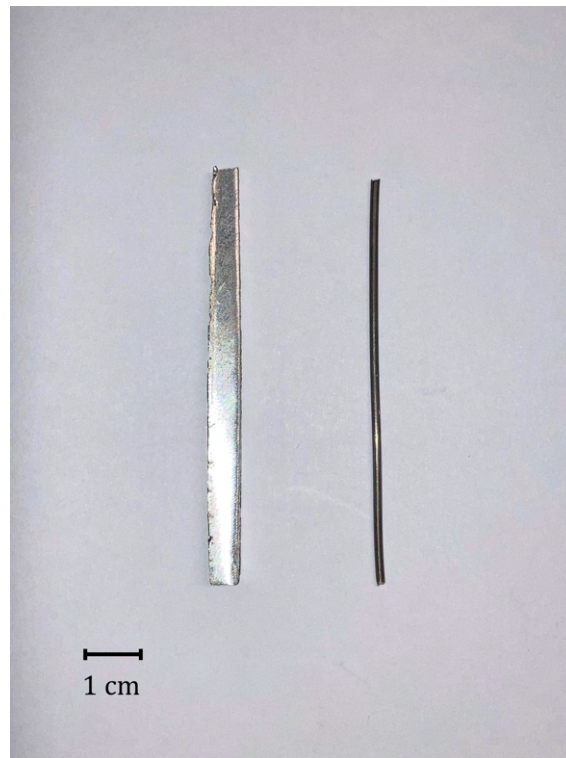


Figure I.2: Photograph of the printed WAAM substrate (left) and the commercial wire (right), side by side

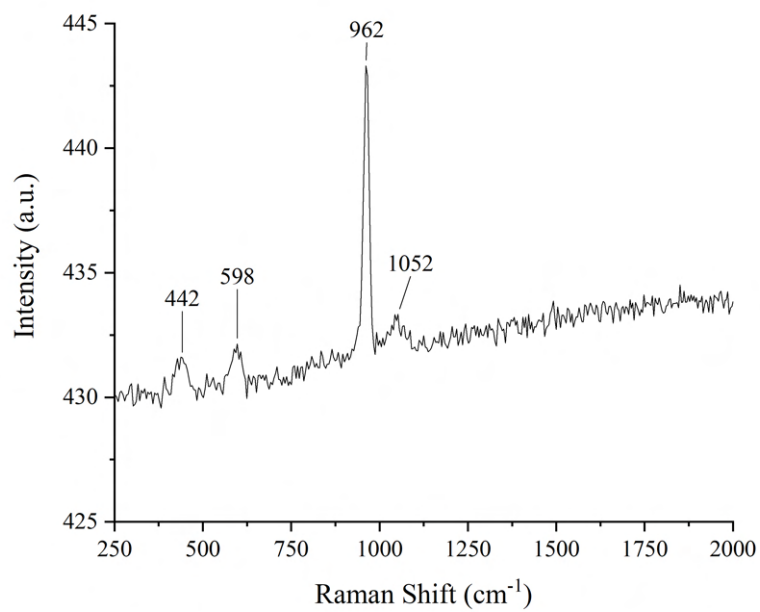

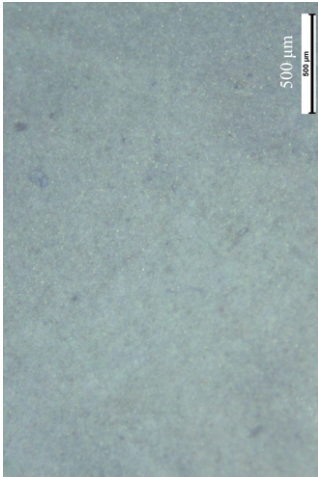

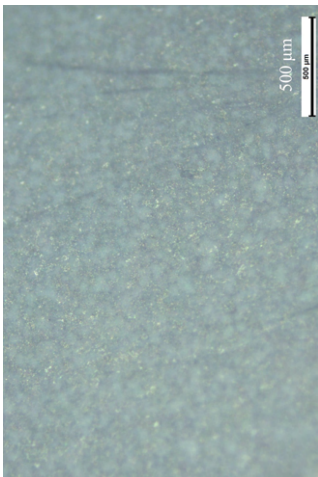

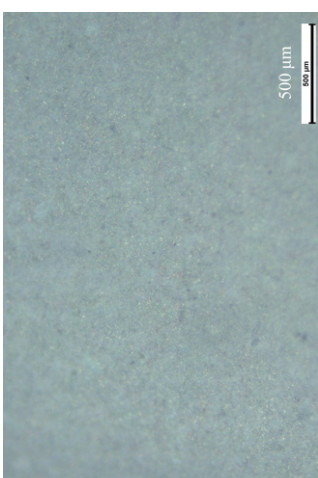


Figure I.3: Raman Spectroscopy of the Hydroxyapatite commercial powder

Table I.2: Photographs and microscopic images of the substrates after the electrodepositions at voltages 3V, 3.5V and 4V, with a duration of 2 hours, after the immersion in NaOH

Voltage	Photographs	Microscopic
3V		
3.5V		
4V		

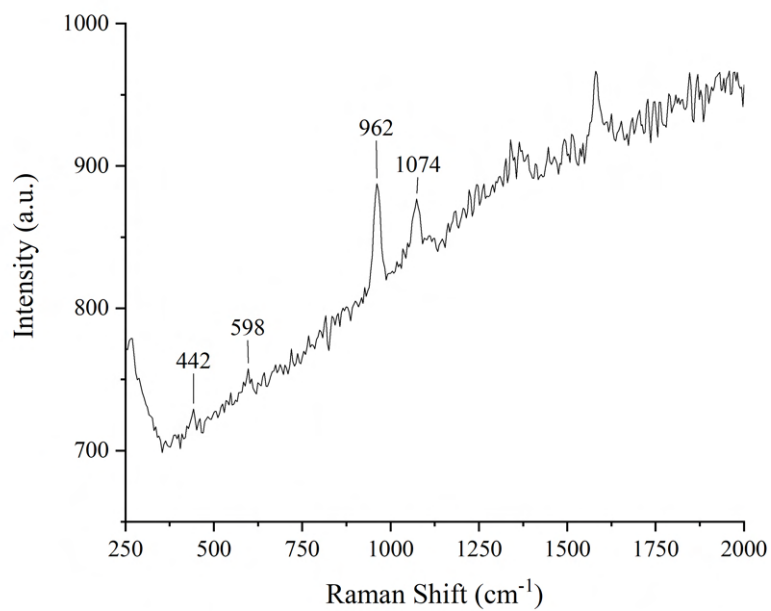


Figure I.4: Raman Spectroscopy of a substrate after the immersion in NaOH, with a electrodeposition of 3V for 2 hours

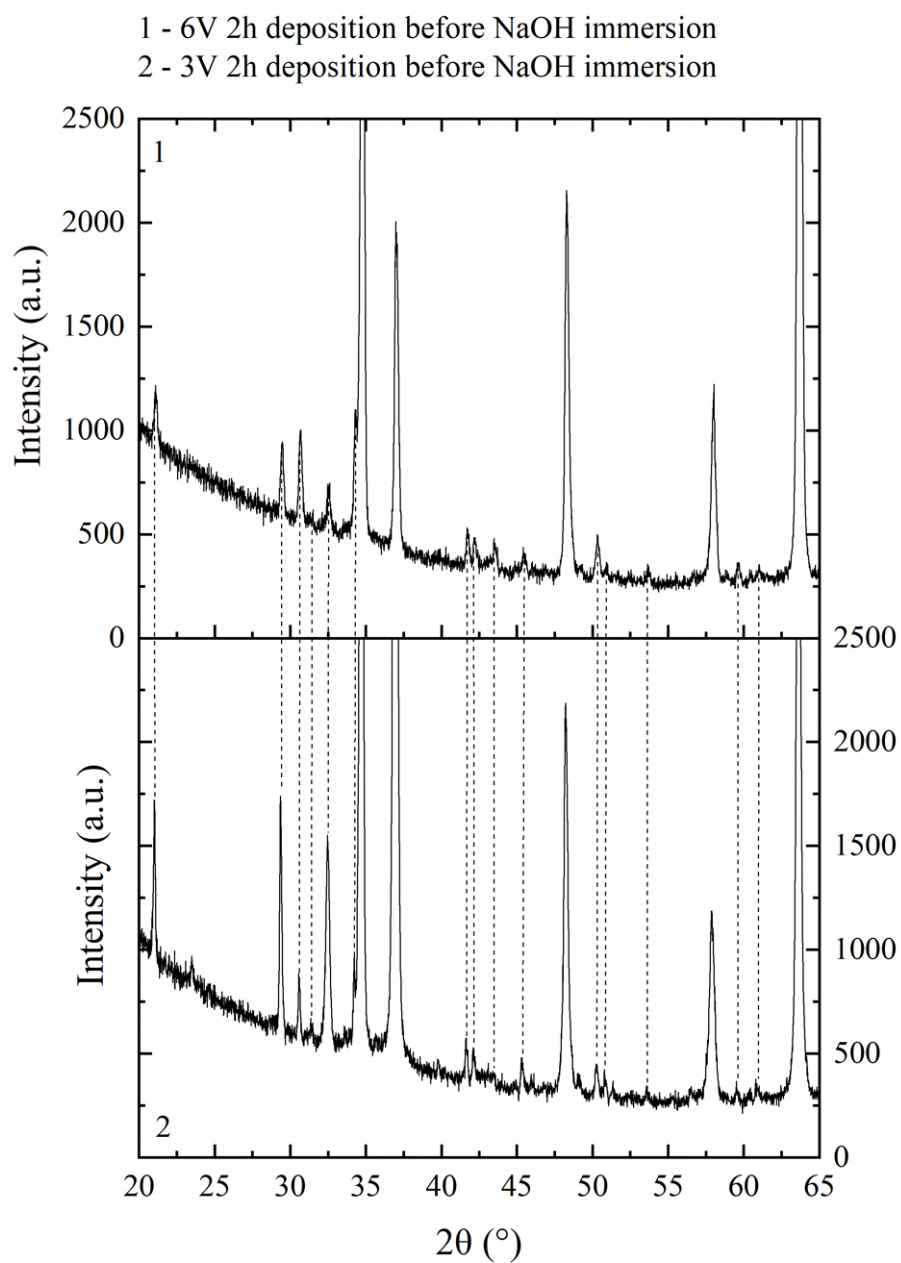


Figure I.5: Comparison of the XRD of the as-deposited coating of depositions of 6V (1) and 3V (2), both for 2 hours

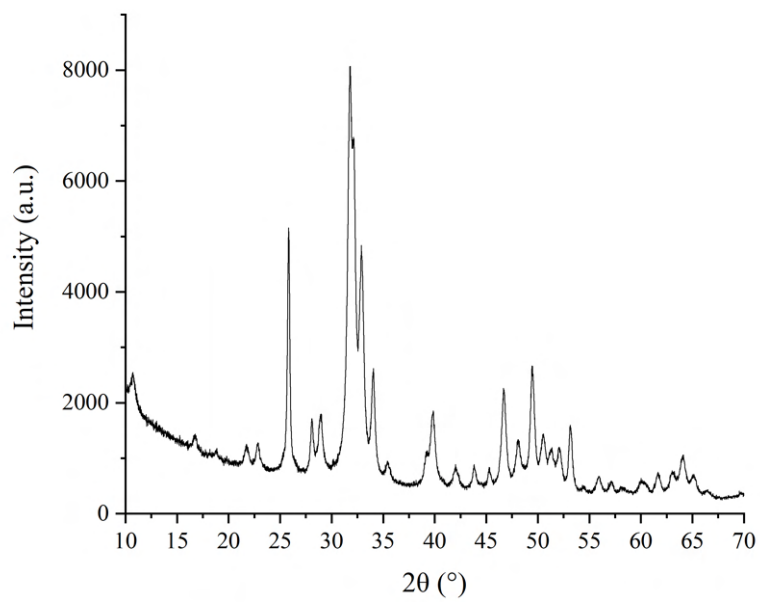


Figure I.6: XRD of the commercial Hydroxyapatite powder

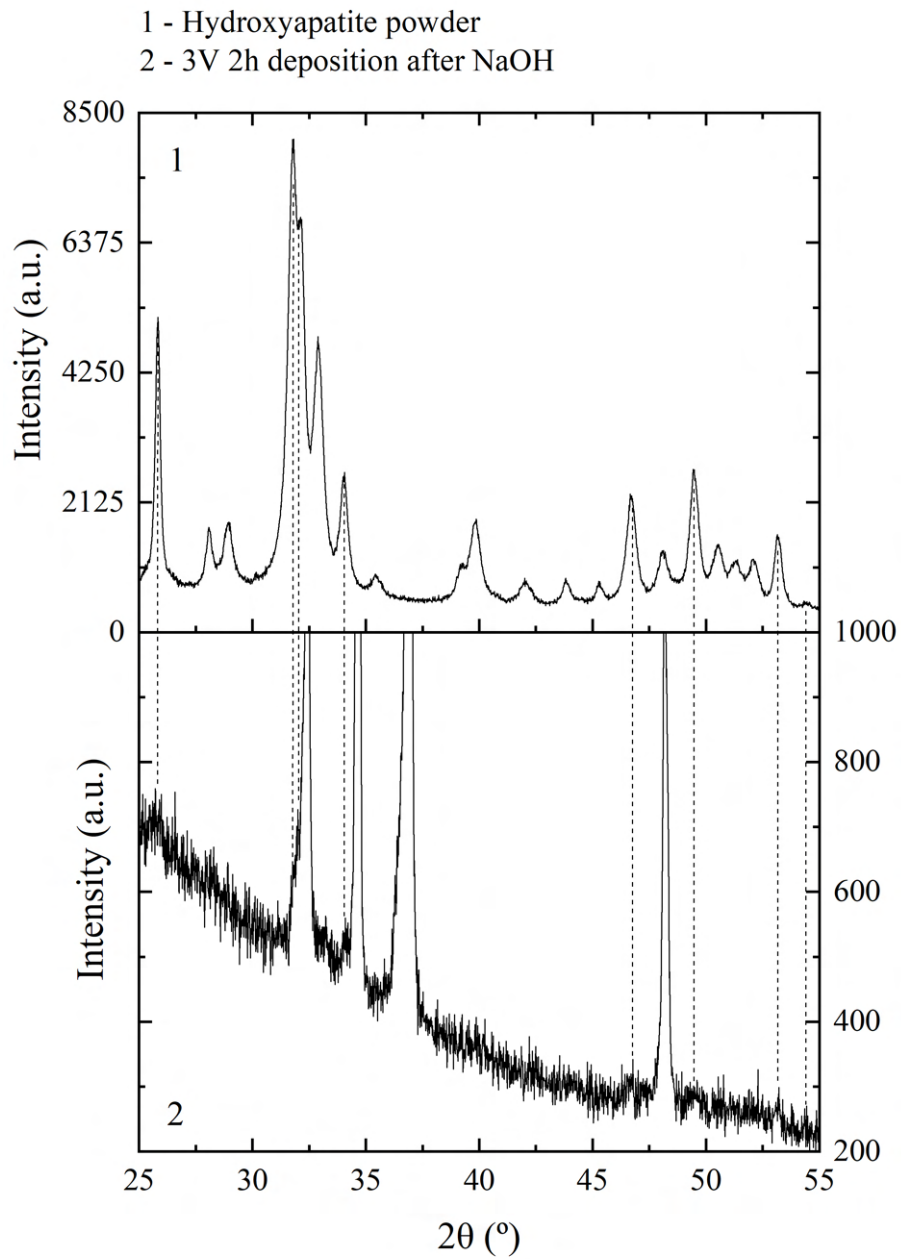


Figure I.7: XRD of the HA commercial powder (1) and of the coating after the immersion in NaOH with a deposition of 3V for 2 hours (2)

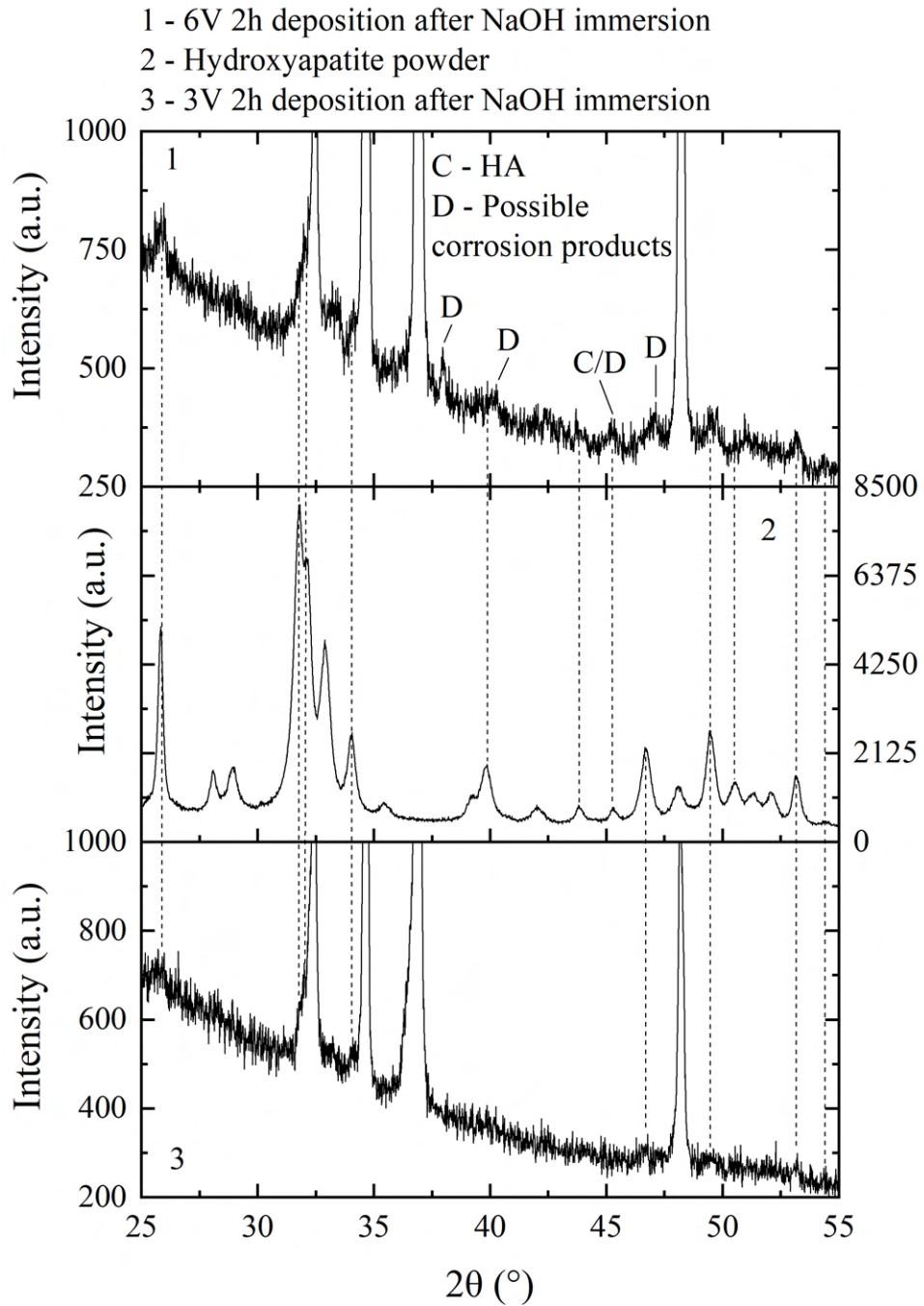


Figure I.8: Comparison of the XRD of the coating after the alkaline treatment of depositions of 6V and 3V, both for 2 hours (1 and 3, respectively) and of the HA commercial powder (2)

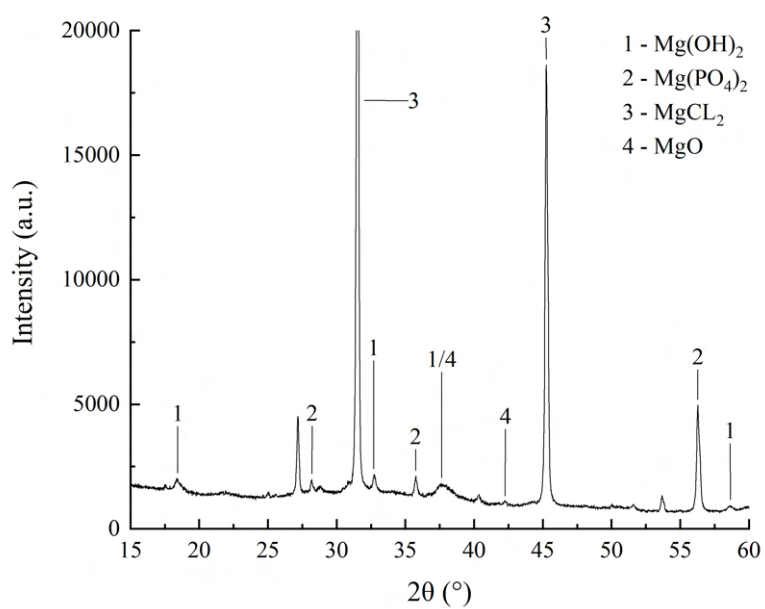


Figure I.9: XRD of the corrosion precipitate formed during the CV experiment with neutral pH

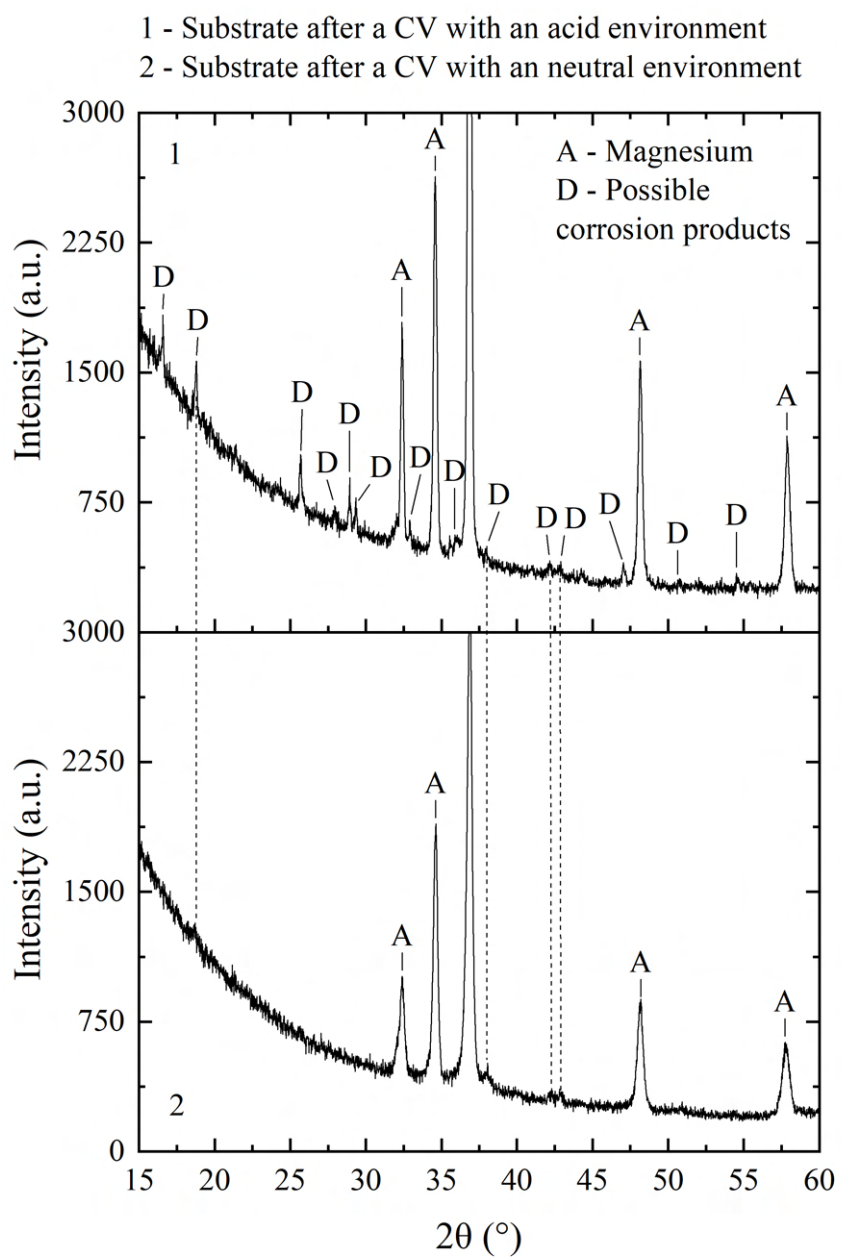


Figure I.10: XRD of the substrates after two CV experiments - acid environment (1) neutral environment (2)

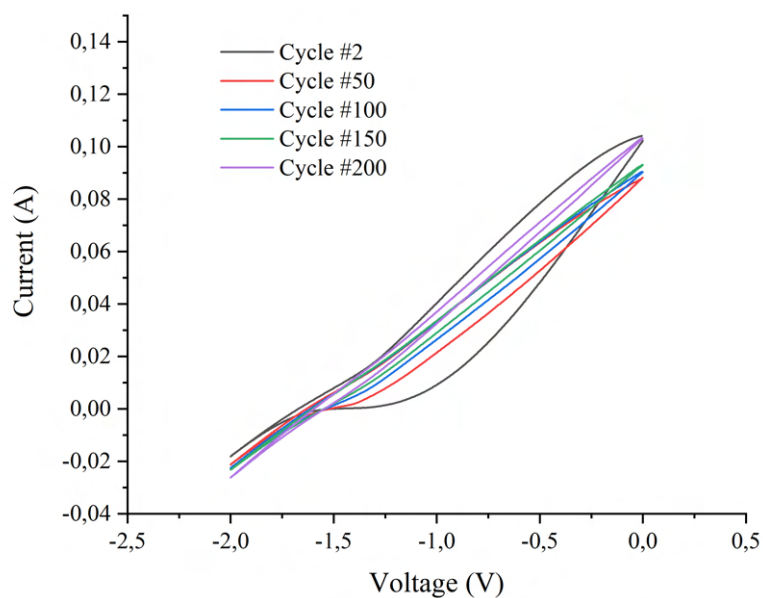


Figure I.11: CV of the WAAM printed substrate with 200 consecutive cycles with a pH of 7.4 (Scan Rate of 200 mV/s), after an electrodeposition of 3V for 2 hours

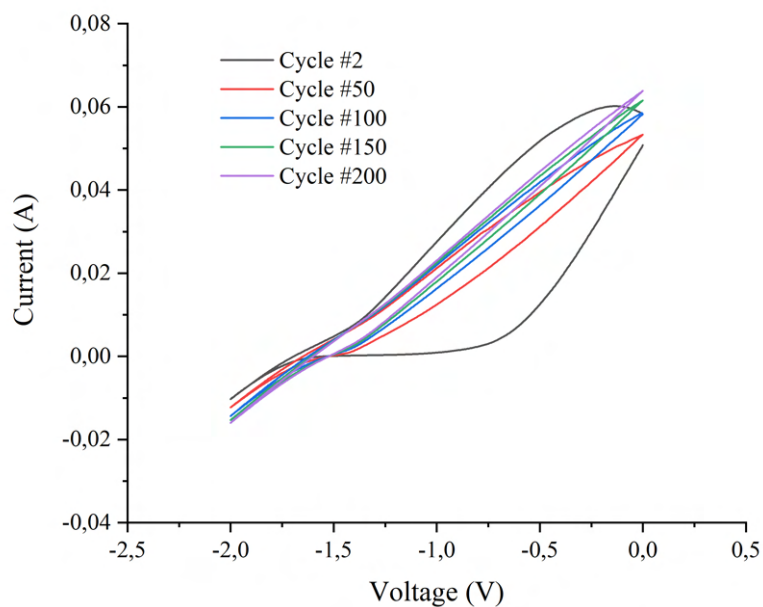


Figure I.12: CV of the WAAM printed substrate with 200 consecutive cycles with a pH of 7.4 (Scan Rate of 200 mV/s), after an electrodeposition of 3.5V for 2 hours

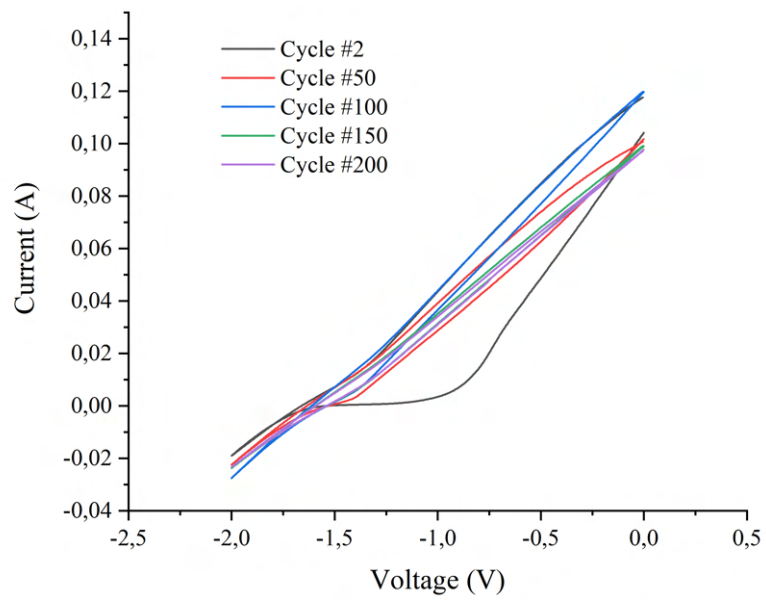


Figure I.13: CV of the WAAM printed substrate with 200 consecutive cycles with a pH of 7.4 (Scan Rate of 200 mV/s), after an electrodeposition of 4V for 2 hours

